National Aeronautics and
Space Administration

Lyndon B. Johnson Space Center
Houston, Texas 77058

NASA-CR-151776
19790078847

DMS-DR-2453
NASA CR-151,776

BASE PRESSURE AND HEAT TRANSFER TESTS OF THE 0.0225-SCALE SPACE SHUTTLE PLUME SIMULATION MODEL (19-OTS) IN THE NASA/CALSPAN LUDWIEG TUBE WIND TUNNEL (IH75)

SPACE SHUTTLE AEROTHERMODYNAMIC DATA REPORT

Data Management SERVICES

SPACE DIVISION CHRYSLER CORPORATION

April, 1979

DMS-DR-2453
NASA CR-151,776

BASE PRESSURE AND HEAT TRANSFER TESTS OF THE 0.0225-SCALE SPACE SHUTTLE PLUME SIMULATION MODEL (19-OTS) IN THE NASA/CALSPAN LUDWIEG TUBE WIND TUNNEL (IH75)

by

J. W. Foust
STS Aerosciences
Rockwell International
Space Systems Group

and

C. E. Wittliff
Aerodynamic Research Department
Calspan Corporation

Prepared under NASA Contract Number NAS9-13247

by

Data Management Services
Chrysler Corporation Michoud Defense-Space Division
New Orleans, La, 70189

for

Engineering Analysis Division

Johnson Space Center
National Aeronautics and Space Administration
Houston, Texas

WIND TUNNEL TEST SPECIFICS:

Test Number:	Calspan LT I95-100
NASA Series Number:	IH75
Model Number:	19-OTS
Test Dates:	September 23, 1977 to December 12, 1977
Occupancy Hours:	320

FACILITY COORDINATOR:

C. E. Wittliff
Aerodynamic Research Department
Calspan Corporation
P. O. Box 235
Buffalo, New York 14221

Phone: (716) 632-7500, Ext. 720

PROJECT ENGINEERS:

J. W. Foust
M. Quan
Mail Code AD38
Rockwell International
Space Systems Group
12214 Lakewood Boulevard
Downey, CA 90241

Phone: (213) 922-1451

C. E. Wittliff
Aerodynamic Research Department
P. O. Box 235
Buffalo, New York 14221

Phone: (716) 632-7500, Ext.720

DATA MANAGEMENT SERVICES:

Prepared by: Liaison--D. W. Hersey
Operations--G. R. Lutz

Reviewed by: G. G. McDonald

Approved: J. L. Glynn
J. L. Glynn, Manager
Data Operations

Concurrence:
N. D. Kemp, Manager
Data Management Services

Chrysler Corporation Michoud Defense-Space Division assumes no responsibility for the data presented other than display characteristics.

BASE PRESSURE AND HEAT TRANSFER TESTS OF THE 0.0225-SCALE SPACE SHUTTLE PLUME SIMULATION MODEL (19-OTS) IN THE NASA/CALSPAN LUDWIEG TUBE WIND TUNNEL (IH75)

by

J. W. Foust
Rockwell International
Space Systems Group

and

C. E. Wittliff
Calspan Corporation

ABSTRACT

Test IH75 was conducted in the NASA/Calspan Ludwieg Tube Wind Tunnel to determine heat transfer and pressure distributions and gas recovery temperatures in the base regions of a rocket firing model of the space shuttle integrated vehicle. The distributions are a direct result of rocket plume gas recirculation and impingement at simulated first-and second-stage flight trajectory conditions. The objective of this test was to extend the existing experimental data envelope to higher Mach numbers and altitudes.

First-and second-stage flight trajectory conditions were simulated by simultaneous flow of the space shuttle model rocket engines and Ludwieg Tube Wind Tunnel into a vacuum environment. First-stage flight consisted of space shuttle main engine (SSME) and SRB rocket motor simulation. Second-stage flight consisted of SSME simulation only. The Ludwieg Tube Wind Tunnel simulated Mach numbers of 3.5 and 4.5 over an altitude range of 100,000 to 170,000 feet with varying tunnel total temperature, model angle-of-attack, nozzle gimbal angle, and SRB chamber

pressure. For first-stage flight, the altitude range was 100,000 to 140,000 feet at Mach 3.5 and 100,000 to 160,000 feet at Mach 4.5. For second-stage flight, the altitude range was 130,000 to 170,000 feet at Mach 4.5.

All objectives of Test IH75 were fulfilled. Four runs were obtained at Mach 3.5 to collect repeat data to verify that IH75 test techniques would produce satisfactory data. At Mach 4.5, twenty-three first-stage runs and fifteen second-stage runs were obtained.

Tabulated heat transfer and pressure data are not presented with this report; they may be obtained as shown in Appendix A. Gas recovery temperature data derived from the thirteen gas temperature probe runs are presented in Appendix B.

The model configuration, instrumentation, test procedures, and data reduction are described in this report.

Procedures and data from the flow calibration of the Mach 3.5 nozzle used with the Ludwieg Tube Wind Tunnel for Test IH75 are presented in Appendix D.

TABLE OF CONTENTS

TABLE OF CONTENTS (Concluded)

INDEX OF MODEL FIGURES

INDEX OF MODEL FIGURES (Concluded)

INTRODUCTION

Not being a conventional rocket launch vehicle, the space shuttle experiences complex heating and pressure conditions in its base regions during first-and second-stage ascent due to solid rocket booster and main engine plume interaction in the presence of the surrounding airstream. Since these heat transfer and pressure conditions cannot be adequately defined by existing analytical methods, they must be determined experimentally. The experimental data will assist the design of thermal protection in the space shuttle vehicle base regions.

This investigation, Test IH75, was undertaken to measure heating rates and pressures and to determine gas recovery temperatures in the base regions of a scaled model of the space shuttle vehicle with orbiter and SRB firing rocket engines simulating plume recirculation and impingement in an altitude environment. Forty-two runs were obtained at Mach 3.5 and 4.5 with various altitudes and various model parameters simulating numerous shuttle first-and second-stage flight trajectory conditions. The model parameters included angle-of-attack, nozzle gimbal angle, and SRB chamber pressure. The results of the investigation are presented in this report.

NOMENCLATURE

PLOT SYMBOL	MNEMONIC	DEFINITION
	Tunnel Parameters (Freestream)	
M_∞	MACH	Mach number
PALT		altitude pressure, psi
P_∞	PS	static pressure, psia
P_O	PO	stagnation pressure, psia
Re	REB	Reynolds number, 1/ft
T_∞		static temperature, ^oR
T_O	TO	stagnation temperature, ^oR
μ_∞		absolute viscosity, lb-sec/ft^2
	Model Parameters	
α	ALPHA or ALPHAB	angle-of-attack, degrees
δ_{E_I}	ELEVON CONF.	inboard elevon deflection, degrees
δ_{E_O}	ELEVON CONF.	outboard elevon deflection, degrees
P		SRB and SSME nozzle gimbal pitch angle, degrees
Y		SRB and SSME nozzle gimbal yaw angle, degrees
	Pressure and Heat Transfer Parameters	
CAL		oscillograph calibration, mV/in or V/in
DEFL		measured deflection on oscillograph, inches
GAIN		system gain
K_b		thin-film gauge calibration sensitivity, ohms/^oF
K'		thin-film gauge sensitivity corrected for abrasion and normal wear, ohms/^oF

NOMENCLATURE (Continued)

PLOT SYMBOL	MNEMONIC	DEFINITION
		Pressure and Heat Transfer Parameters
P	PRESS	absolute pressure, psia
P_{REF}		transducer pre-run ambient pressure, psi
$\dot{q}$	$\dot{q}$	heat transfer rate, BTU/ft^2-sec
c_p		analog q-meter proportionality factor
R_b		thin-film gauge calibration resistance, ohms
R_L		thin-film gauge circuit line resistance, ohms
R_T		thin-film gauge measured pre-run resistance, including line resistance, ohms
S		pressure transducer calibration sensitivity, mV/psi
		Gas Recovery Temperature Parameters
A		wire cross sectional area, cm^2
D		wire diameter, cm
h		convective heat transfer coefficient, cal/sec-cm^2-^oK
h_c	h	corrected convective heat transfer coefficient, cal/sec-cm^2-^oK
k		wire thermal conductivity, cal/cm-sec-^oK
ℓ		wire length, cm
q_c		heat input to the wire from the gas, cal/sec
q_j		heat due to current flow, cal/sec
q_k		heat conduction to wire supports, cal/sec
q_{rw}		heat loss by radiation from the wire, cal/sec

NOMENCLATURE (Concluded

PLOT SYMBOL	MNEMONIC	DEFINITION
	Gas Recovery Temperature Parameters (Continued)	
q_s		heat accumulated in the wire, cal/sec
q_{wg}		heat gained by radiation from the gas, cal/sec
R_o		wire resistance at T_o, ohms
R_w		measured wire resistance, ohms
T_o		initial wire temperature, ^oK (20^oC)
T_r		gas recovery temperature, ^oK
T_{r_c}	Tr	corrected gas recovery temperature, ^oK
T_s		wire support temperature, ^oK
T_w		wire temperature, ^oK
$\overline{T}_w$		mean wire temperature, ^oK
X		distance along the wire, cm
α, β		R-T curve fit coefficients
γ		parameter $\sqrt{h/KD}$, $\frac{1}{cm}$
π		constant
σ_o		wire resistivity at T_c($\sigma_o = R_oA/\ell$), ohm-cm
	Subscripts	
1, 2		denotes long and short wires

CONFIGURATIONS INVESTIGATED

The model configuration for Test IH75 was a 0.0225-scale version of the space shuttle integrated vehicle. Designated 19-OTS, the model employed short-duration, rocket firing techniques to simulate the vehicle rocket plumes during ascent. The space shuttle main engines (SSME's) burned hydrogen and oxygen gases, and the solid rocket boosters (SRB's) burned a solid propellant (ANB-3066B) to simulate either first-or second-stage rocket plumes at one-half full-scale chamber pressure.

The integrated vehicle model consisted of the orbiter, external tank (ET), and solid rocket boosters (SRB's) designed to outer mold line vehicle 5 specifications.

Orbiter

The wing, vertical tail, and body flap simulated planform, contour, and thickness distribution. Deflective split elevons were simulated on the wing. Inboard elevons deflected +5, +10, and +15 degrees; outboard elevons deflected -5 and +5 degrees. Elevons remained fixed throughout Test IH75 at $+10^{\circ}$ inboard and 0° outboard. The rudder on the vertical tail was not simulated. The body flap remained fixed in the nominal position (zero deflection).

The base heat shield was divided into four segments to facilitate gimbal angle changes and to provide easy access to the instrumentation.

Nozzles

SSME and SRB nozzle internal surfaces were geometrically duplicated. External surfaces were smooth except for one extra SSME nozzle which

simulated the external hatbands; the hatband nozzle was used in the #1 SSME location during gas temperature probe runs. SSME and SRB nozzle walls were structurally thickened to withstand nozzle heating.

Both SSME and SRB nozzles had gimbaling capability. Gimbal angle blocks defined specific pitch and yaw nozzle displacements. When required, each gimbal block rotated about its central axis to simulate various gimbal configurations; all gimbal blocks were designed to be positioned at 45-degree intervals around the circumference. Null position for the SSME and SRB nozzles was as follows:

Left and Right SRB's:	Pitch = 0, Yaw = 0
#1 SSME:	Pitch = 16° up, Yaw = 0
#2 and #3 SSME:	Pitch = 10° up, Yaw = 0

For both SSME and SRB nozzles, deflections were as shown in Figure 1.

Two non-firing SSME nozzles were provided with the model for simulating engine-out operation. Although the two non-firing nozzles could replace any of the three firing nozzles, they were not used for this test program.

OMS nozzles were non-functional. They were simulated internally and externally at their "stowed" ascent position which is six degrees pitch down from null and seven degrees yaw outboard from null.

External and Support Hardware

External and support hardware on the orbiter, ET, and SRB's were not simulated except for the aft support hardware on the ET consisting of

struts, cross beam, diagonal cross strut, and LO_2 and LH_2 feed lines. These hardware were simulated to scale but were not detailed or capable of carrying support loads.

Support between the orbiter and external tank was provided by an adapter which contained propulsion supply passages, autovalve control passages and instrumentation wire passages. The adapter also provided a mounting surface for the orbiter wing.

The SRB's were supported at the center of the external tank by mounting pads. A small strut also attached just aft of the SRB nose. The mounting pad provided for ignition gas passage to the SRB and a transducer installation to monitor chamber pressure.

Model Support

A thin-blade strut was mounted to the bottom of the external tank. The strut was bolted to a base fixture which was rigidly mounted to the floor of the Ludwieg Tube Wind Tunnel receiver tank. Thus, the model was mounted upright just downstream of the nozzle exit. Model angle-of-attack was determined by the bolt hole pattern at the strut/base fixture interface.

Nomenclature

Nomenclature for model 19-CTS was as follows:

Component	Definition
B_{64}	fuselage body
C_{16}	canopy

Component	Definition
E_{63}	elevon
F_{14}	body flap
M_{18}	OMS pod
N_{92}	OMS nozzle
N_{94}	SSME nozzle
V_{23}	vertical tail
W_{129}	wing
S_{22}	solid rocket booster
N_{106}	solid rocket booster nozzle
T_{33}	external tank

These components of the space shuttle vehicle are identified in Figures 2 and 3.

Dimensional Data

Dimensional data for model 19-OTS are presented in Table III.

Model Drawings

Further description of the model including model drawings can be found in Reference 1.

Propulsion Systems

(Orbiter)

The orbiter propulsion system consisted of hydrogen and oxygen charge tubes, a fast-acting bipropellant valve (autovalve), hydrogen and oxygen venturis, an injector, a combustion chamber, and the SSME gimbal

block/nozzle assemblies.

The charge tubes were arranged spirally inside the external tank to supply hydrogen and oxygen at approximately 3000 psia through the autovalve to the venturis. When the autovalve opened, the gases were supplied to the venturis at constant conditions for the wave time of the charge tubes. The hydrogen charge tube, being larger, was located in the front of the external tank. The oxygen charge tube, in the back of the external tank, was separated from the hydrogen charge tube by a cavity used to route gas lines and wiring from the orbiter to the model strut.

The autovalve is a pneumatically operated piston type valve. Two solenoid (Valcor) valves, when energized, emitted high-pressure nitrogen (approximately 3000 psia) to chambers within the autovalve for opening or closing. SSME nozzle flow time was controlled by the relative time between solenoid valve operation.

The venturis operated under choked flow conditions. They were designed for an O/F ratio of 6.0. Separate venturis are used for two-engine and three-engine SSME operation to simulate the proper mass flow at each condition; only three-engine SSME operation was simulated for Test IH75.

The injector was composed of twelve doublets designed to impinge on a diameter equivalent to the combustion chamber area mean diameter. Doublet holes were of equal size and angled to balance the radial

momentum of the hydrogen and oxygen streams.

The combustion chamber provided necessary volume for the gases to mix and burn. It was common to all three SSME nozzles. A pyrotechnic ignition source was located in the chamber.

The SSME gimbal block/nozzle assemblies were located downstream of the combustion chamber. The nozzles were scaled and contoured internally.

(Solid Rocket Booster)

Each solid rocket booster consisted of a propellant holder, an ignition gas system, a diaphragm, and a gimbal block/nozzle assembly. SRB flow was controlled by the amount of solid propellant used; propellant thickness determined the burn time while propellant surface area determined chamber pressure level.

The propellant holder was a cylindrical casing which fit inside the SRB. Solid propellant (≈0.050 inch thick) was glued to a thin aluminum sheet (≈0.011 inch thick) and rolled inside the holder. Solid propellant surface areas required to produce the desired chamber pressures are listed in Table IV. Both ends of the propellant holder were capped to enclose the holder during initial propellant burning: a solid cap at the forward end and the diaphragm at the aft end.

An ignition gas composition of ethylene and oxygen filled each SRB just prior to ignition to provide a high-energy source for rapid ignition (<5 msec.) of the solid propellant. Ignition gas pressure was nominally 16.5 psia. The mixture was nominally O/F = 5.6. A pyrotechnic source

in each SRB nose ignited the gas which, in turn, ignited the propellant.

The diaphragm was contained in the aft propellant holder end cap. It consisted of thin sheets of Mylar, 0.040 inch total thickness, sized to burst at slightly above the desired chamber pressure.

The gimbal block/nozzle assemblies were scaled and contoured internally.

The solid propellant, ANB-3066B, was a Class B explosive that functioned by rapid combustion rather than detonation. The burning rate was a function of pressure, temperature and humidity.

INSTRUMENTATION

Heat-Transfer Gauges

Thin-film heat-transfer gauges (References 2-4) were employed for the measurement of model surface heating rates. The sensing elements are thin (order of 0.1 micron) platinum resistance thermometers fused onto the surface of pyrex substrates. The thin-film heat-transfer gauge operates on the principle that the film thickness is much less than the characteristic thermal diffusion depth for the short duration of the test event. Thus, the temperature gradients and heat capacity of the film are negligable, and the instantaneous film temperature can be said to be equal to the instantaneous substrate surface temperature.

The resistance elements are coated with a dielectric film (i.e., M_gF_2) which provides the following beneficial characteristics: (1) it affords mechanical protection for the elements, (2) it improves electric stability of the elements by sealing against the ambient environment, (3) it provides electrical isolation from ionized gas flows, and (4) it provides higher absorptivity to radiant heat flux than can be obtained with uncoated surfaces. Loss of gauge response due to the presence of the coating (approximately one micron thick) is negligible.

During operation, the temperature-induced resistance change of the platinum element is sensed electrically. For those gauges that were recorded directly on oscillographs, the electrical signal was fed to an analog network (known as a "Q-meter"), which converted the indicated surface temperature in real time to an instantaneous heat-transfer rate

by employing the theory of linear heat conduction to an infinite slab (References 2 and 5). This conversion is applicable over a wide range of test conditions, if proper account is taken for gauge resistance changes due to erosion and variations in the physical properties of the substrate with temperature.

For the heat-transfer gauges that were recorded on FM tape, the voltage signal proportional to surface temperature was recorded. After a test run, the tape was played back, and the signals were fed to analog Q-meter networks. The output of these Q-meters was then recorded on an oscillograph.

Two types of heat-transfer gauges were employed during the test: standard and radiative gauges. The physical construction of the two gauge types is similar. The ends of the platinum sensing element are electrically connected to the back of the substrate by silver film deposited on the Pyrex. The lead wires are soft soldered to the silver on the back of the gauge.

Standard Gauge

The standard heat-transfer gauge consists of a platinum film fused onto the surface of the Pyrex substrate which, in turn, conforms to the local contour of the model. This gauge is sensitive to the entire convective heat flux, as well as a portion of the radiative flux. The amount of incident radiation sensed by the gauge is a function of its spectral absorptivity, as well as the spectral radiance of the energy

source.

Radiative Gauge

The radiative heat-transfer gauge consists of a standard gauge upon which a thin coat of aluminum black has been deposited. The coated gauge is mounted within a holder and isolated from convective heating by a synthetic sapphire windor, which has excellent transmittance in the wavelength interval of interest, and also protects the relatively fragile black coating. Essentially, radiation gauges of this type have a uniform spectral absorptivity of about 0.85 over the 1 to 6μ wavelength range.

Pressure Transducers

Model surface and tunnel pressure measurements were made using high-frequency response transducers (References 2 and 6). These devices employ lead-zirconium-titanate piezoelectric ceramics as pressure-sensitive energy sources and include integral field-effect-transistor (FET) circuits for power amplification and impedance matching. The complete transducers are typically 0.37 inch in diameter by 0.23 inch thick. Units with nominal sensitivities of 2000 mv/psi (0-2.5 psi range) 150 mv/psi (0-10 psi range), and 50 mv/psi (0-100 psi range) were used. Typically, transducer sensitivities are linear to within ±2% throughout their respective ranges. To provide acceleration compensation, a second integral, but pressure insensitive, diaphragm/piezoelectric crystal unit is wired in opposition to the active unit. This design reduces acceleration sensitivity to nominally 0.00015 psi/g

and 0.0004 psi/g, respectively, for the low-range and high-range transducers. In order to minimize temperature-induced effects on the transducer diaphragms, copper heat shields were installed to provide line-of-sight shielding from radiant or hot gas sources.

Propellant flow passage and combustion chamber pressures in both the orbiter and the BSRM's were sensed with commercial*, fast-response, piezoelectric pressure transducers. PCB transducers were used for propellant flow passages. Kistler transducers were used for the combustion chambers. Protection of the transducer from the hot combustion gases was provided by a thin layer of RTV** over the diaphragm, a heat shield, and a devious path orifice arrangement. Appropriate impedance matching of the Kistler transducers was provided by external charge amplifiers.

Gas-Temperature Probes

Gas-temperature probe (GTP) measurements in the base regions of the model were used to derive gas recovery temperatures. The gas-temperature probe is a thin wire resistance thermometer consisting of two, thin platinum -10% rhodium wires, approximately 1 and 2 mm long, mounted parallel on the tips of four needles positioned accordingly. Wire resistance due to the rocket plume heating environment is related to the wire temperature and then used to solve the thin wire heat balance

* Kistler Instrument Corporation, Clarence, New York and PCB Piezotronics, Inc., Buffalo, New York.
** Room Temperature Vulcanizing rubber.

equations to produce two unknowns: gas recovery temperature and convective heating rate. The two wires allow independent measurements of the flow field heating environment for simultaneous solution of the heat balance equations.

The gas-temperature probe was mounted in a holder designed to position the two wires 0.10 inch to 0.50 inch from the model surface and to allow rotation for more direct exposure to the flow; wire position was maintained at 0.25 inch throughout Test IH75.

Wire diameter varied with location on the model. Initially, 2.54×10^{-4} cm diameter wires were installed at all gas-temperature locations. This size wire survived the model firing, but the return wave from the Ludwieg Tube Wind Tunnel receiver tank end wall destroyed the wires on the external tank probes. Subsequently, the ET wire diameter was doubled (5.08×10^{-4} cm).

An iron-constantan "Type J" thermocouple was mounted in the tip of one needle on each probe to monitor probe temperature during model firing.

Further description and procedures for the gas-temperature probe can be found in References 7, 8, and 9.

Instrumentation Locations

Pressure, heat transfer, and gas-temperature probe locations on the model are shown on Figures 4a through 4t. The instrumentation is summarized below and itemized on each figure.

INSTRUMENTATION (Concluded)

Standard heat-transfer gauges	188
Radiative heat-transfer gauges	22
Pressure transducers	33
Gas-temperature probes	7

The instrumentation numbering system used on Figures 4a through 4t is summarized in Table V.

Instrumentation on the model actually used for Test IH75 is categorized according to instrumentation configuration in Table VI.

TEST FACILITY DESCRIPTION

A short-duration tube wind tunnel (Ludwieg tube) (Reference 10), provided aerodynamic flow about the test model to simulate specific regimes of the Space Shuttle launch trajectory. Figure 5 depicts the facility and identifies its main components.

In operation, the test gas is initially loaded into the 42-inch diameter supply tube and contained by a mylar diaphragm located just upstream of the nozzle. To initiate flow, the diaphragm is cut by mechanical means. A centered expansion wave then propagates upstream in the supply tube and accelerates the test gas to a steady velocity. The gas expands through the nozzle into the initially evacuated receiver tank (See Table I). Meanwhile, the expansion wave in the supply tube propagates upstream at acoustic speed. The nozzle supply conditions remain constant, and flow is steady until that wave, reflected from the upstream end of the supply tube, returns to the nozzle inlet. A schematic diagram of this operation is shown in Figure 6. For the 60-foot long supply tube, steady nozzle inlet conditions are maintained for approximately 90 milliseconds (ms) when the test gas is ambient temperature air or nitrogen.

The test gas, expanding through the nozzle into the receiver tank, provides the desired ambient test conditions in the free jet test section at the nozzle exit. The test flow continues downstream in the receiver tank at high velocity, until it is brought to rest when it encounters the receiver tank end wall. The incoming test gas develops a stagnated

volume at the end wall, which continues to grow in the unconstrained upstream direction. A shock front (i.e., the interfacial boundary between the incoming high velocity test gas and the stagnated gas) thus propagates upstream until it encounters and (usually) breaks down the test section conditions established by the nozzle flow. Prior to testing, flow breakdown time in the receiver tank was estimated to be approximately equal to the supply-tube wave time for the external flow conditions of this program.

For some of the test runs, the supply-tube gas charge was heated during its residence in the charge tube in order to effect a more reasonable simulation of the shuttle flight trajectory conditions. Strip heaters, covered with high-temperature insulation, were distributed uniformly on the outside surface of the tube. The heating system provided the capability of raising the wall temperature to 600°F. Separate "on-off" temperature controllers, with adjustable setpoints, were used to control the longitudinal temperature distribution. One effect of heating the gas in the supply tube was to reduce the time during which steady pressure was available at the nozzle inlet from approximately 90 ms for ambient temperature gas to about 65 ms for gas at 600°F.*

* That is, because of the higher sound speed in the hot gas, the expansion wave velocity is greater.

To maintain the pre-run strength and integrity of the mylar diaphragm, a water ccoling system consisting of internal and external jacket coils was installed at the diaphragm station. Pre-run gas temperature in the portion of the supply tube just upstream of the diaphragm was consequently reduced to 300 to 400°F. Although this environment proved suitable for diaphragm survivability, it also produced an axial temperature gradient in the supply tube gas charge. Thus, as the supply-tube gas passed through the nozzle and expanded into the test section, the total temperature varied during the early portion of the test time. It was constant during the time the data were read.

The Mach 3.5 and 4.5 nozzles, fabricated of glass-reinforced polyester resin, were contoured to provide uniform, parallel test section flow. In order to comply with existing facility length constraints, the final four feet of the theoretical full-expansion length were omitted (e.g., see Figure 7). The resulting maximum free jet test rhombus diameter was somewhat smaller than the nominal five-foot exit diameter of the nozzle.

TEST PROCEDURE

Installation

Model 19-CTS was installed in the upright position just downstream of the nozzle exit plane (see Figure 7). The model sat atop a thin-bladed strut which was inserted into a base fixture rigidly attached to the receiver tank floor. Model angle-of-attack was determined by selecting the proper bolt hole pattern at the strut-base fixture interface.

Model instrumentation wiring and propulsion lines were routed through a shroud, attached to the trailing edge of the strut, to the lower base region of the strut. Propulsion lines were then routed through a pressure bulkhead at the receiver tank wall. Once outside, the lines extended to isolated sources (K-bottles) or to vent areas. Instrumentation wires were soldered to a patchboard at the base of the strut. Tunnel wiring relayed the instrumentation signals from the patchboard to the appropriate data acquisition systems. While enroute to the data acquisition systems, the wiring passed through sealed bulkhead fittings at the receiver tank wall and through a switching panel.

Control panels for regulating gas flow to the model propulsion systems were located in the control room. Gases required to operate the model were:

Oxygen	-	orbiter charge tubes and SRB ignition
Hydrogen	-	orbiter charge tubes
Ethylene	-	SRB ignition
Helium	-	orbiter and ET leak checking

Nitrogen - autovalve operation, charge tubes for orbiter cold flow runs, charge tube purging, and SRB leak checking

Front and rear views of the first-and second-stage model configurations installed in the Ludwieg tube wind tunnel are shown in Figure 9.

Instrumentation Calibrations

The calibration methods utilized at Calspan are described in detail in References 2 through 4 and 6, along with the theoretical considerations from which they are derived. Calibration records are maintained at Calspan. However, the following comments are appropriate with respect to their application to the test.

Pressure

Prior to the start of the test program, all pressure transducers used in the model were pneumatically calibrated with a series of step pressure inputs covering the anticipated range of usage. The voltage output variations of the transducers were typically linear within ±2%.

The Kistler pressure transducers used for combustion-chamber pressure measurements were dynamically calibrated prior to the test program by means of a high-pressure pneumatic calibration system. Linearity was again typically well within the nominal ±2% bandwidth.

Heat Transfer

The standard calibration procedure for a thin-film heat-transfer gauge is explained in detail in Reference 3. Its resistance is measured at three temperatures in order to obtain the gauge's temperature

sensitivity $K = \Delta R/\Delta T$. The temperature range is nominally 70° to 150°F.

Gas-Temperature Probes

Prior to installation in the model, gas-temperature probes were calibrated over their operating temperature range to determine resistance change with wire temperature. Calibrations were also required following repair or following the test program to determine changes that could account for data anomalies.

Recording System

A complete gain calibration of each oscillograph recording channel with its associated conditioning amplifier was performed prior to the start of the test program. Routine checks, during the course of the test program, disclosed no appreciable variations (i.e., drift or fluctuations).

Operating Procedure

The test objectives required simultaneous realization of steady exhaust plumes from three scale SSME rocket nozzles, as well as from the two solid propellant SRB engines during the short duration of steady external flow produced about the 19-OTS model. After initiation of the external flow, model operation was characterized by ignition of SRB and SSME propellants sequenced to attain simultaneous, steady-state plume flow.

As a result of experience with the model during previous tests, proper synchronization of the three flow events (i.e., orbiter SSME

rockets, SRB motors, and Ludwieg tube external flow) did not present significant problems. Test runs 1 through 3 were required before full synchronization was achieved. After that, the only operating problems were occasional relay failures, wherein igniters failed to fire.

Test runs were categorized according to the instrumentation being recorded. Instrumentation configurations were distinguished by model configuration and type of instrumentation (Reference Table 6). The general run sequence was:

1. First-stage configuration runs (Instr. Config. 1)
2. Second-stage configuration runs (Instr. Config.3)
3. Second-stage gas temperature probe runs (Instr. Config. 4)
4. First-stage gas temperature probe runs (Instr. Config. 2)

Test runs producing good data are listed in Table II.

Procedure to achieve synchronization of the three flow events with the data acquisition systems was similar for all runs. Gas-temperature probe runs required additional monitoring to insure probe integrity at the start of the run. The general procedure was as follows:

1. Following model refurbishment and Ludwieg tube diaphragm replacement, the tunnel was closed for receiver tank evacuation. The target evacuation pressure was always less than one-tenth of the nominal freestream static pressure during tunnel flow (See Table I). The target pressure was not always attainable, especially at the high altitudes where leaks around the receiver tank were of the same order as the evacuation rate.

2. Approximately one hour before model firing, the orbiter propulsion gas systems were roughly set to the desired pressures. Any system leaks could be detected before model firing. Final pressure adjustment occurred just prior to model firing.

3. At about the same time period, the Vidar data acquisition system was prepared for recording, i.e., gains were set, signal full span was verified, and signal zero was verified. The Vidar system was continuously monitored until model firing.

4. Approximately one-half hour before model firing, thin-film gauge resistance readings were manually recorded on a digital volt meter.

5. Approximately five minutes before model firing, the ignition gas mixture was loaded into the SRB's. At about the same time, pre-run gas-temperature probe readings, total resistance and line resistance, were recorded.

6. When time for the model firing, all model and data acquisition systems were given a final check. If ready, the final step was to load the Ludwieg tube driver section to the desired charge pressure.

7. Following model firing, the receiver tank required about thirty minutes of evacuation, before model refurbishment could begin, to exhaust SRB propellant residue from the tank.

Time between runs was usually dictated by evacuation of the receiver tank. Two or three runs were typical for an eight-hour work period.

Synchronization of the three flows, Ludwieg tube, orbiter SSME, and SRB, was controlled by a series of timing relays initiated by a single pushbutton fire switch. The relays were set to first; initiate SRB flow, second; initiate Ludwieg tube flow, and third; initiate SSME flow. SSME flow duration was typically 60 milliseconds with the first 10 milliseconds required for flow stabilization; duration was determined by proper sequencing of the autovalve opening and closing pressures. SRB flow duration was determined by propellant thickness (≈0.050 inch); total duration was typically 180 milliseconds with the first 30 milliseconds required for flow stabilization. Ludwieg tube flow duration

was as described in the Test Facility section: typically 90 milliseconds for ambient temperature driver gas and 65 milliseconds for 600°F driver gas; Ludwieg tube flow stabilization was typically less than 10 milliseconds. When synchronizing the three flows, SRB flow timing was most critical, not because of the relatively long stabilization time but because of its effect on the receiver tank environment. Flow breakdown time, described in the Test Facility section, was significantly decreased due to the mass of the SRB flow adding to the stagnated volume returning from the receiver tank end wall. Thus, data had to be recorded during early SRB flow before flow breakdown. Pressure measurements at the Ludwieg tube nozzle exit plane determined when flow breakdown occurred. Flow breakdown varied with SRB chamber pressure and Ludwieg tube flow conditions. Maximum operating conditions with Model 19-OTS in the Ludwieg tube wind tunnel based on the flow breakdown process are presented in Table VIII. Typical model and tunnel operating data are presented in Figures 9a and 9b.

It should be noted at this time that static pressure of the Ludwieg tube flow at a simulated altitude is one-half of the actual altitude pressure. Actual altitude pressures were determined from Reference 11. With the model SSME and SRB propulsion systems operating at one-half full-scale chamber pressure and the Ludwieg tube wind tunnel operating at one-half actual altitude pressure, the scaled SSME plume flow field was duplicated.

Model refurbishment between runs consisted of model configuration changes, new SRB propellant, and new SRB and SSME igniters. Model configuration changes were usually SSME and SRB nozzle gimbal angle changes. Following propellant and igniter replacement, an SRB ignition gas leak check procedure insured that the new propellant holders were installed correctly. Loss of ignition gas during a run would cause SRB misfire. To leak check, nitrogen was loaded into the propellant holders at approximately 30 psia. An acceptable leak rate was 0.2 psi per minute. For a good propellant holder installation, which was common, there would be no leak during the first minute.

Data Acquisition

Both oscillographs and an FM-Multiplex tape recorder system were used to record test data. A total of 128 channels were available during the test. However, since the total number of model measurements was too large to record simultaneously, four different instrumentation set-ups were used.

A total of 62 data channels were recorded on 5 twelve-or-fourteen-channel direct-writing, light-beam oscillographs, employing galvanometers having a flat frequency response bandwidth of 0.600 Hz. A chart speed of 32 inches/second provided adequate time resolution and frequency response. Two types of conditioning amplifiers, having a variable gain from 1 to 100 or 1 to 1000, provided the amplification necessary to drive the galvanometers.

The FM-Multiplex tape recorder system was a portable Vidar system consisting of 12 tape tracks with 6 channels each. Only eleven tape tracks were available for this test program to comprise the remaining 66 data channels. The Vidar VCO amplifiers provided system gains of 0.40, 1, 3.33, 10, 33.33, and 100. To provide additional amplification, separate pre-amplifiers with gains of 1 to 1000 were connected in series to the Vidar VCO amplifiers. Full-scale input to the Vidar tape recorder was 1-volt. The standard procedure was to use the pre-amplifiers and the VCO amplifiers to boost the anticipated instrumentation output (heat-transfer gauge or gas-temperature probe) to 1/2-volt for input to the Vidar tape. For data playback, two tape tracks (12 channels) at a time were patched through a q-meter circuit (see Data Reduction) and output on to a fourteen-channel, direct-writing, light-beam oscillograph. Playback amplifier gains were set to provide 1-inch deflection for a full-scale 1-volt tape signal. A schematic of the Vidar data acquisition and playback is presented in Figure 10.

Of the 128 channels available to record test data, from 90 to 100 channels were used to record model data. A summary of the model data recorded for each instrumentation configuration is presented at the end of Table VI. Channels not used for model data recorded the following essential information:

1. Model operating pressures (propellant flow passage and combustion chamber)
2. Model timing events
3. Tunnel operating data (pressures and temperature)

A summary of the data recorded by the Vidar and oscillograph data acquisition systems for each instrumentation configuration is presented in Table IX.

Signal conditioning for the Kistler pressure transducers was provided by external charge amplifiers. Signal conditioning for the PCB pressure transducers was provided by a 110V multi-channel power unit built specifically for the transducers. The power supply unit supplied 22V and 12mA current excitation for each transducer. Being highly sensitive, the pressure transducers did not require additional amplification.

Thin-film gauge signal conditioning consisted of circuitry with the gauge connected in series with a 10K-ohm series resistor and a 220-ohm coupling capacitor resistor. Excitation voltage for the circuit was 30V. For a nominal 100-ohm thin-film gauge, the circuit current was 2.91mA. All thin-film gauges recorded on the Vidar FM-Multiplex tape recorder system and oscillographs required amplification.

Gas-temperature probe signal conditioning was provided by a power supply panel which allowed the current to be adjusted to match the probe wire size. The panel supplied 15VDC excitation to each probe. Further details of the power supply panel are given in Reference 9.

SSME nozzle position and instrumentation orientation depended on the use of gas-temperature probes. Without gas-temperature probes, the #1 and #2 SSME instrumented nozzles were used in SSME positions 1 and 2 as shown in Figure 11a. With gas-temperature probes, the hatband nozzle

was added, and all three instrumented nozzles were positioned as shown in Figure 11b. The figures are viewed looking forward along each nozzle axis.

Data were reviewed immediately after each model firing to:

1. Verify satisfactory model operation.
2. Verify sufficient data and their integrity.

Oscillograph records of the tunnel and model operating data were examined first to verify model operation. Then, all Vidar data were played back onto the oscillograph and along with remaining on-line oscillograph data were examined to verify data integrity. All model data were reviewed after each test run.

DATA REDUCTION

Test Conditions

The Mach 4.5 nozzle was calibrated prior to Test IH75 and found to provide satisfactory flow at the design Mach number over the pressure range of the tests. Because the Mach 3.5 nozzle had not been previously calibrated, this was done prior to the present program, and the results are summarized in Appendix D. The average test section Mach number, used in the data reduction, was 3.484.

Thus, test section static pressure and static temperature were computed by:

M_∞	3.484	4.5	
P_∞	.01341 P_o	.003455 P_o	(psia)
T_∞	.2917 T_o	.1980 T_o	(^oR)

where P_o and T_o were the average nozzle stagnation conditions measured on each run during the data acquisition time. The respective simulated test altitude was determined from a pressure equal to twice the calculated static pressure (PALT = 2 P_∞) to account for the 1/2 reduction in the combustion chamber pressure. The altitudes corresponding to the pressure PALT were found using the 1963 Patrick Atmosphere Tables (Reference 11).

The test section unit Reynolds number, derived from isentropic flow relations using nitrogen as an ideal gas, was calculated by using the expression

$$Re/ft = 4.11 \frac{P_o}{\mu_\infty} \sqrt{\frac{1}{T_o}} \left[\frac{M_\infty}{(1 + 0.2 M_\infty^2)^3} \right] \qquad (1)$$

where the viscosity μ_∞ for nitrogen was based on

$$\mu_\infty = 3.46 \times 10^{-7} \left(\frac{T_\infty}{492}\right)^{1.5} \left(\frac{690}{T_\infty + 198}\right) \text{ (lb-sec/ft}^2\text{)} \qquad (2)$$

with T_∞ in $^\circ$R.

Pressure

All of the pressure transducers employed during this program operate on a differential basis in that they sense the change between the local pressure applied to the model during the run and the pre-run ambient pressure. Accordingly, the receiver tank pre-run absolute pressure was added to the measured pressure change for all transducers exposed to the tunnel environment. For the SRB's, however, the initial ignition gas pressure of 16.5 psia was added to the transducer output to derive the absolute pressure. Absolute pressures were calculated according to Equation (3).

$$P = \frac{\text{CAL X DEFL.}}{\text{S X GAIN}} + P_{REF} \qquad \text{(psia)} \qquad (3)$$

where

CAL = oscillograph calibration (mV/in)

DEFL = measured deflection on oscillograph due to transducer output (inches)

S = transducer calibration sensitivity (mV/psi)

GAIN = system gain

P_{REF} = transducer pre-run ambient pressure (psi)

Heat Transfer

The thin-film gauge is a resistance thermometer which responds to the local surface temperature of the substrate. The classical theory of heat conduction in a homogeneous body is used to relate the surface temperature history to the rate of heat transfer. Due to the considerable effort required to convert temperature-time records into equivalent heating rate histories, an analog network, referred to as a "q-meter," has been developed to convert the temperature signal directly into a heat flux in real time for presentation on the oscillograph (Reference 5). All thin-film gauge, heat-transfer data for this study were obtained through the use of q-meters.

For the heat-transfer data recorded directly on the oscillographs, each channel was equipped with a q-meter. The heat-transfer gauges recorded on the FM-Multiplex tape recorder system were handled somewhat differently. The outputs of the thin-film gauges (which are proportional to the surface temperature of the gauge) were recorded on the FM tape. After each test run, the tape was played back through an analog q-meter and the signals proportional to heat-transfer rate were recorded on an oscillograph.

Signals from the q-meter analog circuit, proportional to the heat-transfer rate, were converted to heating rates by the following equations:

$$K' = \frac{K_b \times (R_T - R_L)}{R_b} \qquad (\text{ohms}/^{\circ}F) \qquad (4)$$

where

K' = gauge sensitivity corrected for abrasion and normal wear

K_b = calibration sensitivity (ohms/°F)

R_b = calibration resistance (ohms)

R_L = circuit line resistance (ohms)

R_T = measured pre-run gauge resistance, including line resistance (ohms)

$$q_p = \frac{[R_T + 10220]^2}{306600 \times K'} \qquad (5)$$

q_p is the analog q-meter proportionality factor to convert gauge output in volts to heating rate.

$$\dot{q} = \frac{q_p \times CAL \times DEFL}{GAIN} \quad (BTU/ft^2\text{-sec}) \qquad (6)$$

where

$\dot{q}$ = heating rate

CAL = oscillograph calibration (V/in)

DEFL = measured deflection on oscillograph due to gauge output; the deflection may be directly recorded through a q-meter or played back from the Vidar through a q-meter (inches)

GAIN = system gain

Recovery Temperature (Gas-Temperature Probes)

Gas-temperature probe data reduction at the test site was minimal. Information were presented for calculating gauge output in millivolts only for comparison during later off-site data reduction at REMTECH, Inc. To facilitate data reduction by REMTECH, the Vidar FM tapes containing

gas temperature probe data were first digitized at the Rockwell International, Los Angeles Division Dynamics Laboratory. Two time frames of data, 270 msec/frame, were digitized at a rate of 3000 samples per second. The time frames covered the period from 100 milliseconds before the SRB ignition signal, T_2, to 440 milliseconds after. Digitized data tapes received by REMTECH, Inc. were converted to engineering units, reformatted, and used as outlined below to calculate gas-recovery temperatures and heat-transfer coefficients.

Gas-recovery temperature data reduction procedures, in general, remain unchanged from those used for previous impulse base heating tests. These procedures are documented in References 7 and 8. For test IH75, however, there were improvements to the data reduction program used for calculating gas recovery temperature. These improvements are detailed in Reference 9 and outlined briefly in the remainder of this section.

Previous data reduction required simultaneous solution of the complete heat balance equation for two thin wires. The equation is:

$$q_s = q_j + q_c - q_k - q_{rw} + q_{wg} \qquad (7)$$

where

q_s = heat accumulated in wire

q_j = heat due to current flow

q_c = heat input to the wire from gas

q_k = heat conduction to wire supports

q_{rw} = heat loss by radiation from wire

q_{wg} = heat gained by radiation from gas

This equation was non-linear in two unknowns, T_r and h, and required a numerical iteration scheme via a computer code called SNEBE [4] to obtain solutions. Improvements were made in Reference [8] where a linearized semi-closed form solution to the wire heat balance equation provided initial estimates of the recovery temperature and heat-transfer coefficient for the non-linear numerical technique, thereby saving considerable data reduction time.

Further modifications to the linearized semi-closed form solution have produced a complete linear solution which agrees very well with results of the non-linear numerical technique. The results are much more data in much less data reduction time; specifically, gas-recovery temperature and heat-transfer coefficient can now be obtained as a function of test time, instead of a single average value, allowing more detailed analysis.

Experience with previous gas temperature probe data has shown that most heat transfer associated with the wires is due to convective heat input and conduction. Eliminating other types of heat, Equation 7 simplifies to:

$$q_c = q_k \tag{8}$$

Substituting:

$$h\pi D(T_r - T_w) = -A \frac{\partial^2 k\, T_w}{\partial X^2} \tag{9}$$

where

h = heat transfer coefficient

D = wire diameter

T_r = gas recovery temperature

T_w = wire temperature

A = wire cross section area

k = wire thermal conductivity

X = distance along wire

Assuming k does not vary with temperature and substituting for A,

$$h\pi D(T_r - T_w) = k \frac{\pi D^2}{4} \frac{d^2T_w}{dX^2} \tag{10}$$

Equation 10 can be transformed into a simple homogeneous differential equation (Reference 12) which has the solution:

$$T_w(X) = T_r - (T_r - T_s) \frac{\cosh\left(X\sqrt{4h/kD}\right)}{\cosh\left(\ell\sqrt{4h/kD}/2\right)} \tag{11}$$

where

T_s = wire support temperature

ℓ = wire length

To obtain the average wire temperature for a finite length wire, Equation 11 is integrated over the wire length.

$$\overline{T}_w = T_r - (T_r - T_s)\frac{\tanh\left(\ell\sqrt{h/kD}\right)}{\ell\sqrt{h/kD}} \tag{12}$$

Solving for T_r and inserting parameter $\gamma = h/kD$,

$$T_r = \frac{(\ell\gamma)\,\overline{T}_w - T_s \tanh(\ell\gamma)}{\gamma\ell - \tanh(\ell\gamma)} \tag{13}$$

Equation 13 is an explicit expression of finite length single-wire heating with two unknowns, T_r and h. Two distinct equations can be written for the two different gas-temperature probe wire lengths, denoted by subscripts 1 and 2, and solved simultaneously to obtain an equation of only one unknown, h.

$$\frac{\ell_2\gamma - \tanh(\ell_2\gamma)}{\ell_1\gamma - \tanh(\ell_1\gamma)} = \frac{\ell_2\gamma\,\bar{T}_{w2} - T_s \tanh(\ell_2\gamma)}{\ell_1\gamma\,\bar{T}_{w1} - T_s \tanh(\ell_1\gamma)} \qquad (14)$$

For practical use of the preceding equations, γ must first be obtained from Equation 14. From γ, h is calculated and used in Equation 13 to obtain T_r. Parameters T_s, $\bar{T}_w$, ℓ used in Equations 13 and 14 are obtained as follows: T_s, the wire support temperature, is measured by an iron-constantan thermocouple in the tip of one of the gas-temperature probe short wire support needles. $\bar{T}_w$, the average wire temperature, is calculated by Equation 15.

$$R_w = R_o\left[1 + \alpha(\bar{T}_w - T_o) + \beta(\bar{T}_w - T_o)^2\right] \qquad (15)$$

where

R_w = measured wire resistance

R_o = wire resistance at temperature T_o

T_o = 20°C = 293°K

α, β = R-T curve fit coefficients

Wire length, ℓ, is calculated by Equation 16.

$$\sigma_o = R_o \frac{A}{\ell} = 1.853\times10^{-5} \text{ ohm-cm for Platinum -10\% Rhodium wire} \qquad (16)$$

where

σ_o = manufacturer's stated value of resistivity at T_o

With all parameters known, γ is still not directly obtained from Equation 14 due to the hyperbolic functions. An efficient method for obtaining accurate values of γ is known as the Fibonacci series search routine. It is an interval elimination search method which sets upper and lower bounds to an **initial heat transfer coefficient estimate** ($h_{initial} = 1 \times 10^{-2}$ cal/cm^2 - sec - ^oK) and then proceeds to reduce the interval in which the optimum value occurs until a final value is reached. If the final value is equivalent to the upper or lower bounds, it becomes the new initial estimate, and the procedure is repeated.

The final solutions to Equations 13 and 14, i.e., h and T_r, must satisfy the following boundary conditions; if not, the solutions are considered non-convergent.

$$T_r > T_{w1} > T_{w2} > T_s$$

$$T_r < 4000^oK$$

$$1 \times 10^{-5} < h < 1.0 \quad cal/cm^2 - sec - {}^oK$$

As gas temperature increases, the non-linear terms of the wire heat balance equation, ignored for the preceding simplified solution, cause the linear gas recovery temperature to diverge from the true non-linear solution. Correction Equations 17 and 18 are applied to the linear gas-recovery temperature and heat-transfer coefficient solutions to account for non-linearity.

$$T_{r_c} = 4.6805 \times 10^{-7}\ T_r^3 - 9.4521 \times 10^{-4}\ T_r^2 + 1.6682\ T_r - 152.02 \qquad (17)$$

$$h_c = 2.8598 \times 10^{-10}\ h^4 + 6.1589 \times 10^{-7}\ h^3 - 5.0279\ h^2 + 0.13456\ h + h \qquad (18)$$

To use the simplified linear equations, the following assumptions must be made:

1. The gas-temperature probe wires are at a steady state heating condition.

2. The convective heat-transfer coefficient and gas-recovery temperature are identical for both wires.

3. The wire supports do not significantly disturb the flow in wich the measurement is made.

RESULTS AND DISCUSSION

The basic Test IH75 reduced data consisted of steady-state heating rates, pressures, and gas recovery temperatures. The data were measured at a time corresponding to steady model combustion chamber pressures and tunnel flow. Pressure and heating rate raw data were hand measured at the steady-state time from the oscillograph traces and entered into a computer program for final reduction. Accuracy of these data can most likely be directly related to the hand measurements. Gas-temperature probe data were reduced entirely by computer. Improvements in the computer programs, mentioned briefly in the preceding section and outlined thoroughly in Reference 9, allowed wire resistance, wire temperature, recovery temperature, and convective heating coefficient to be plotted as a function of model firing time. These time plots allowed visual evaluation of the overall gas-temperature probe response and insured that steady-state conditions existed.

Vidar and oscillograph data quality were hampered by low signal-to-noise ratio. Data on oscillographs and on Channels 1-41 of the Vidar system seemed to have the best quality with the noise not inhibiting the steady-state data level; however, data recorded on Channels 1-41 of the Vidar system employing Calspan amplifiers were in error as discussed later. Data on Channels 42-66 of the Vidar system employing Incor amplifiers were of the lowest quality; in general, the noise and data levels were of the same order.

After completion of the test program, it was noted that some of the

data recorded on the Vidar FM tape system exhibited a droop indicative of a limited DC response. This was traced to the use of amplifiers having a 100K ohm input impedance with heat transfer conditioning circuits that had a 1 μfd coupling capacitor in the output. This resulted in a system time constant of only 0.1 sec. for Channels 1-41 on the Vidar FM-Multiplex tape recorder system. The effect of this time constant on the output of the q-meters was analyzed, and correction factors were determined and applied to the data. The analysis and correction factors derived by Calspan are presented in Appendix C.

A discrepancy in the magnitude of the gas-temperature probe data recorded during second-stage configuration runs 39 - 43 tends to discredit these data. Specifically, the recorded wire resistances produce wire temperatures and recovery temperatures twice as large as expected and twice as large as any previous data. Oscillograph playback data from the Vidar and digitized data from the Vidar FM tape compare in magnitude, which points to the Vidar input as the problem. However, investigation did not prove that the Vidar input channels were incorrectly spanned or that the gains were in error. Thus, the gas-temperature probe data were evaluated two ways: (1) using the actual recorded data referred to as "literal data" in Appendix B and (2) using one-half of the actual recorded data referred to as "literal data ÷ 2" or "input data ÷ 2" in Appendix B. Analysis of the results of both types of data, detailed in Reference 9, did not conclude that either set of data was correct.

Tabulated source data are not supplied with this document but are available through the Rockwell International, STS Aerosciences Department as shown in Appendix A.

Oscillograph traces of the raw data, including Vidar playback, are also available as shown in Appendix A.

Gas-recovery temperatures and convective heat transfer coefficients, derived from the gas-temperature probe resistance and thermocouple time history data as described in the preceding section and Reference 9, are presented in Appendix B. The data were extracted from Reference 9. Both literal data and literal data ÷ 2 are presented. Steady-state gas-recovery temperatures and convective heat-transfer coefficients are presented in Tables B1 - B4. Figures B1 - B4 show an example of time histories of the gas-temperature probe data. Gas-recovery temperatures, plotted as a function of simulated altitude, are presented in Figures B5 - B11. Convective heat-transfer coefficients, plotted as a function of simulated altitude, are presented in Figures B12 - B15.

REFERENCES

1. Quan, M., "Information for Base Pressure and Heat Transfer Tests of the 0.0225-Scale Space Shuttle Plume Simulation Model 19-OTS in the NASA/Calspan Ludwieg Tube Wind Tunnel (IH75A)." SD76-SH-0143, Rockwell International, Space Division, dated April 11, 1977.

2. Bogdan, L., "Instrumentation Techniques for Short-Duration Test Facilities," Calspan Report No. WTH-030, Buffalo, New York, dated March, 1967.

3. Bogdan, L., and Garberoglio, J. E., "Transient Heat-Transfer Measurements with Thin-Film Resistance Thermometers -- Fabrication and Application Technology," Technical Report AFAPL-TR-67-72, Calspan Corporation, Buffalo, New York, dated June; 1967.

4. Vidal, R. J., "Transient Surface Temperature Measurements," Calspan Report No. 114, dated March, 1962.

5. Skinner, G. T., "Analog Network to Convert Surface Temperature to Heat Flux," Calspan Report No. 100, dated February, 1960.

6. Martin, J. F., Duryea, G. R., Stevenson, L. M., "Instrumentation for Force and Pressure Measurements in a Hypersonic Shock Tunnel," Calspan Report No. 113, dated January, 1962.

7. Fuller, C. E., III, and Engel, Dr. C. D., "Gas Temperature Probe Development and Short Duration Space Shuttle Testing Support," REMTECH, Incorporated RTR015-1, dated December, 1974.

8. Fuller, C. E., Morrison, M. W., Powell, R. T., and Levie, J. K., III, "Utilization of a Gas Recovery Temperature Probe on Space Shuttle Short Duration Base Heating Model Tests OH78 and IH39," REMTECH, Incorporated RTR019-2, dated July, 1977.

9. Fuller, C. E., Levie, J. K., III, Powell, R. T., "Utilization of a Gas Recovery Temperature Probe on Space Shuttle Short Duration Base Heating Model Tests IH75 and IH83," REMTECH, Incorporated RTR019-3, dated July, 1978.

10. Sheeran, W. J., Hendershot, K. C., and Wilson, H. B., Jr., "Applications of a Tube Wind Tunnel in Supersonic Testing," AIAA Paper No. 69-335, presented at 4th Aerodynamic Testing Conference, Cincinnati, Ohio, 1969.

11. Smith, O. E., and Weidner, D. K., "A Reference Atmosphere for Patrick AFB, Florida, Annual (1963 Revision)," NASA TM X-53139, NASA-Marshall Space Flight Center, dated September 23, 1964.

REFERENCES (Concluded)

12. Sandborn, V. A., "Resistance Temperature Transducers," Metrology Press, Fort Collins, Colorado, 1972.

TABLE I. TEST CONDITIONS

MACH NO.	ALTITUDE	T_o	P_c	P_∞*	P_∞	CHARGE TUBE PRESSURE	RECEIVER TANK PRESSURE
	Kft.	°F	PSIA	PSIA	μHg	PSIA	μHg
3.5	100	300	6.265	0.0821	4249	7.78	< 400
↓	110	↓	4.046	0.0531	2744	4.95	< 200
	130		1.756	0.0231	1192	2.10	< 100
↓	140	↓	1.180	0.0155	800	1.40	< 75
4.5	100	600	23.770	0.0821	4249	26.62	< 400
	120	↓	10.048	0.0347	1795	11.26	< 170
	140	↓	4.477	0.0155	800	5.02	< 75
	100	70	23.770	0.0821	4249	26.62	< 400
	110		15.352	0.0531	2744	17.19	< 250
	120		10.048	0.0347	1795	11.26	< 170
	130		6.664	0.0230	1192	7.46	< 100
	140		4.477	0.0155	800	5.02	< 75
	150		3.042	0.0105	544	3.41	< 50
	160		2.082	0.00719	372	2.33	< 35
↓	170	↓	1.426	0.00493	255	1.60	< 25

* $P_\infty = 1/2\ P_{ALTITUDE}$

TABLE II. DATA SET/RUN NUMBER COLLATION SUMMARY

TEST IH75

SPACE DIVISION
NORTH AMERICAN ROCKWELL CORPORATION

Prepared By: | Page No. of
Checked By: | Report No.
Date: | Model No.

1	2	3	4	5	6	7	8		9		10		11		12		13	14	15
							NOZZLE GIM BAL ANGLES										Chamber	Pressure	
Dataset Identification	Run	Config.	M_∞	T_0 (°F)	Altitude (K ft)	α (Deg.)	#1 SSME		#2 SSME		#3 SSME		LSRB		RSRB		SSME (PSIA)	SRB (PSIA)	Instr. Satisfy.
							P	Y	P	Y	P	Y	P	Y	P	Y			
001	4	OTS	3.5	300	100	+5	0	0	0	0	0	0	0	0	0	0	1500	290	1
002	5	↓	↓	↓	110	↓	↓	↓	↓	↓	↓	↓	↓	↓	↓	↓	↓	↓	↓
003	6				130													145	
004	7		↓	↓	140													↓	
005	10		4.5	600	↓													290	
006	11		↓	↓	100													↓	
007	13			70	↓														
008	14			↓	110														
009	15				120														
010	17				130													↓	
011	19				↓													100	
012	20				140													↓	
013	21				150														
014	23				160													↓	
015	24				130													200	
016	25				140	↓												↓	
017	26				120	+10												290	
018	27	↓	↓	↓	↓	-10	↓	↓	↓	↓	↓	↓	↓	↓	↓	↓	↓	↓	↓
019	28				140	+5	-5	0	-5	0	-5	0	-1	0	-1	0		100	
020	29	OT			↓		↓	↓	↓	↓	↓	↓	-	-	-	-		-	3
021	30				160														
022	31				↓		0	0	0	0	0	0							
023	32				170														
024	33				150														
025	34	↓	↓	↓	140	↓	↓	↓	↓	↓	↓	↓	↓	↓	↓	↓	↓	↓	↓

TABLE II. DATA SET/RUN NUMBER COLLATION SUMMARY (Concluded)

TEST IH75

SPACE DIVISION
NORTH AMERICAN ROCKWELL CORPORATION

Prepared By:
Checked By:
Dates:

Page No. of
Report No.
Model No.

1	2	3	4	5	6	7	8		9		10		11		12		13	14	15
							NOZZLE				GIM		BAL ANGLES						
Dataset Identifier	Run	Config.	M_∞	T_0 (°F)	Altitude (K ft)	α (Deg.)	#1 SSME		#2 SSME		#3 SSME		LSRB		RSRB		Chamber SSME (P$_{c}$ in A)	Transducers SRB (P$_{c}$ in A)	Instr. Set-114-
							P	Y	P	Y	P	Y	P	Y	P	Y			
026	35	OT	4.5	70	130	+5	0	0	0	0	0	0	–	–	–	–	1500	–	3
027	36	↓	↓	↓	140	+10	↓	↓	↓	↓	↓	↓	↓	↓	↓	↓	↓	↓	↓
028	37	↓	↓	↓	↓	-10	↓	↓	↓	↓	↓	↓	↓	↓	↓	↓	↓	↓	4
029	39	OT/GTP	↓	↓	130	+5	↓	↓	↓	↓	↓	↓	↓	↓	↓	↓	↓	↓	↓
030	40	↓	↓	↓	140	↓	↓	↓	↓	↓	↓	↓	↓	↓	↓	↓	↓	↓	↓
031	41	↓	↓	↓	150	↓	↓	↓	↓	↓	↓	↓	↓	↓	↓	↓	↓	↓	↓
032	42	↓	↓	↓	160	↓	↓	↓	↓	↓	↓	↓	↓	↓	↓	↓	↓	↓	↓
033	43	↓	↓	↓	170	↓	↓	↓	↓	↓	↓	↓	↓	↓	↓	↓	↓	↓	↓
034	44	↓	↓	↓	140	↓	-5	0	-5	0	-5	0	↓	↓	↓	↓	↓	↓	↓
035	45	OTS/GTP	↓	↓	↓	↓	↓	↓	↓	↓	↓	↓	-1	0	-1	0	↓	100	2
036	46	↓	↓	↓	100	↓	0	0	0	0	0	0	0	0	0	0	↓	290	↓
037	47	↓	↓	↓	120	↓	↓	↓	↓	↓	↓	↓	↓	↓	↓	↓	↓	↓	↓
038	49	↓	↓	↓	140	↓	↓	↓	↓	↓	↓	↓	↓	↓	↓	↓	↓	100	↓
039	50	↓	↓	↓	130	↓	↓	↓	↓	↓	↓	↓	↓	↓	↓	↓	↓	↓	↓
040	51	↓	↓	600	120	↓	↓	↓	↓	↓	↓	↓	↓	↓	↓	↓	↓	290	↓
041	52	↓	↓	↓	100	↓	↓	↓	↓	↓	↓	↓	↓	↓	↓	↓	↓	↓	↓
042	53	OTS	↓	↓	120	↓	↓	↓	↓	↓	↓	↓	↓	↓	↓	↓	↓	↓	1

TABLE III. MODEL DIMENSIONAL DATA

MODEL COMPONENT: BODY - B64

GENERAL DESCRIPTION: The body is to the Baseline Definition Space Shuttle Vehicle Configuration 5, MCR 200, Rev. 7 dated 10-17-74.

MODEL SCALE: .0225

DRAWING NUMBER: VC70-000002, #MDV-70 Baseline IML

DIMENSIONS:	FULL SCALE	MODEL SCALE
Length: OML X_O = 235-1528.3 in.	1293.3	29.099
Ref. Length: OML X_O = 238-1528.3 in.	1290.3	29.032
Length (IML X_O = 239.5) in.	1288.8	28.998
OML Max. Width, in. X_O = 1516.801	262.710	5.911
IML Max. Width, in. X_O = 1516.301	260.718	5.866
OML Max. Depth, in. X_O = 1463.316	248.575	5.593
IML Max.Depth, in. X_O = 1463.316	246.575	5.548
OML Fineness Ratio	5.203	5.203
IML Fineness Ratio	5.227	5.227
Area - Ft^2		
Max. Cross-Sectional @ X_O = 1463.316	340.82	0.173

TABLE III. MODEL DIMENSIONAL DATA (Continued)

MODEL COMPONENT: CANOPY - C_{16}

GENERAL DESCRIPTION: Orbiter 102 Canopy per MCR 1750 R1 Baseline

MODEL SCALE: 0.0225

DRAWING NUMBER: VC70-000002A, MD-V70

DIMENSIONS:	FULL SCALE	MODEL SCALE
Length, in., X_o = 433.0793 to X_o = 670	236.9207	5.331
Max. Width, in., @ X_o = 594	194.4394	4.375
Max. Depth, in., @ X_o = 492	58.8007	1.323
Area - Ft^2		
Max. Cross-Sectional @ X_o = 520	45.6558	0.0231

TABLE III. MODEL DIMENSIONAL DATA (Continued)

MODEL COMPONENT: ELEVON - E_{63}

GENERAL DESCRIPTION: Elevon for Configuration 5, hingeline at X_O = 1387, Elevon split line, Y_O = 312.5 6.0" gaps beveled edges, and centerbodies "CML"used on W_{129} Ref. MCR 200, Rev. 7, dated 10-17-74.

MODEL SCALE: 0.0225

DRAWING NUMBER: VC70-000002A

DIMENSIONS:	FULL SCALE	MODEL SCALE
Area used for C_{H_e} computation	210.0	0.106
Area, Ft^2	206.57	0.105
Span (equivalent), In.	346.44	7.795
Inb'd equivalent chord, In.	116.50	2.621
Outb'd equivalent chord, In.	55.219	1.242
Ratio movable surface chord/ total surface chord		
At Inb'd equiv. chord	0.2137	0.2137
At Outb'd equiv. chord	0.3999	0.3999
Sweep Back Angles, degrees		
Leading Edge	0.00	0.00
Trailing Edge	- 10.056	- 10.056
Hingeline	0.00	0.00
Area Moment (Area X MAC) - Ft^3	1540.74	0.0175
Mean Aerodynamic Chord, In.	89.50	2.014

TABLE III. MODEL DIMENSIONAL DATA (Continued)

MODEL COMPONENT: BODY FLAP (OUTER MOLD LINES): F_{14}

GENERAL DESCRIPTION: Orbiter body flap vehicle 5 Configuration, MCR 200, Rev. 7. "OML" to be used with B_{64} Hingeline X_O 1532.0 Y_O = -1280.

MODEL SCALE: 0.0225

DRAWING NUMBER: VC70-000002, MDV-70

DIMENSIONS:	FULL SCALE	MODEL SCALE
Area, (Total), Ft^2	134.125	0.068
Span (equivalent), In.	238.00	5.355
Inb'd equivalent chord, In.	81.00	1.823
Outb'd equivalent chord, In.	81.00	1.823
Ratio movable surface chord/ total surface chord		
At Inb'd equiv. chord		
At Outb'd equiv. chord		
Sweep Back Angles, degrees		
Leading Edge	0.0	0.0
Trailing Edge	0.0	0.0
Hingeline	0.0	0.0
Area Moment (Product of $\bar{c}$ & area), Ft^3	905.344	0.0103
Mean Aerodynamic Chord, In.	81.0	1.823

TABLE III. MODEL DIMENSIONAL DATA (Continued)

MODEL COMPONENT: OMS PODS (OML) - M_{18}

GENERAL DESCRIPTION: Vehicle 5 configuration MCR 200, Rev. 7, Orbiter OMS pod - short pod.

MODEL SCALE: 0.0225

DRAWING NUMBER: VC70-000002, VL70-008410, MDV-70

DIMENSIONS:	**FULL SCALE**	**MODEL SCALE**
Length, in. (X_O1311 to 1511)	200.00	4.500
Max. Width, in. (X_P304, X_O1511)	135.75	3.054
Max. Depth, in. (X_P304, X_O1511)	74.50	1.676
Fineness Ratio	1.937	1.937
Area - Ft^2		
Max.Cross-Sectional @ X_P 304	58.169	0.029

TABLE III. MODEL DIMENSIONAL DATA (Continued)

MODEL COMPONENT: CMS NOZZLES - N_2O_2

GENERAL DESCRIPTION: The two orbiter maneuvering system nozzles are laval-bell shaped and are located at the aft end of the CMS pod. CMS nozzles in stowed position are outboard 9° and down 7° from null position.

MODEL SCALE: 0.0225

DRAWING NUMBER: VD70-000002, SS-A01240

DIMENSIONS:	**FULL SCALE**	**MODEL SCALE**
MACH NO.		
Length, in.		
Gimbal Point to Exit Plane	56.00	1.260
Throat to Exit Plane		
Diameter, in.		
Exit	50.00	1.125
Throat	27.778	0.625
Area, ft.^{2}		
Exit	13.634	0.0069
Throat	4.205	0.0021
Gimbal Point (Station), in.		
Left Nozzle		
X_O	1518.00	34.155
Y_O	- 88.00	- 1.980
Z_O	492.00	11.070
Right Nozzle		
X_O	1518.00	34.155
Y_O	+ 88.0	+ 1.980
Z_O	492.0	11.070
Null Position, Deg.		
Left Nozzle		
Pitch	15°49' Up	15°49' Up
Yaw	6°30' Outb'd	6°30' Outb'd
Right Nozzle		
Pitch	15°49' Up	15°49' Up
Yaw	6°30' Outb'd	6°30' Outb'd

TABLE III. MODEL DIMENSIONAL DATA (Continued)

MODEL COMPONENT: MPS NOZZLES - N94

GENERAL DESCRIPTION: The main propulsion nozzles are laval-bell shaped and are located on the aft planes of the orbiter. The dimensions are external and not to be scaled for plume tests.

MODEL SCALE: 0.0225

DRAWING NUMBER: VC70-000002, VL70-008144, RS09189, SS-A01216

DIMENSIONS:	**FULL SCALE**	**MODEL SCALE**
MACH NO.		
Length, in.		
Gimbal Point to Exit Plane	156.69	3.526
Diameter, in.		
Exit	93.75	2.109
Area, $ft.^2$		
Exit	1445.00	0.732
Gimbal Point (Station), in.		
Upper Nozzle		
X_O	1445.00	32.513
Y_O	0.00	0.0
Z_O	443.00	9.968
Lower Nozzle		
X_O	1468.170	33.034
Y_O	± 53.00	± 1.193
Z_O	34.264	0.771
Null Position, Deg.		
Upper Nozzle		
Pitch	16°0 Up	16°0 Up
Yaw	0.0	0.0
Lower Nozzle		
Pitch	10.0 Up	10.0 Up
Yaw	3.5 Outb'd	3.5 Outb'd

TABLE III. MODEL DIMENSIONAL DATA (Continued)

MODEL COMPONENT: VERTICAL - V_{23}

GENERAL DESCRIPTION: The vertical tail is double wedge shaped and mounted dorsally on the aft fuselage. These data correspond to Vehicle 5 configuration, MCR 200, Rev. 7.

MODEL SCALE: 0.0225

DRAWING NUMBER: VC70-000002, master dimensions.

DIMENSIONS:	FULL SCALE	MODEL SCALE
TOTAL DATA		
Area (Theo.), ft^2		
Planform	413.253	0.209
Span (Theo.), in.	315.72	7.104
Aspect Ratio	1.675	1.675
Rate of Taper	0.507	0.507
Taper Ratio	0.404	0.404
Sweep Back Angles, degrees		
Leading Edge	45.00	45.00
Trailing Edge	26.25	26.25
0.25 Element Line	41.13	41.13
Chords:		
Root (Theo.) WP	268.50	6.041
Tip (Theo.) WP	108.47	2.441
MAC	199.81	4.496
Fus. Sta. of .25 MAC	1463.50	32.929
W.P. of .25 MAC	635.52	14.299
B.L. of .25 MAC	0.0	0.0
Airfoil Section		
Leading Wedge Angle, deg.	10.0	10.0
Trailing Wedge Angle, deg.	14.92	14.92
Leading Edge Radius	2.00	0.045
Void Area	13.17	0.007
Blanketed Area	0.00	0.00

TABLE III. MODEL DIMENSIONAL DATA (Continued)

MODEL COMPONENT: WING - W129

GENERAL DESCRIPTION: The wing is the primary lifting device and is mounted horizontally and is symmetric about the plane $Y_0 = 0$. A cuff fairs the fuselage to the wing's leading edge @ T_0 940 to 1084.

MODEL SCALE: 0.0225 DRAWING NO.:

DIMENSIONS:	FULL SCALE	MODEL SCALE
TOTAL DATA		
Area (Theo.), ft^2		
Planform	2690.00	1.362
Span (Theo.), in.	936.68	21.075
Aspect Ratio	2.265	2.265
Rate of Taper	1.177	1.177
Taper Ratio	0.200	0.200
Dihedral Angle, degrees	3.500	3.500
Incidence Angle, degrees	0.500	0.500
Aerodynamic Twist, degrees		
Sweep Back Angles, degrees		
Leading Edge	45	45
Trailing Edge	10.056	10.056
0.25 Element Line	35.209	35.209
Chords:		
Root (Theo.) B.P.0.0.	689.243	15.500
Tip, (Theo.) B.P.	137.849	3.102
MAC	474.812	10.683
Fus. Sta. of .25 MAC	1136.834	25.579
W.P. of .25 MAC	290.857	6.544
B.L. of .25 MAC	182.132	4.098
EXPOSED DATA		
Area (Theo.), ft^2	1751.50	0.887
Span, (Theo.), in. BP108	720.68	16.215
Aspect Ratio	2.060	2.060
Taper Ratio	0.245	0.245
Chords		
Root BP108	562.090	12.64
Tip 1.00 b/2	137.849	3.102
MAC	392.826	8.839
Fus. Sta. of .25 MAC	1186.50	26.696
W.P. of .25 MAC	293.683	6.608
B.L. of .25 MAC	251.769	5.665
Airfoil Section (Rockwell Mod NASA) XXXX-64		
Root b/2 =	0.1136	0.1136
Tip b/2 =	0.120	0.120
Data for (1) of (2) Sides		
Leading Edge Cuff		
Planform Area, ft^2	145.4	0.074
Leading Edge Intersects Fus M.L. @ Sta	500.0	11.25
Leading Edge Intersects Wing @ Sta	1084.0	24.39

TABLE III. MODEL DIMENSIONAL DATA (Continued)

MODEL COMPONENT: BOOSTER SOLID ROCKET MOTOR - S_{22}

GENERAL DESCRIPTION: The BSRM is an external propulsion system which is jettisoned and recoverable after burnout. The BSRM's can be refurbished and reused after recovery.

MODEL SCALE: 0.0225

DRAWING NUMBER: VC77-000002C VC70-000002A; VC72-000002C

DIMENSIONS:	FULL SCALE	MODEL SCALE
Length, in.	1789.60	40.266
Max. Width Tank Dia., in.	146.00	3.285
Max. Depth, Aft Shroud Dia., in.	208.20	4.685
Fineness Ratio	8.596	8.596
Area, $Ft.^2$		
Max. Cross-Sectional	236.423	0.120
WP of BSRM centerline (Z_T)	400.0	9.000
FS of BSRM nose (X_T)	743.0	16.718
BP of BSRM centerline (Y_T)	250.5	5.636

TABLE III. MODEL DIMENSIONAL DATA (Continued)

MODEL COMPONENT: SOLID ROCKET BOOSTER NOZZLES - N_{106}

GENERAL DESCRIPTION: SRB nozzle to new lines to use with S_{22}

MODEL SCALE: 0.0225

DRAWING NUMBER: VC77-000002D

DIMENSIONS:	**FULL SCALE**	**MODEL SCALE**
Diameter, D_{ex} - In. (I.D.)	145.64	3.277
Diameter, D_{ex} - In. (C.D.)	147.64	3.322
Diameter, DT - In.	----	----
Diameter, D_{in} - In.	----	----
Area, $Ft.^2$	115.688	0.059
Gimbal Point (Station) - In.		
Left Nozzle		
X_B - cold	1863.458	41.928
X_B - hot	1875.358	42.196
Y_O -	- 250.50	- 5.636
Z_T	400.0	9.000
Right Nozzle		
X_B - cold	1863.458	41.928
X_B - hot	1875.358	42.196
Y_O -	250.50	5.636
Z_T	400.0	9.000
Null Position, Deg.		
Left Nozzle		
Pitch	0	0
Yaw	0	0
Right Nozzle		
Pitch	0	0
Yaw	0	0

TABLE III. MODEL DIMENSIONAL DATA (Concluded)

MODEL COMPONENT: EXTERNAL TANK - T_{33}

GENERAL DESCRIPTION: External tank with spike nose. Dimensions are calculated to the outer mold line (OML).

MODEL SCALE: 0.0225

DRAWING NUMBER: VC78-000002B Spike nose Dwg. No.: 82600203049

DIMENSIONS:	FULL SCALE	MODEL SCALE
Length, In.	1852.486	41.681
Max. Dia. (OML), In.	333.00	7.493
Fineness Ratio	5.563	5.563
Area		
Max. Cross-Sectional	604.807	0.306

TABLE IV. SOLID PROPELLANT SURFACE AREA

SRB NOMINAL CHAMBER PRESSURE	PROPELLANT SURFACE AREA (EACH SRB)
PSIA	IN^2
290	130
200	100
145	85
100	72

TABLE V. INSTRUMENTATION NUMBERING SYSTEM

Component Or Instrumentation	Number Series	Actual Numbers	
		Comp. or Instr.	Numbers
Orbiter	1 - 200	Total Thin-Film Gauges	1 - 119
		Radiation Gauges	120 - 134
		PCB Transducer Locations	135 - 161
External Tank	201 - 300	Total Thin-Film Gauges	201 - 229
		Radiation Gauges	230 - 233
		PCB Transducer Locations	234 - 236
SRB's	301 - 400	Total Thin-Film Gauges	301 - 320, 326 - 330
		Radiation Gauges	321 - 322, 331
		PCB Transducers Locations	323 - 325
*Reference Static Pressures	501 - 600	Orbiter	501 - 513
		External Tank	514 - 516
		SRB (Left Hand)	517
Thermocouples	601 - 699	See Table VII for listing	
Model Operating Pressures	700 - 750	SSME Pc	700
		Left SRB Pc	701
		Right SRB Pc	702
		O_2 Venturi	703
		H_2 Venturi	704
		O_2 Injector	705
		H_2 Injector	706
Gas Temperature Probes	751 - 799	Orbiter	752 - 754
		External Tank	756 - 758
		SRB (Left Hand)	759
Hatband Nozzle	166 - 180	Total Thin-Film Gauges (Flat and contoured)	166 - 180 (HB1-HB15)

* Not applicable to Test IH75

TABLE VI. INSTRUMENTATION CONFIGURATIONS

COMPONENT	PARAMETER NUMBER	PARAMETER TYPE		CONFIGURATION OR SET-UP			
				1	2	3	4
			DESCRIPTION	OTS*	OTS W/GTP	OT**	OT W/GTP
			DATASET IDENTIFIER	1-19, 42	35-41	20-28	29-34
Orbiter Side	9	Standard Gauge				X	
	10	↓				X	
Orbiter Top	14	Standard Gauge				X	
	15	↓				X	
Wing Upper Surface	23	Standard Gauge			X		
	24	↓			X	X	
	25				X	X	
	27				X		

* OTS is first stage shuttle configuration (orbiter, external tank, SRB)
** OT is second stage shuttle configuration (orbiter, external tank)

TABLE VI. INSTRUMENTATION CONFIGURATIONS (Continued)

COMPONENT	PARAMETER NUMBER	PARAMETER TYPE	DESCRIPTION / DATASET IDENTIFIER	CONFIGURATION OR SET-UP 1 OTS* 1-19, 42	2 OTS W/GTP 35-41	3 OT** 20-28	4 OT W/GTP 29-34
Vertical Tail	30	Standard Gauge				X	
	31	↓			X		
	32				X	X	
	33					X	
	34				X	X	
Body Flap	35	Standard Gauge		X		X	
	36	↓				X	X
	37			X		X	
	38					X	X
	39					X	X

* OTS is first stage shuttle configuration (orbiter, external tank, SRB)
** OT is second stage shuttle configuration (orbiter, external tank)

TABLE VI. INSTRUMENTATION CONFIGURATIONS (Continued)

COMPONENT	PARAMETER NUMBER	PARAMETER TYPE	DESCRIPTION / DATASET IDENTIFIER	CONFIGURATION OR SET-UP 1 OTS* 1-19, 42	2 OTS W/GTP 35-41	3 OT** 20-28	4 OT W/GTP 29-34
Body Flap (Continued)	43	Standard Gauge				X	X
	45	↓		X	X	X	X
	46					X	
	125	Radiative Gauge		X		X	X
	139	Pressure			X	X	X
Left OMS Pod	55	Standard Gauge				X	
	56	↓				X	
Left OMS/RCS - Inside Surfaces	57	Standard Gauge		X		X	X
	58			X		X	X
	59	↓		X	X	X	X

* OTS is first stage shuttle configuration (orbiter, external tank, SRB)
** OT is second stage shuttle configuration (orbiter, external tank)

TABLE VI. INSTRUMENTATION CONFIGURATIONS (Continued)

COMPONENT	PARAMETER NUMBER	PARAMETER TYPE	DESCRIPTION / DATASET IDENTIFIER	CONFIGURATION OR SET-UP 1	2	3	4
			DESCRIPTION	OTS*	OTS W/GTP	OT**	OT W/GTP
			DATASET IDENTIFIER	1-19, 42	35-41	20-28	29-34
Left OMS/RCS - Inside Surfaces (Continued)	60	Standard Gauge		X		X	
	61	↓		X		X	
Left OMS/RCS - Aft Surfaces	62	Standard Gauge				X	
	63					X	X
	64			X		X	X
	65			X	X	X	X
	66			X		X	X
	67	↓		X		X	X
Orbiter Base Heat Shield	68	Standard Gauge		X		X	X
	69	↓		X		X	

* OTS is first stage shuttle configuration (orbiter, external tank, SRB)
** OT is second stage shuttle configuration (orbiter, external tank)

TABLE VI. INSTRUMENTATION CONFIGURATIONS (Continued)

COMPONENT	PARAMETER NUMBER	PARAMETER TYPE		CONFIGURATION OR SET-UP			
				1	2	3	4
			DESCRIPTION	OTS*	OTS W/GTP	OT**	OT W/GTP
			DATASET IDENTIFIER	1-19, 42	35-41	20-28	29-34
Orbiter Base Heat Shield (Continued)	70	Standard Gauge		X	X	X	X
	71			X	X	X	X
	72			X	X	X	X
	73			X	X	X	X
	74					X	
	75					X	
	76			X		X	
	77					X	X
	78			X		X	X
	79					X	X
	80					X	

* OTS is first stage shuttle configuration (orbiter, external tank, SRB)
** OT is second stage shuttle configuration (orbiter, external tank)

TABLE VI. INSTRUMENTATION CONFIGURATIONS (Continued)

COMPONENT	PARAMETER NUMBER	PARAMETER TYPE		CONFIGURATION OR SET-UP			
				1	2	3	4
			DESCRIPTION	OTS*	OTS W/GTP	OT**	OT W/GTP
			DATASET IDENTIFIER	1-19, 42	35-41	20-28	29-34
Orbiter Base Heat Shield (Continued)	81	Standard Gauge		X		X	X
	82			X	X	X	X
	83			X	X	X	X
	84			X	X	X	X
	85			X		X	X
	86			X		X	
	87			X		X	X
	88			X		X	X
	89			X	X	X	X
	90			X		X	
	91			X	X	X	X

* OTS is first stage shuttle configuration (orbiter, external tank, SRB)
** OT is second stage shuttle configuration (orbiter, external tank)

TABLE VI. INSTRUMENTATION CONFIGURATIONS (Continued)

COMPONENT	PARAMETER NUMBER	PARAMETER TYPE	DESCRIPTION / DATASET IDENTIFIER	CONFIGURATION OR SET-UP 1 OTS* 1-19, 42	2 OTS W/GTP 35-41	3 OT** 20-28	4 OT W/GTP 29-34
Orbiter Base Heat Shield (Continued)	92	Standard Gauge		X		X	X
	93			X		X	X
	94					X	
	95					X	
	96					X	
	97			X	X	X	X
	98			X		X	X
	99			X	X	X	
	100					X	
	130	Radiative Gauge		X			
	131			X			

* OTS is first stage shuttle configuration (orbiter, external tank, SRB)
** OT is second stage shuttle configuration (orbiter, external tank)

TABLE VI. INSTRUMENTATION CONFIGURATIONS (Continued)

COMPONENT	PARAMETER NUMBER	PARAMETER TYPE	DESCRIPTION / DATASET IDENTIFIER	CONFIGURATION OR SET-UP 1 OTS* 1-19, 42	2 OTS W/GTP 35-41	3 OT** 20-28	4 OT W/GTP 29-34
Orbiter Base Heat Shield (Continued)	133	Radiative Gauge		X			
	134	↓		X			
	145	Pressure		X	X	X	X
	146	↓		X	X	X	X
	148			X	X	X	X
	149					X	X
	150			X	X	X	X
	155				X	X	X
	158	↓				X	X
	162	Standard Gauge					X
	163	↓		X		X	X

* OTS is first stage shuttle configuration (orbiter, external tank, SRB)
** OT is second stage shuttle configuration (orbiter, external tank)

TABLE VI. INSTRUMENTATION CONFIGURATIONS (Continued)

COMPONENT	PARAMETER NUMBER	PARAMETER TYPE	DESCRIPTION	CONFIGURATION OR SET-UP 1	2	3	4
				OTS*	OTS W/GTP	OT**	OT W/GTP
			DATASET IDENTIFIER	1-19, 42	35-41	20-28	29-34
Orbiter Base Heat Shield (Continued)	164	Standard Gauge		X		X	X
	165	↓		X		X	
	622	GTP Thermo-couple			X		X
	623	↓			X		X
	624	↓			X		X
	752S	GTP (Short Wire)			X		X
	752L	(Long Wire)			X		X
	753S	(Short Wire)			X		X
	753L	(Long Wire)			X		X
	754S	(Short Wire)			X		X
	754L	↓ (Long Wire)			X		X

* OTS is first stage shuttle configuration (orbiter, external tank, SRB)
** OT is second stage shuttle configuration (orbiter, external tank)

TABLE VI. INSTRUMENTATION CONFIGURATIONS (Continued)

COMPONENT	PARAMETER NUMBER	PARAMETER TYPE	DESCRIPTION / DATASET IDENTIFIER	CONFIGURATION OR SET-UP 1 OTS* 1-19, 42	2 OTS W/GTP 35-41	3 OT** 20-28	4 OT W/GTP 29-34
Nozzle #1	101	Standard Gauge		X	X	X	X
	102			X	X	X	
	103			X	X	X	
	104			X	X	X	X
SSME Firing Nozzles	105			X	X	X	X
	106			X	X	X	X
	107			X	X	X	X
	108			X	X	X	X
	109			X	X	X	X
	110			X	X	X	X

* OTS is first stage shuttle configuration (orbiter, external tank, SRB)
** OT is second stage shuttle configuration (orbiter, external tank)

TABLE VI. INSTRUMENTATION CONFIGURATIONS (Continued)

COMPONENT	PARAMETER NUMBER	PARAMETER TYPE	DESCRIPTION / DATASET IDENTIFIER	CONFIGURATION OR SET-UP 1 OTS* 1-19, 42	2 OTS W/GTP 35-41	3 OT** 20-28	4 OT W/GTP 29-34
Nozzle #2							
SSME Firing Nozzles	111	Standard Gauge		X	X	X	X
	112			X	X	X	X
	113			X	X	X	X
	114			X	X	X	X
	115			X	X	X	X
	116			X	X	X	X
	117			X	X	X	X
	118			X	X	X	X
	119			X	X	X	X
Hatband Nozzle	166	Standard Gauge			X		X
	167				X		X

* OTS is first stage shuttle configuration (orbiter, external tank, SRB)
** OT is second stage shuttle configuration (orbiter, external tank)

TABLE VI. INSTRUMENTATION CONFIGURATIONS (Continued)

COMPONENT	PARAMETER NUMBER	PARAMETER TYPE	DESCRIPTION / DATASET IDENTIFIER	CONFIGURATION OR SET-UP 1 OTS* 1-19, 42	2 OTS W/GTP 35-41	3 OT** 20-28	4 OT W/GTP 29-34
Hatband Nozzle (Continued)	168	Standard Gauge			X		X
	169				X		X
	170				X		X
	171				X		X
	172				X		X
	173				X		X
	174				X		X
	175				X		X
	176				X		X
	177				X		X
	178				X		X

* OTS is first stage shuttle configuration (orbiter, external tank, SRB)
** OT is second stage shuttle configuration (orbiter, external tank)

TABLE VI. INSTRUMENTATION CONFIGURATIONS (Continued)

COMPONENT	PARAMETER NUMBER	PARAMETER TYPE	DESCRIPTION / DATASET IDENTIFIER	CONFIGURATION OR SET-UP 1 OTS* 1-19, 42	2 OTS W/GTP 35-41	3 OT** 20-28	4 OT W/GTP 29-34
Hatband Nozzle (Continued)	179	Standard Gauge			X		X
	180	▼			X		X
External Tank Aft Dome	210	Standard Gauge		X			
	211			X	X	X	X
	212			X	X		
	213			X			
	214			X			
	215			X			
	216			X	X		
	217			X	X		
	218	▼		X			

* OTS is first stage shuttle configuration (orbiter, external tank, SRB)
** OT is second stage shuttle configuration (orbiter, external tank)

TABLE VI. INSTRUMENTATION CONFIGURATIONS (Continued)

COMPONENT	PARAMETER NUMBER	PARAMETER TYPE	DESCRIPTION / DATASET IDENTIFIER	CONFIGURATION OR SET-UP 1 OTS* 1-19, 42	2 OTS W/GTP 35-41	3 OT** 20-28	4 OT W/GTP 29-34
External Tank Aft Dome (Continued)	231	Radiative Gauge		X			
	233	↓		X			
	234	Pressure		X	X	X	X
	235	↓		X			
	236	↓		X	X	X	X
	626	GTP Thermo-couple			X		
	627	↓			X		
	628	↓			X		
	756S	GTP (Short Wire)			X		
	756L	(Long Wire)			X		
	757S	(Short Wire)			X		

* OTS is first stage shuttle configuration (orbiter, external tank, SRB)
** OT is second stage shuttle configuration (orbiter, external tank)

TABLE VI. INSTRUMENTATION CONFIGURATIONS (Continued)

COMPONENT	PARAMETER NUMBER	PARAMETER TYPE	DESCRIPTION	CONFIGURATION OR SET-UP 1	2	3	4
				OTS*	OTS W/GTP	OT**	OT W/GTP
			DATASET IDENTIFIER	1-19, 42	35-41	20-28	29-34
External Tank Aft Dome (Continued)	757L	GTP (Long Wire)			X		
	758S	(Short Wire)			X		
	758L	(Long Wire)			X		
External Tank Hardware	221	Standard Gauge		X			
	228			X			
Left SRB Sidewall	302	Standard Gauge			X		
	303				X		
	305				X		
	306				X		
	307				X		

* OTS is first stage shuttle configuration (orbiter, external tank, SRB)
** OT is second stage shuttle configuration (orbiter, external tank)

TABLE VI. INSTRUMENTATION CONFIGURATIONS (Continued)

COMPONENT	PARAMETER NUMBER	PARAMETER TYPE	DESCRIPTION	CONFIGURATION OR SET-UP 1	2	3	4
				OTS*	OTS W/GTP	OT**	OT W/GTP
			DATASET IDENTIFIER	1-19, 42	35-41	20-28	29-34
Left SRB Sidewall (Continued)	327	Standard Gauge		X			
	328	↓		X			
	329			X	X		
Left SRB Nozzle and Shroud	308	Standard Gauge		X			
	310			X			
	312			X	X		
	313			X	X		
	314			X			
	315			X			
	316	↓		X			
	324	Pressure		X	X		
	325	↓		X	X		

* OTS is first stage shuttle configuration (orbiter, external tank, SRB)
** OT is second stage shuttle configuration (orbiter, external tank)

TABLE VI. INSTRUMENTATION CONFIGURATIONS (Continued)

COMPONENT	PARAMETER NUMBER	PARAMETER TYPE		CONFIGURATION OR SET-UP			
				1	2	3	4
			DESCRIPTION	OTS*	OTS W/GTP	OT**	OT W/GTP
			DATASET IDENTIFIER	1-19, 42	35-41	20-28	29-34
Left SRB Skirt Curtain	317	Standard Gauge		X			
	318	↓		X	X		
	319			X	X		
	320			X			
	629	GTP Thermo-couple			X		
	759S	GTP (Short Wire)			X		
	759L	↓ (Long Wire)			X		
Summary		Standard Gauges		83	69	87	70
		Radiative Gauges		7		1	1
		Pressures		9	10	10	10

* OTS is first stage shuttle configuration (orbiter, external tank, SRB)
** OT is second stage shuttle configuration (orbiter, external tank)

TABLE VI. INSTRUMENTATION CONFIGURATIONS (Concluded)

COMPONENT	PARAMETER NUMBER	PARAMETER TYPE		CONFIGURATION OR SET-UP			
				1	2	3	4
			DESCRIPTION	OTS*	OTS W/GTP	OT**	OT W/GTP
			DATASET IDENTIFIER	1-19, 42	35-41	20-28	29-34
Summary (Continued)		GTP Thermo-couples			7		3
		GTP (Short Wire)			7		3
		GTP (Long Wire)			7		3
		Data Channels		99	100	98	90

* OTS is first stage shuttle configuration (orbiter, external tank, SRB)
** OT is second stage shuttle configuration (orbiter, external tank)

TABLE VII. THERMOCOUPLES

Thermocouple Number	Location	Type
622	Gas Temperature Probe (GTP) 752 (Orbiter)	Iron-Constantan (Type J)
623	GTP 753	↓
624	GTP 754	↓
626	GTP 756 (External Tank)	↓
627	GTP 757	↓
628	GTP 758	↓
629	GTP 759 (Left SRB Skirt Curtain)	↓

TABLE VIII. MAXIMUM MODEL 19-OTS OPERATING CONDITIONS IN THE CALSPAN LUDWIEG TUBE WIND TUNNEL

SRB CHAMBER PRESSURE	MAXIMUM SIMULATED ALTITUDE
290 psia	130,000 ft.
200 psia	140,000 ft.
100 psia	150,000 ft.

TABLE IX. DATA ACQUISITION SUMMARY

DATA ACQUISITION SYSTEMS	INSTRUMENTATION CONFIGURATION			
	1	2	3	4
	OTS	OTS W/GTP	CT	CT W/GTP
MODEL DATA:				
VIDAR:				
Heat-Transfer Gauge Channels	65	42	63	44
Gas-Temperature Probe Channels	--	21	--	9
Total Channels Used	65	63	63	53
OSCILLOGRAPHS:				
Pressure Channels	9	10	10	10
Heat-Transfer Gauge Channels	25	27	25	27
Total Channels Used	34	37	35	37
(1) TOTAL MODEL DATA CHANNELS	99	100	98	90
TUNNEL AND MODEL OPERATING DATA:				
Vidar Channels	1	--	1	1
Oscillograph Channels	26	24	25	25
(2) TOTAL OPERATING DATA CHANNELS	27	24	26	26
UNUSED CHANNELS:				
Vidar	--	3	2	12
Oscillograph	2	1	2	--
(3) TOTAL UNUSED CHANNELS	2	4	4	12
TOTAL TEST DATA CHANNELS [(1) + (2) + (3)]	128	128	128	128

NOTES:
1. Gimbal angle deflection is away from null.
2. Positive pitch is nozzle trailing edge down.
3. Positive yaw is nozzle trailing edge left.
4. (P) is the absolute magnitude of the angle.
5. (Y) is measured counterclockwise from the positive yaw axis.

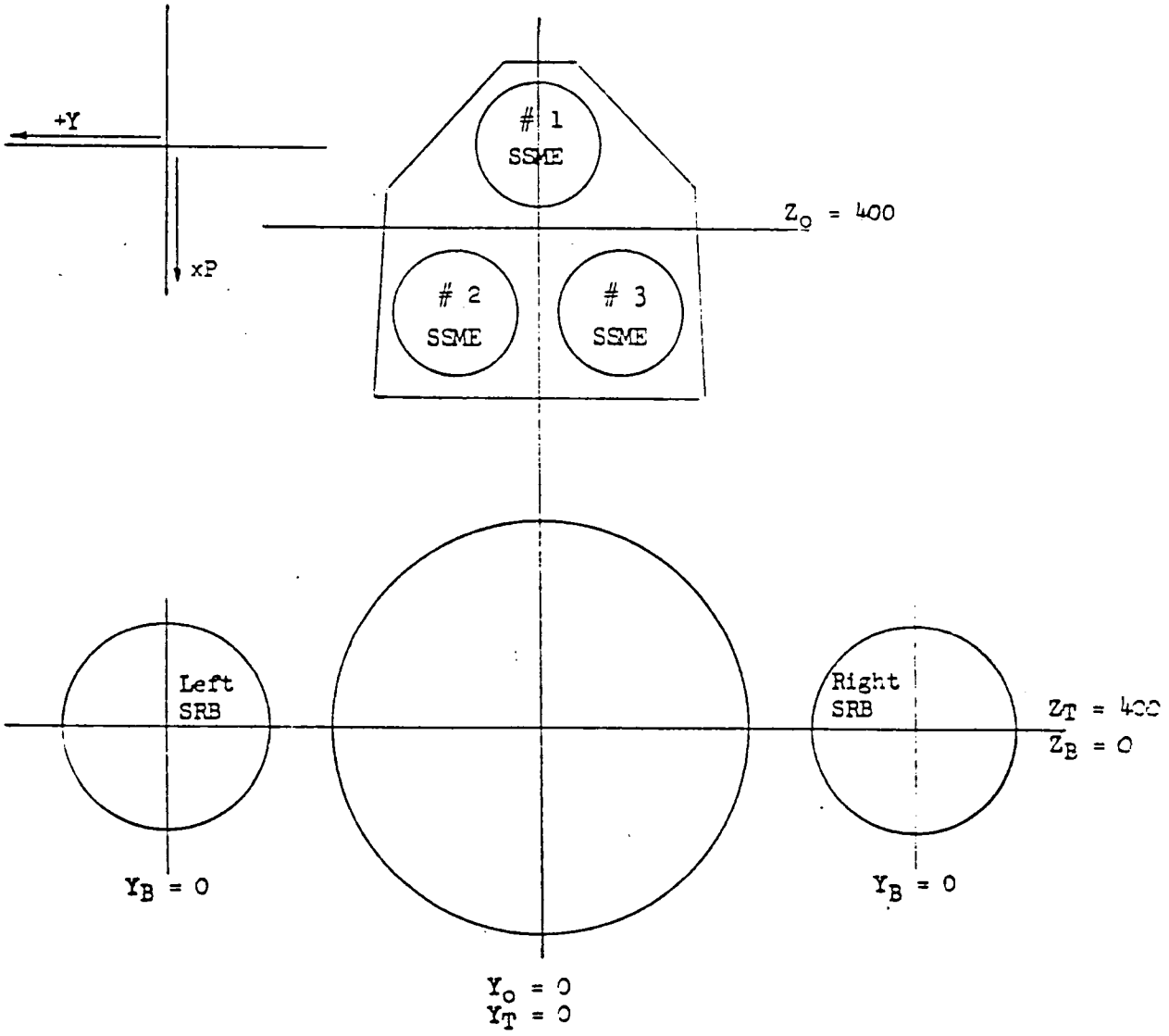

VIEW LOOKING FORWARD

Figure 1. Gimbal angle definition.

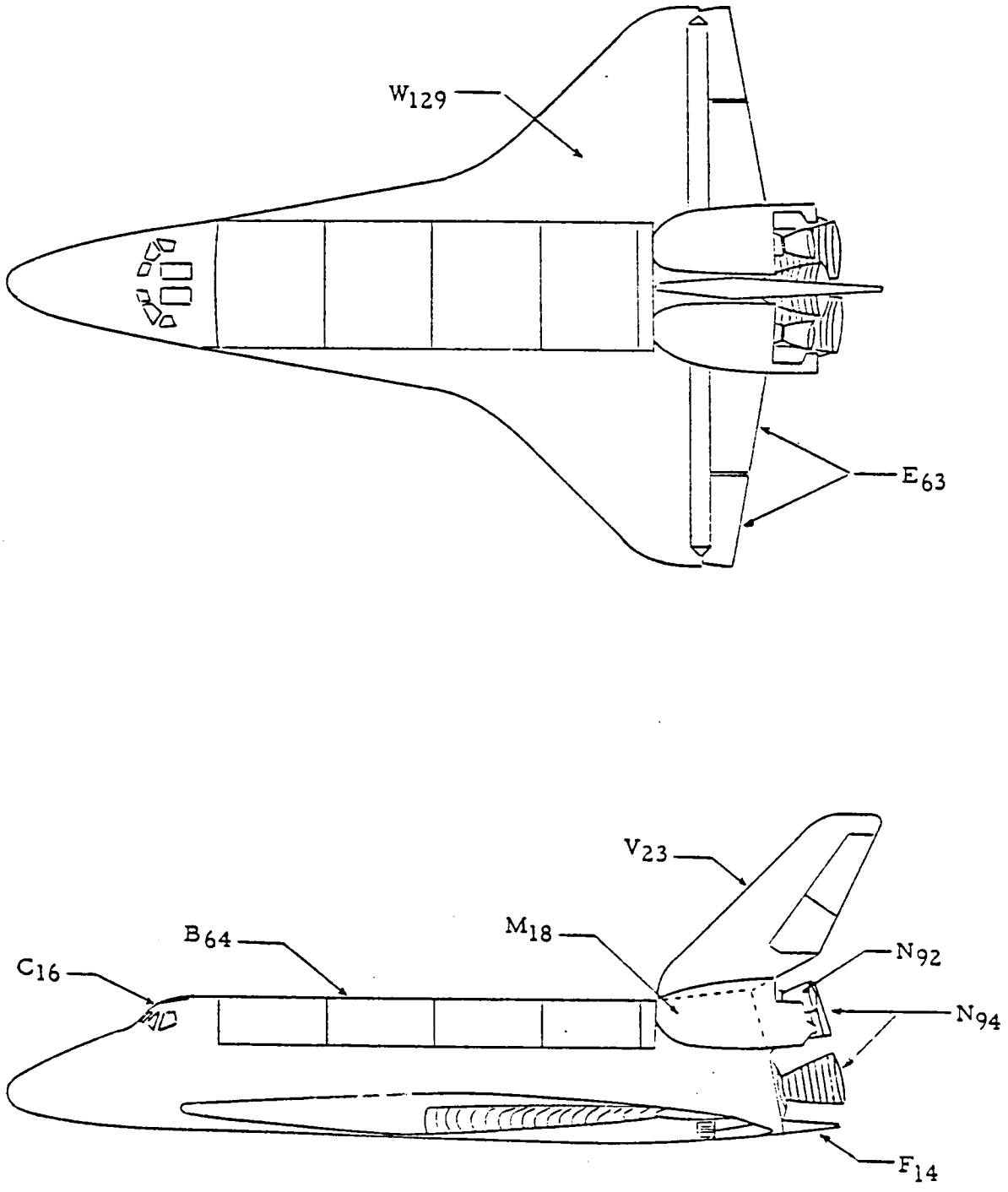

Figure 2. Orbiter vehicle.

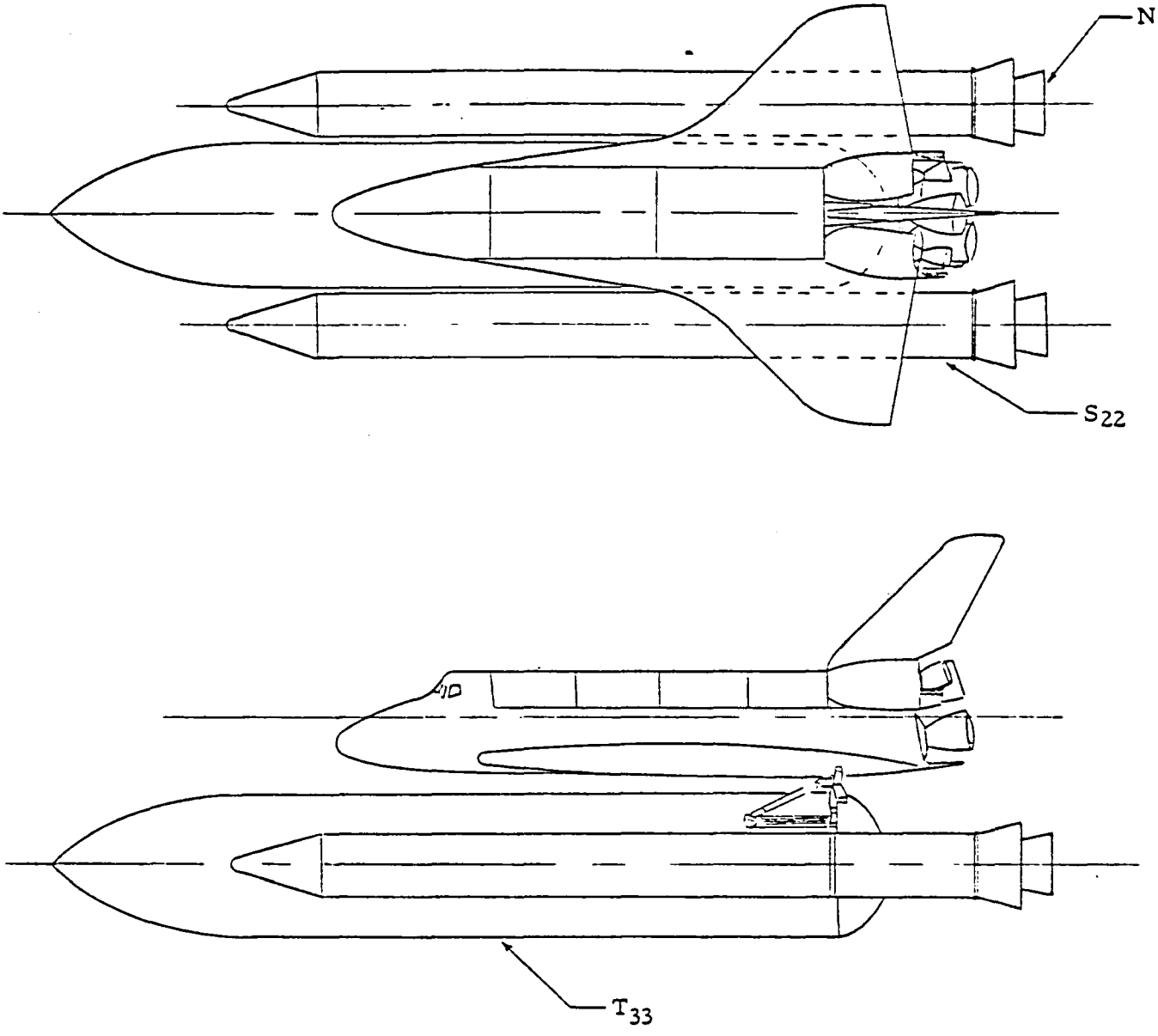

Figure 3. Integrated vehicle.

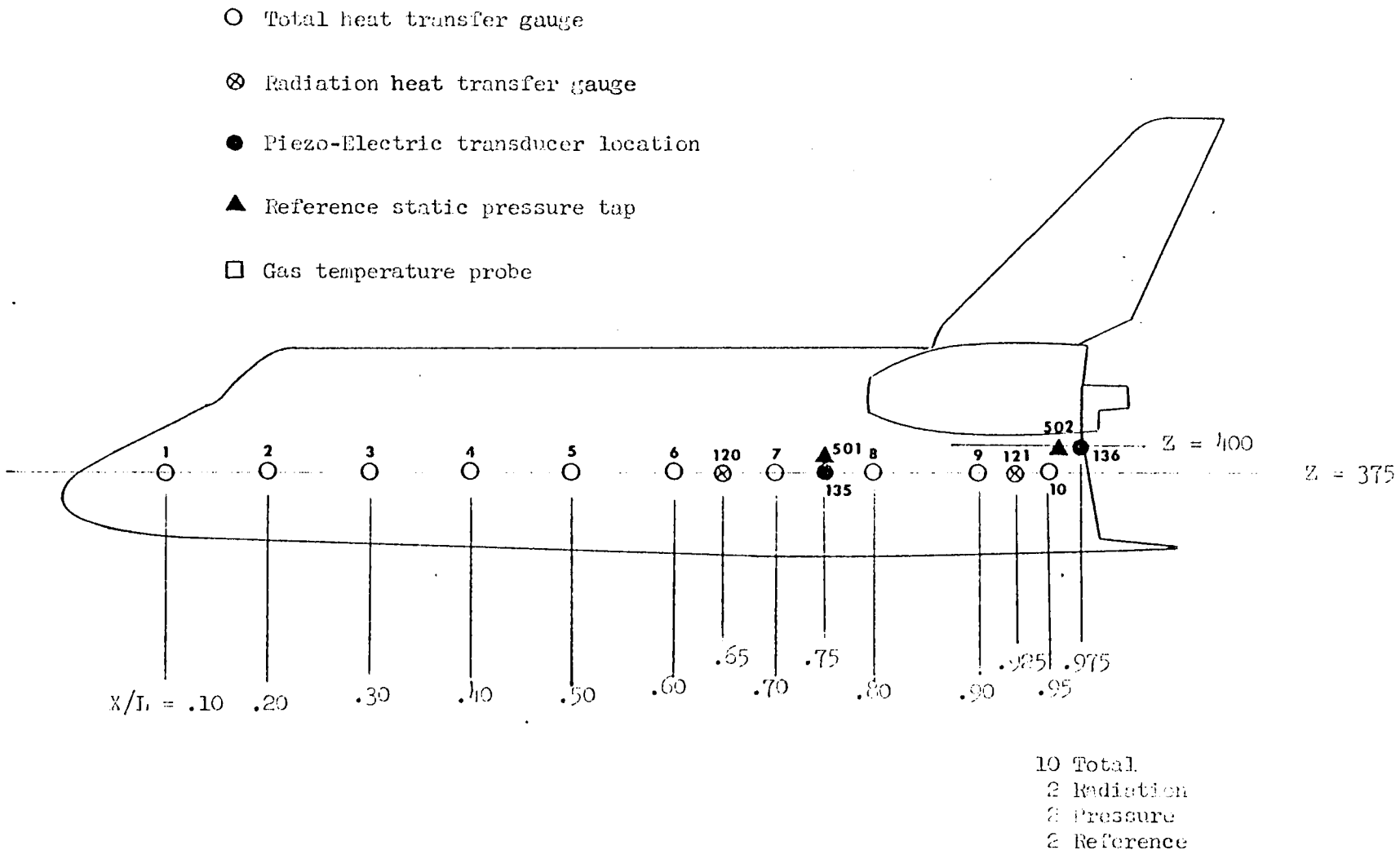

a. Orbiter Side

Figure 4. Instrumentation.

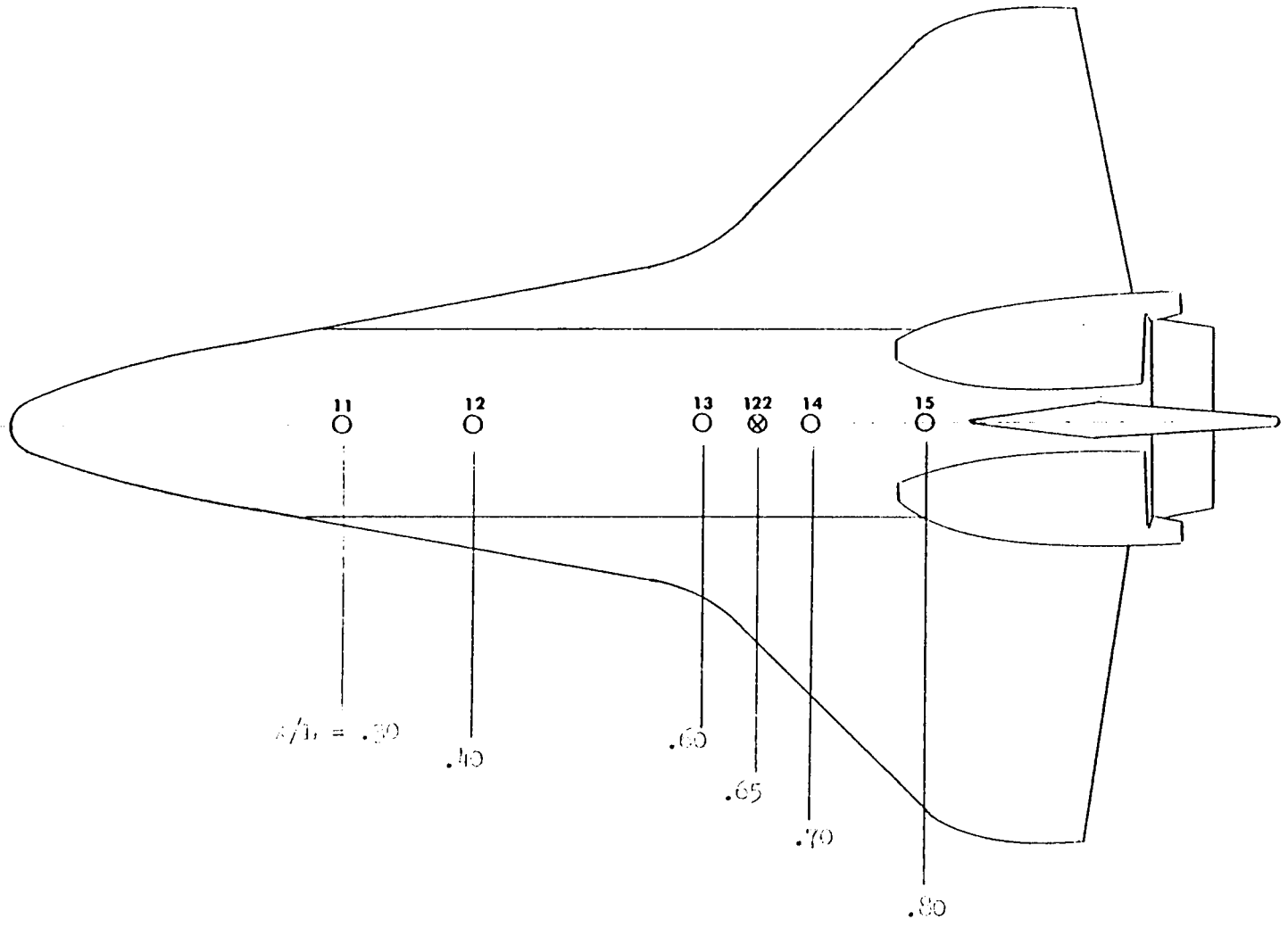

5 Total
1 Radiation

b. Orbiter Top
Figure 4. Continued.

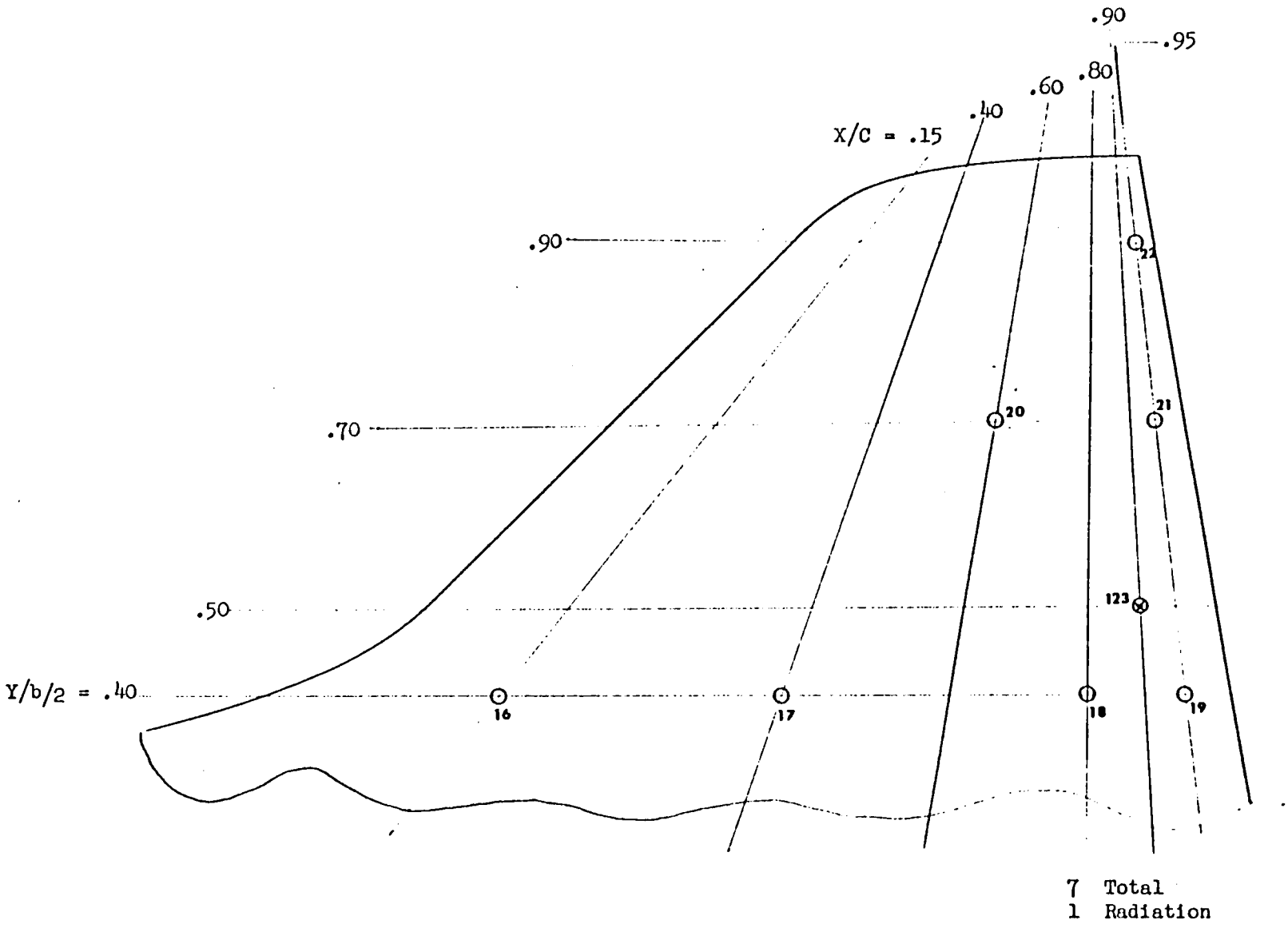

c. Wing Lower Surface
Figure 4. Continued.

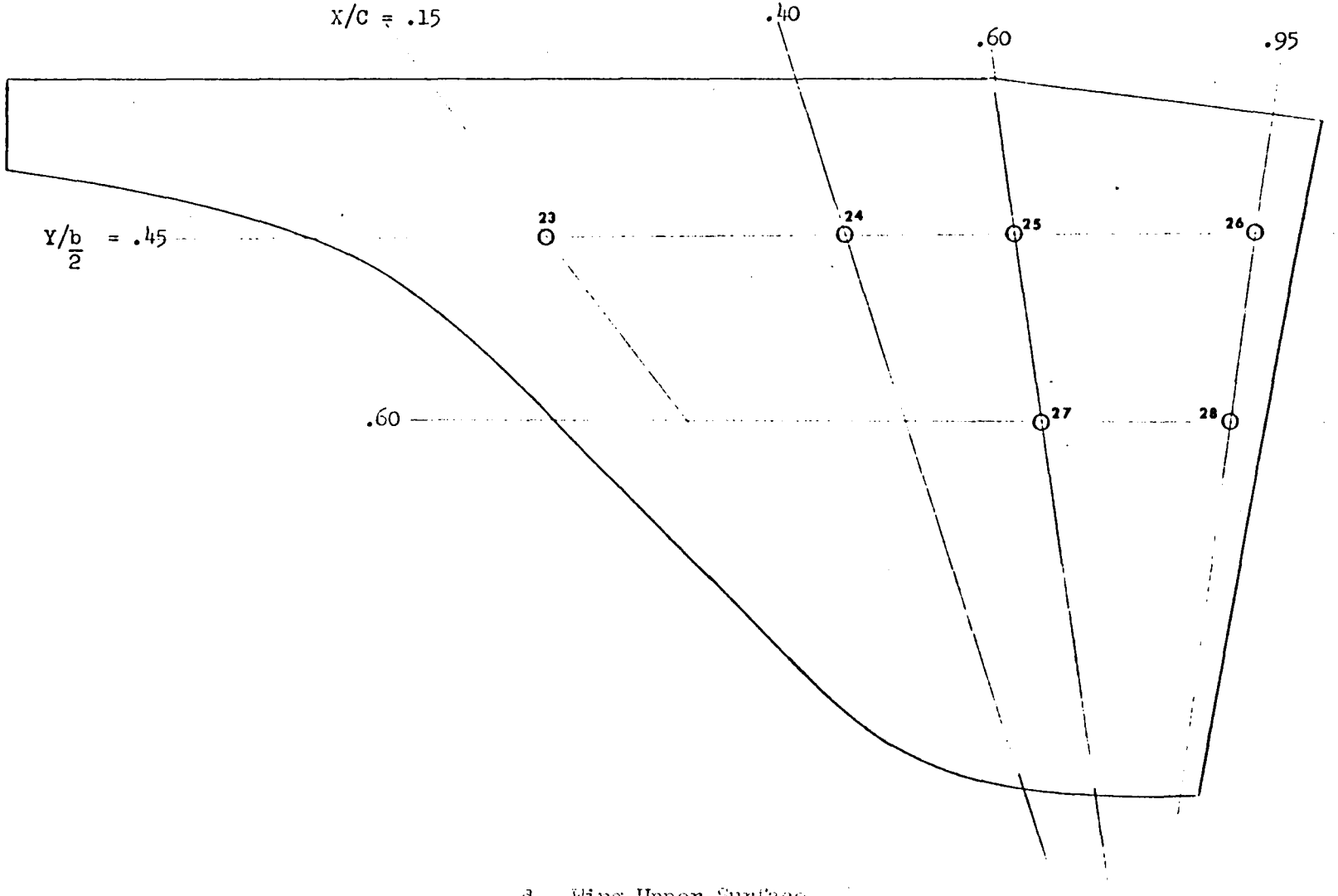

d. Wing Upper Surface

Figure 4. Continued.

6 Total

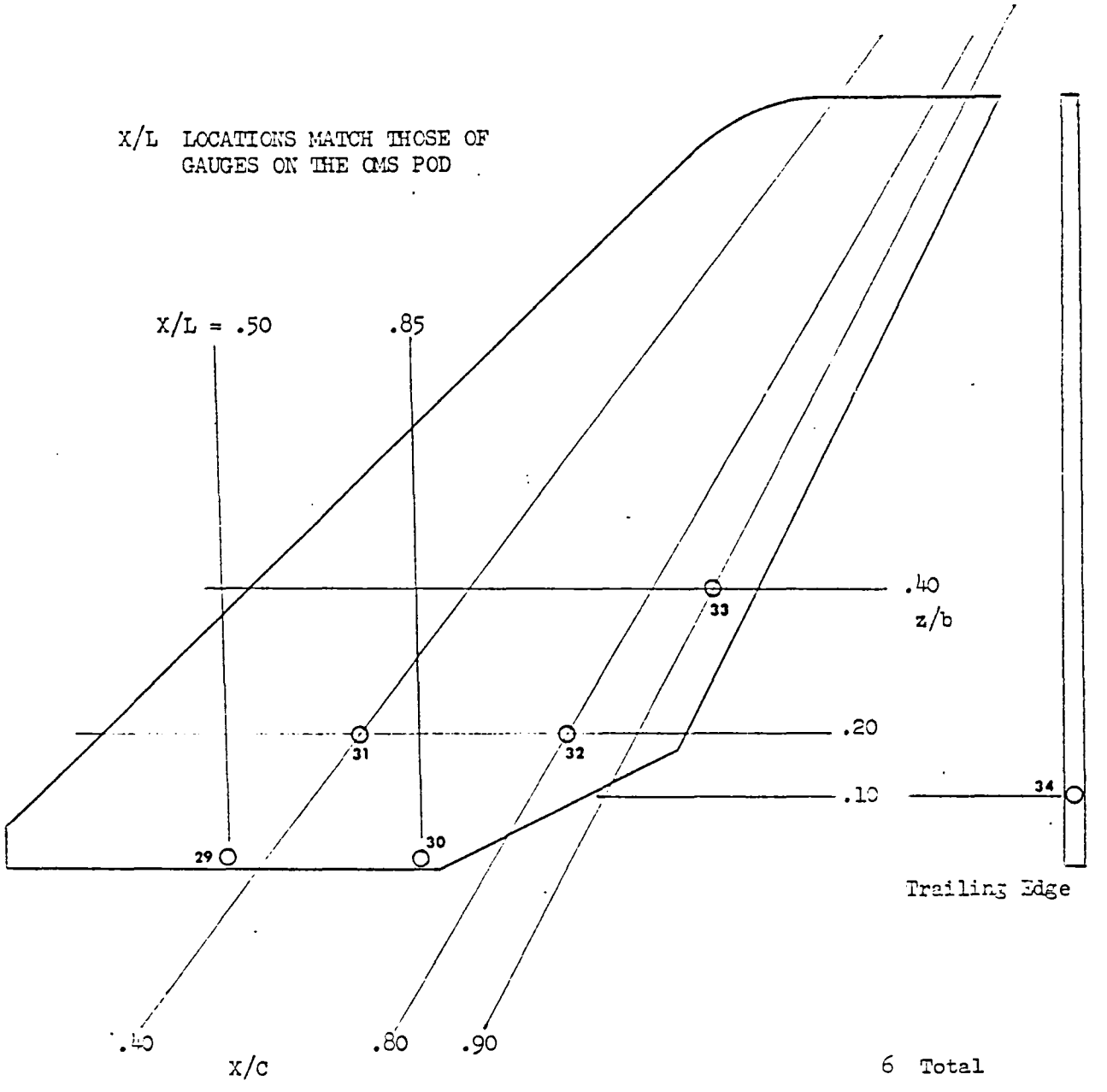

e. Vertical Tail
Figure 4. Continued.

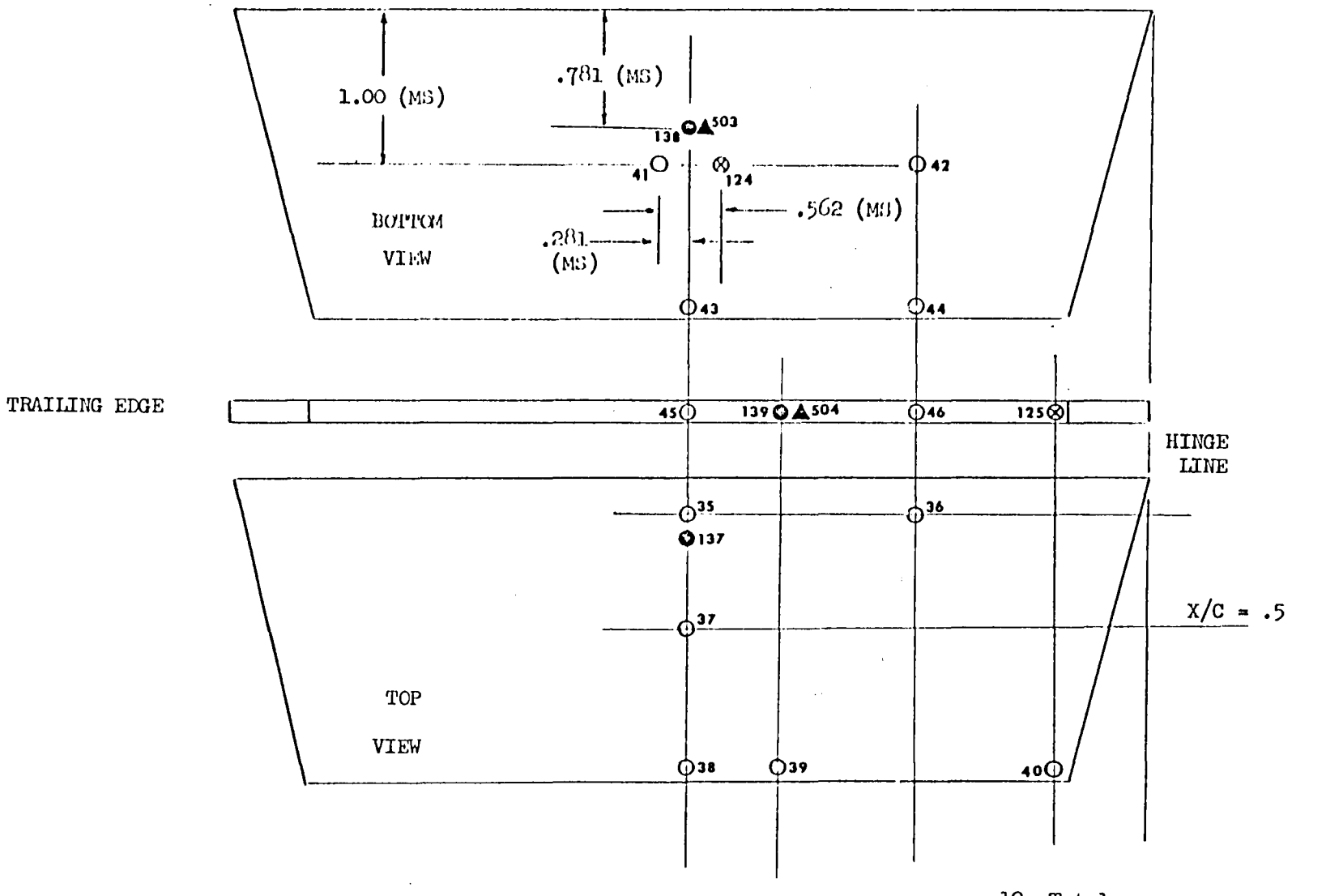

f. Body Flap
Figure 4. Continued.

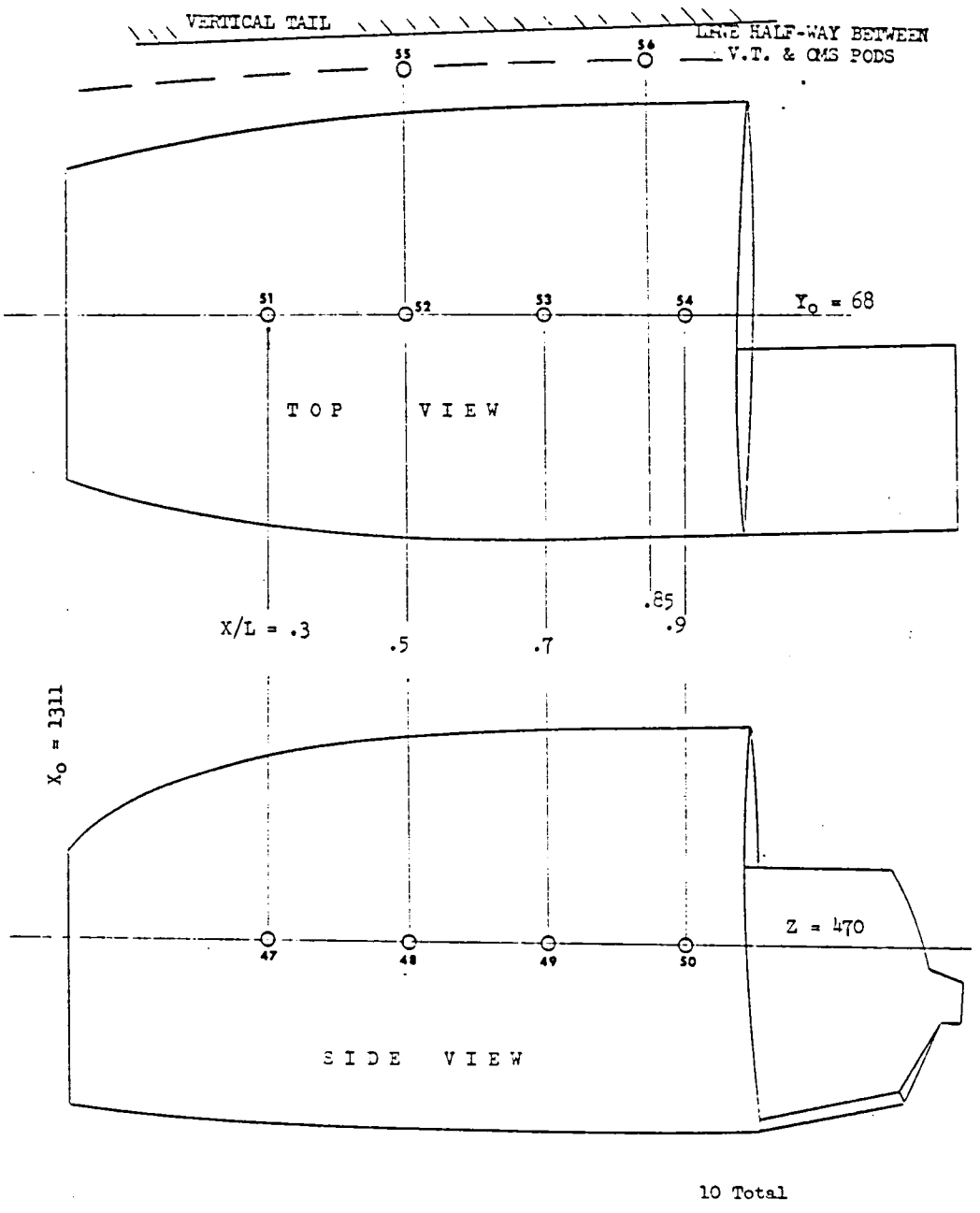

g. Left CMS Pod
Figure 4. Continued.

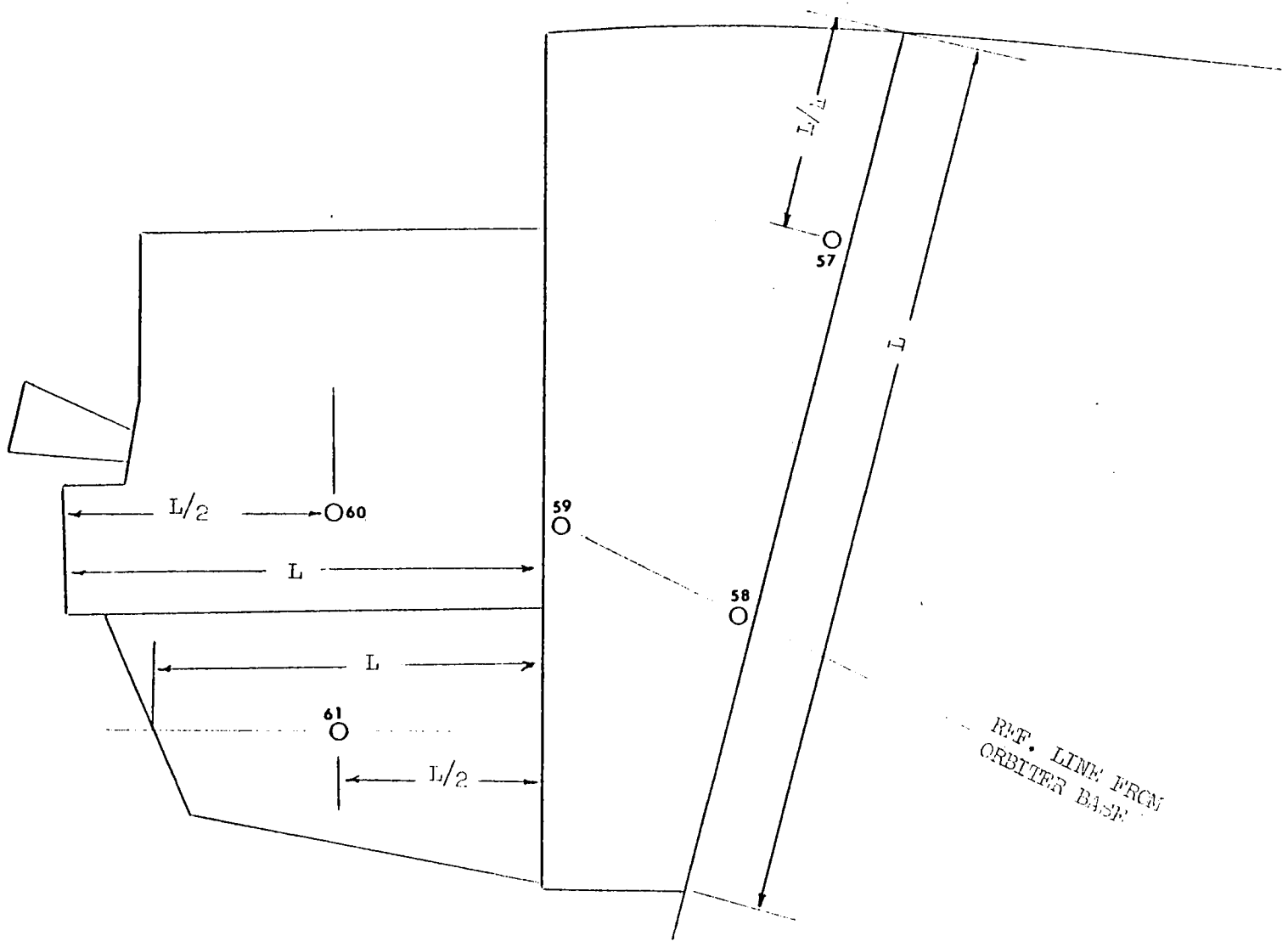

5 Total

h. Left OMS/RCS - Inside Surfaces
Figure 4. Continued.

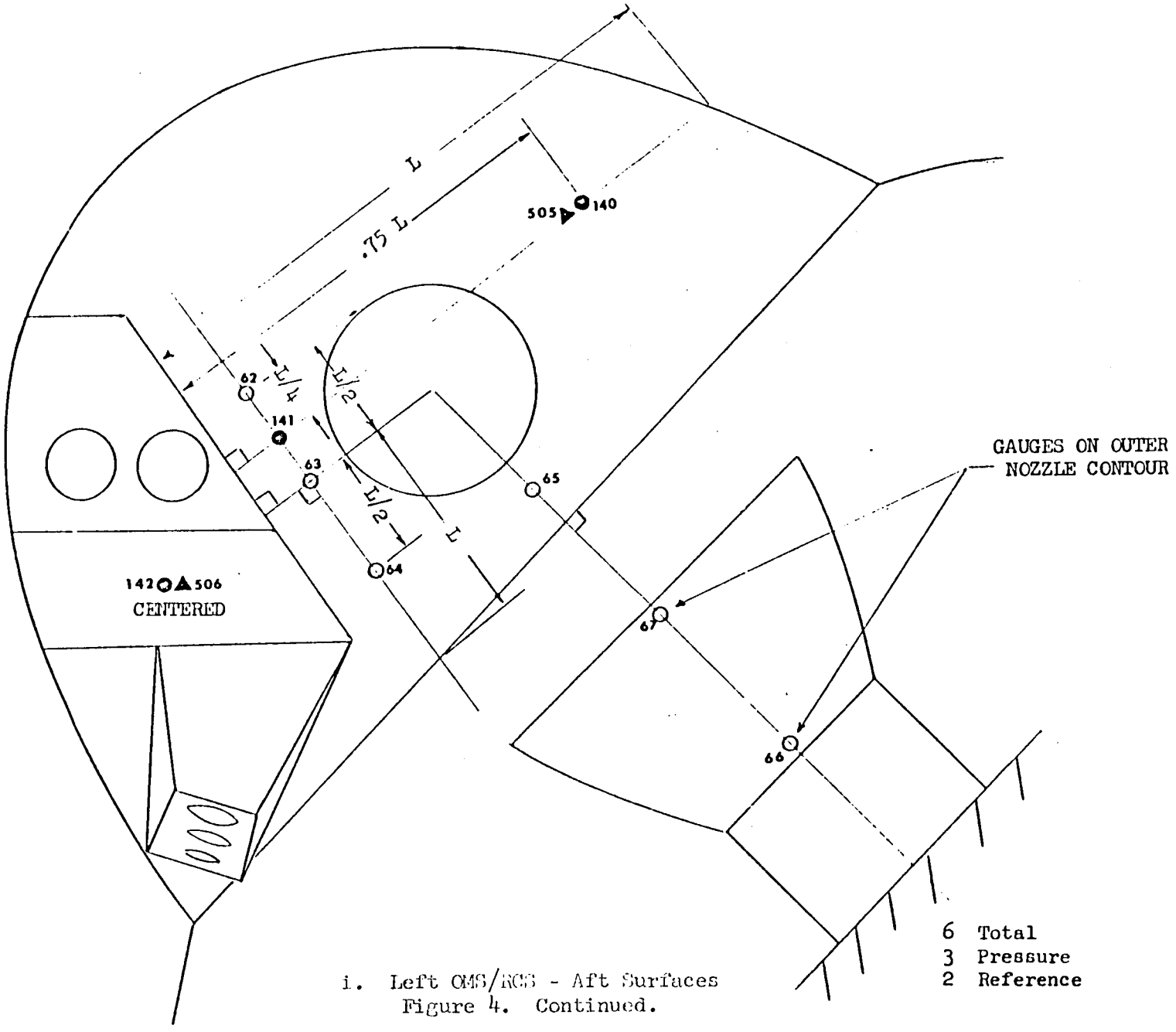

i. Left OMS/RCS - Aft Surfaces
Figure 4. Continued.

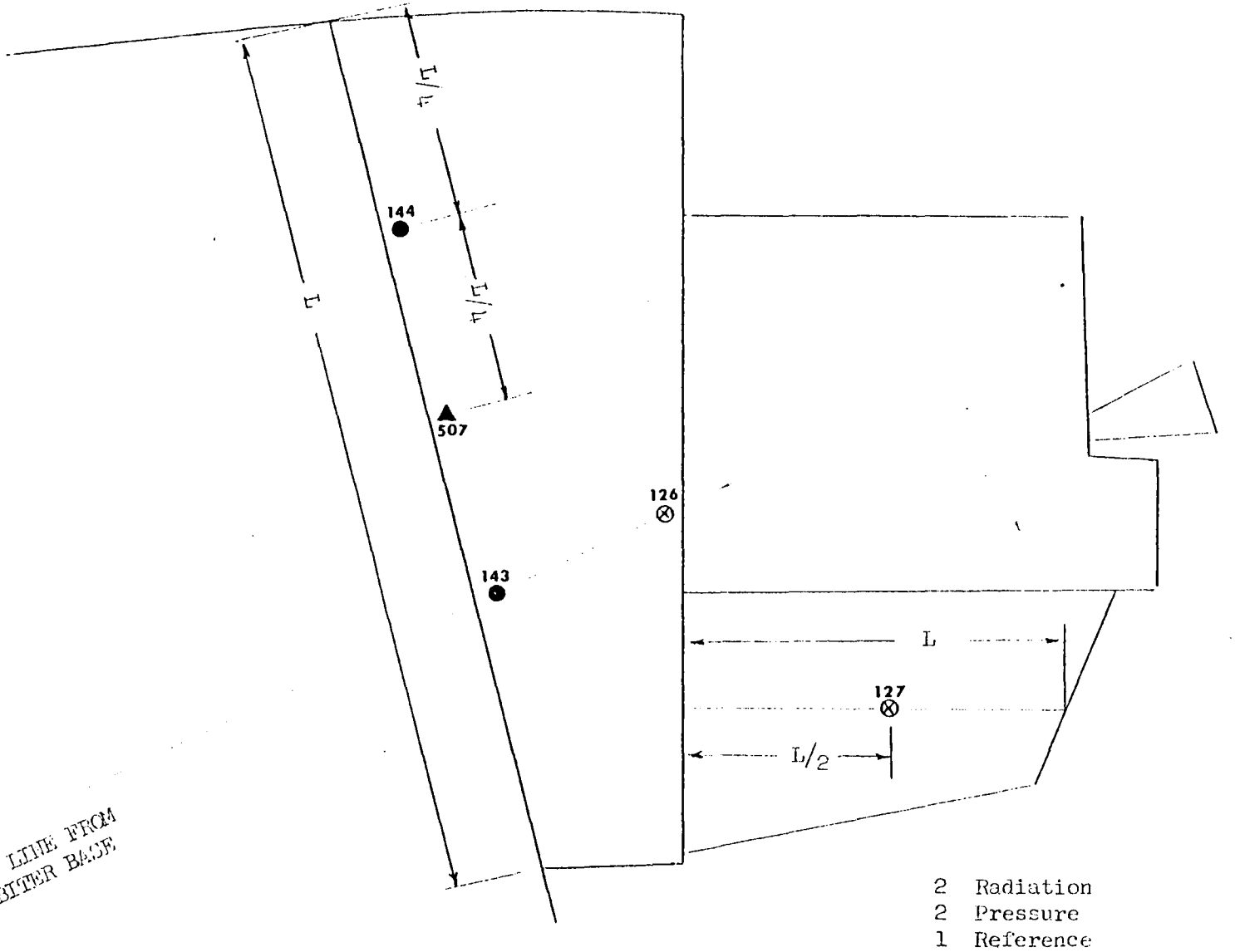

j. Right OMS/RCS - Inside Surfaces
Figure 4. Continued.

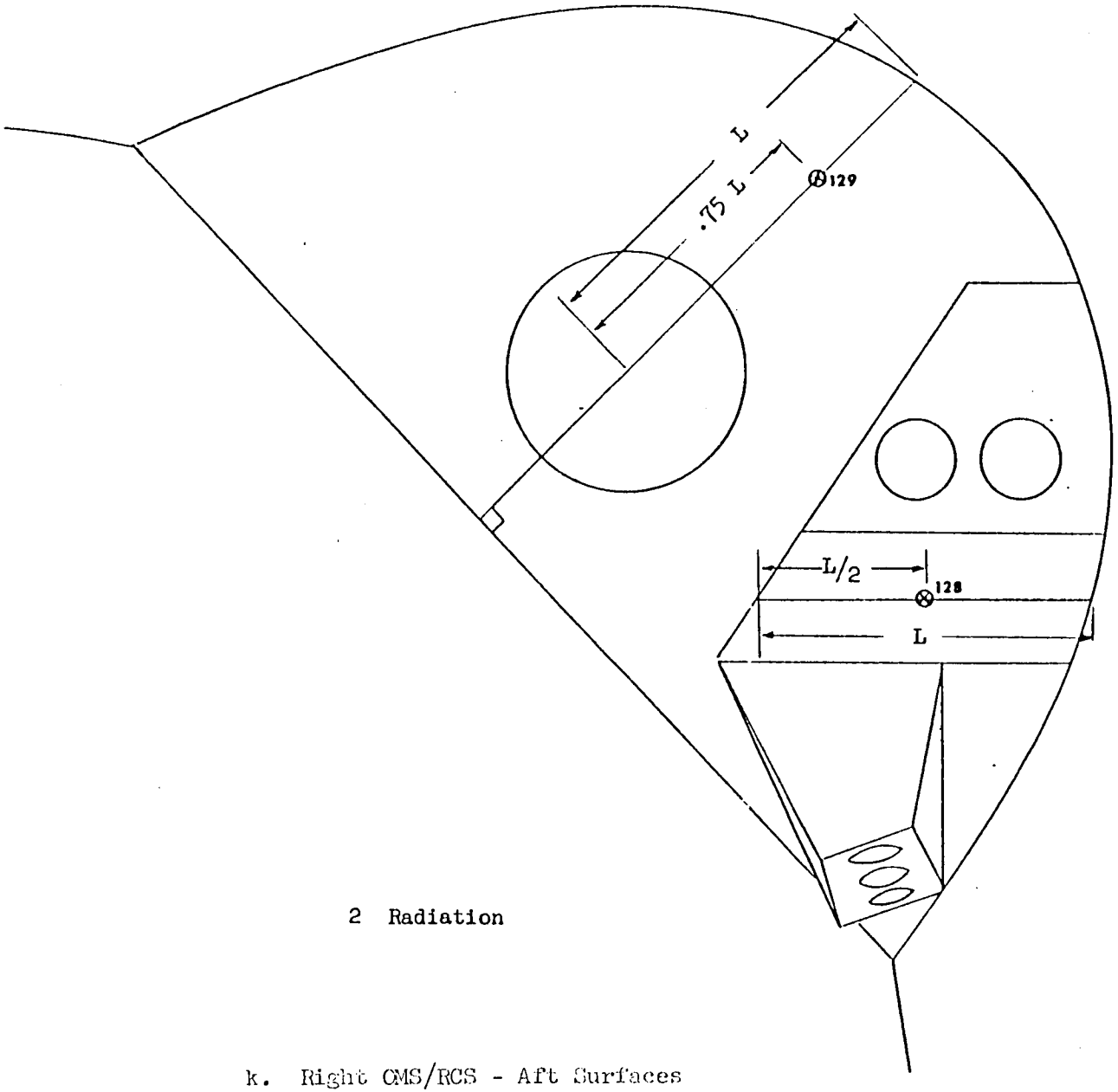

2 Radiation

k. Right OMS/RCS - Aft Surfaces
Figure 4. Continued.

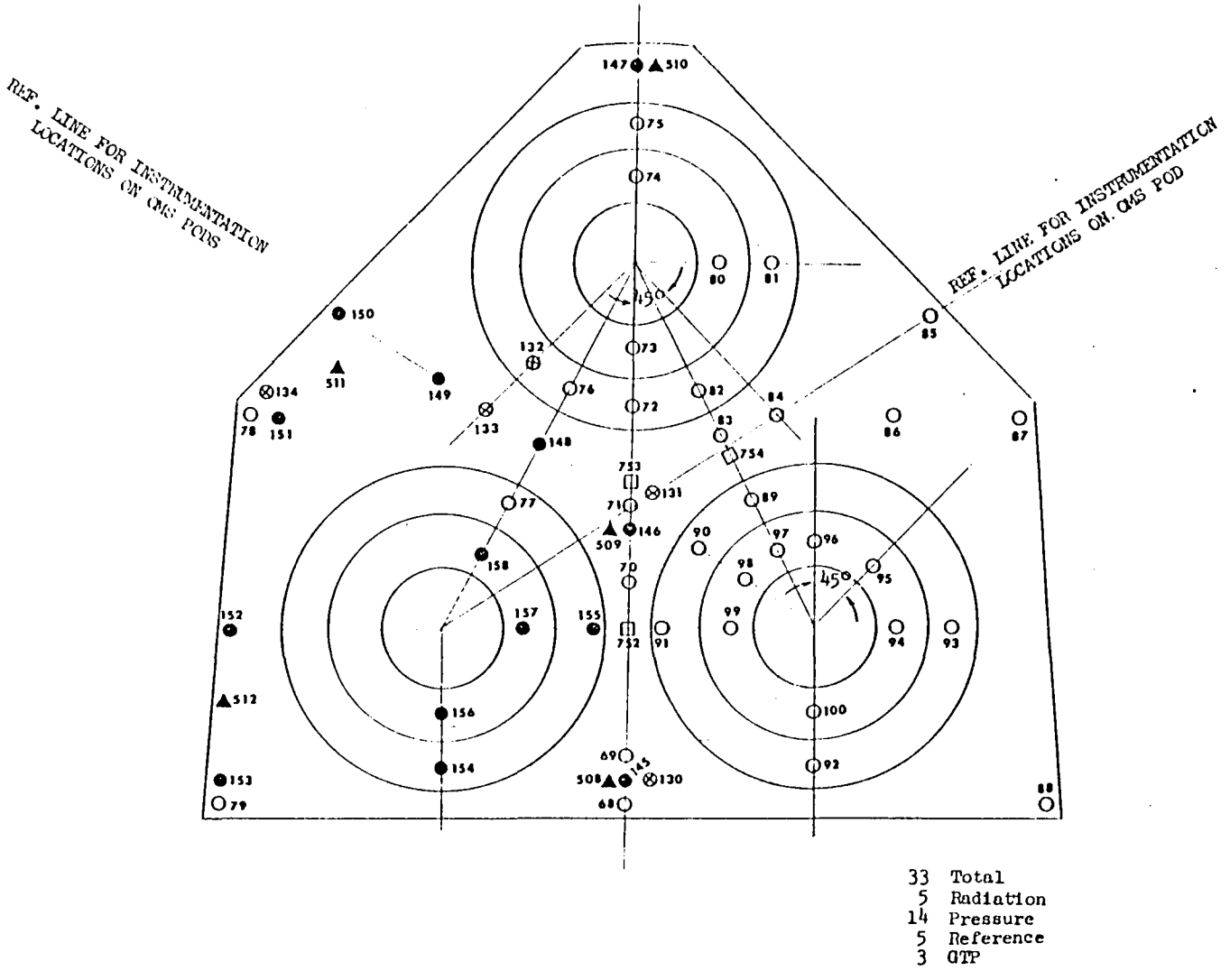

1. Orbiter Base Heat Shield
Figure 4. Continued.

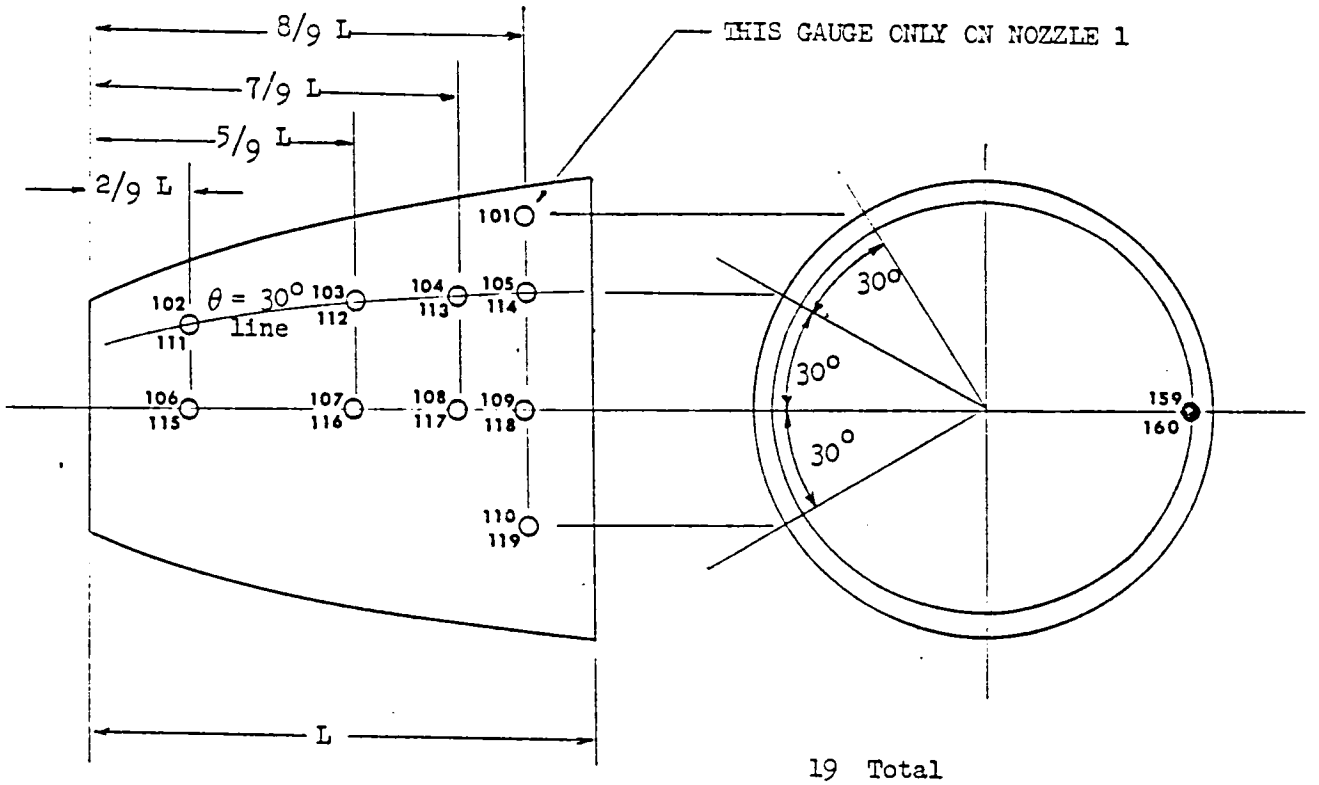

19 Total
2 Pressure

NOZZLES 1 & 2

No.	Nozzle	Type
159	1	Pressure
101-110	1	Total
160	2	Pressure
111-119	2	Total
161	3	Pressure
513	3	Ref. Press.

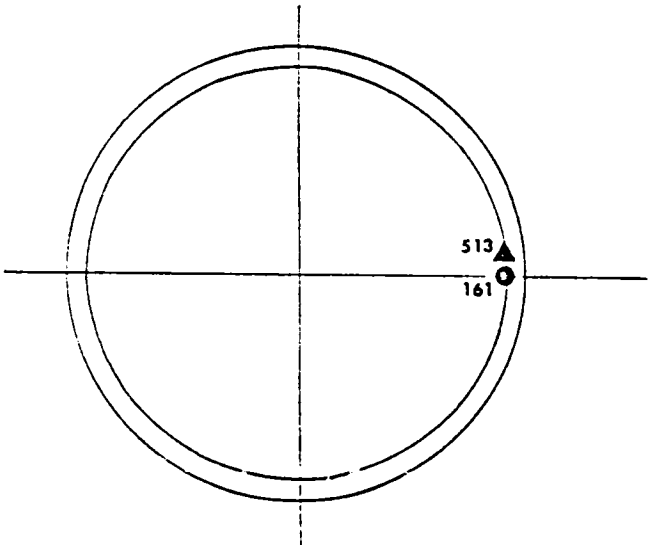

NOZZLE 3

1 Pressure
1 Reference

m. SSME Firing Nozzles
Figure 4. Continued.

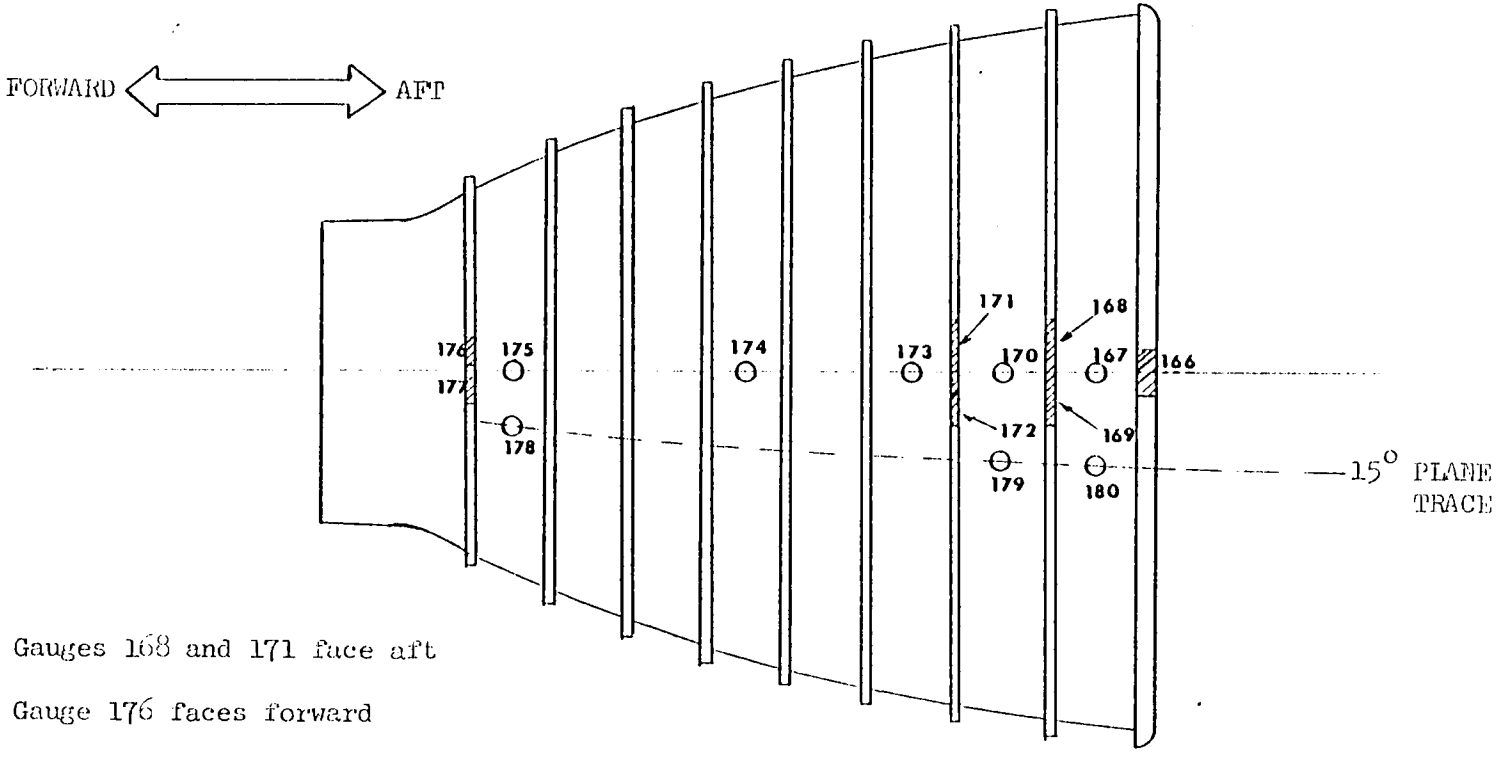

- Gauges 168 and 171 face aft
- Gauge 176 faces forward
- All other gauges are perpendicular to the nozzle surface

15 Total

Gauge numbers 166-180 are synonymous with gauge numbers HB1-HB15.

n. Hatband Nozzle
Figure 4. Continued.

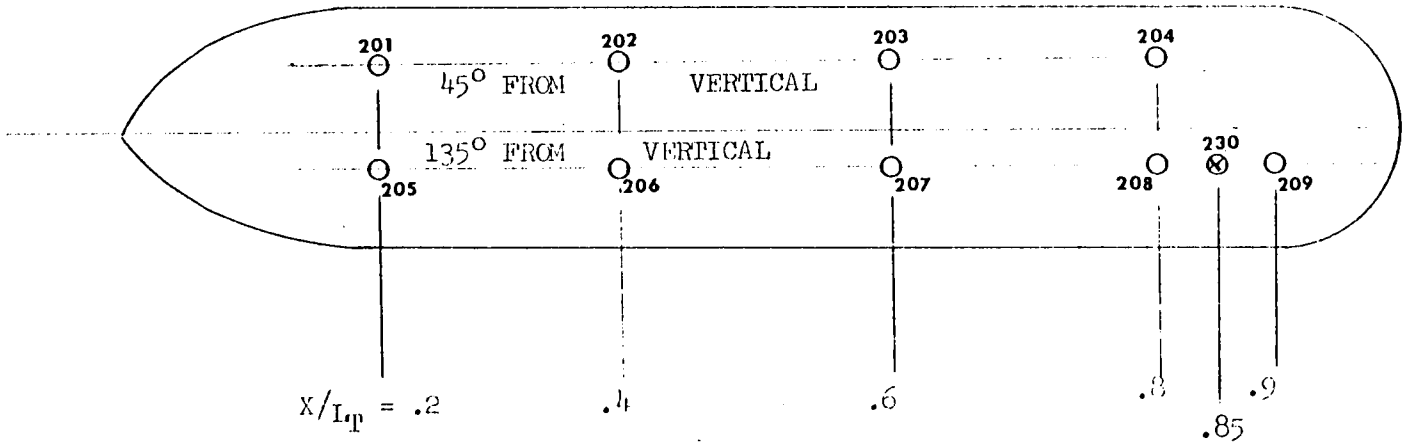

9 Total
1 Radiation

o. External Tank Sidewall
Figure 4. Continued.

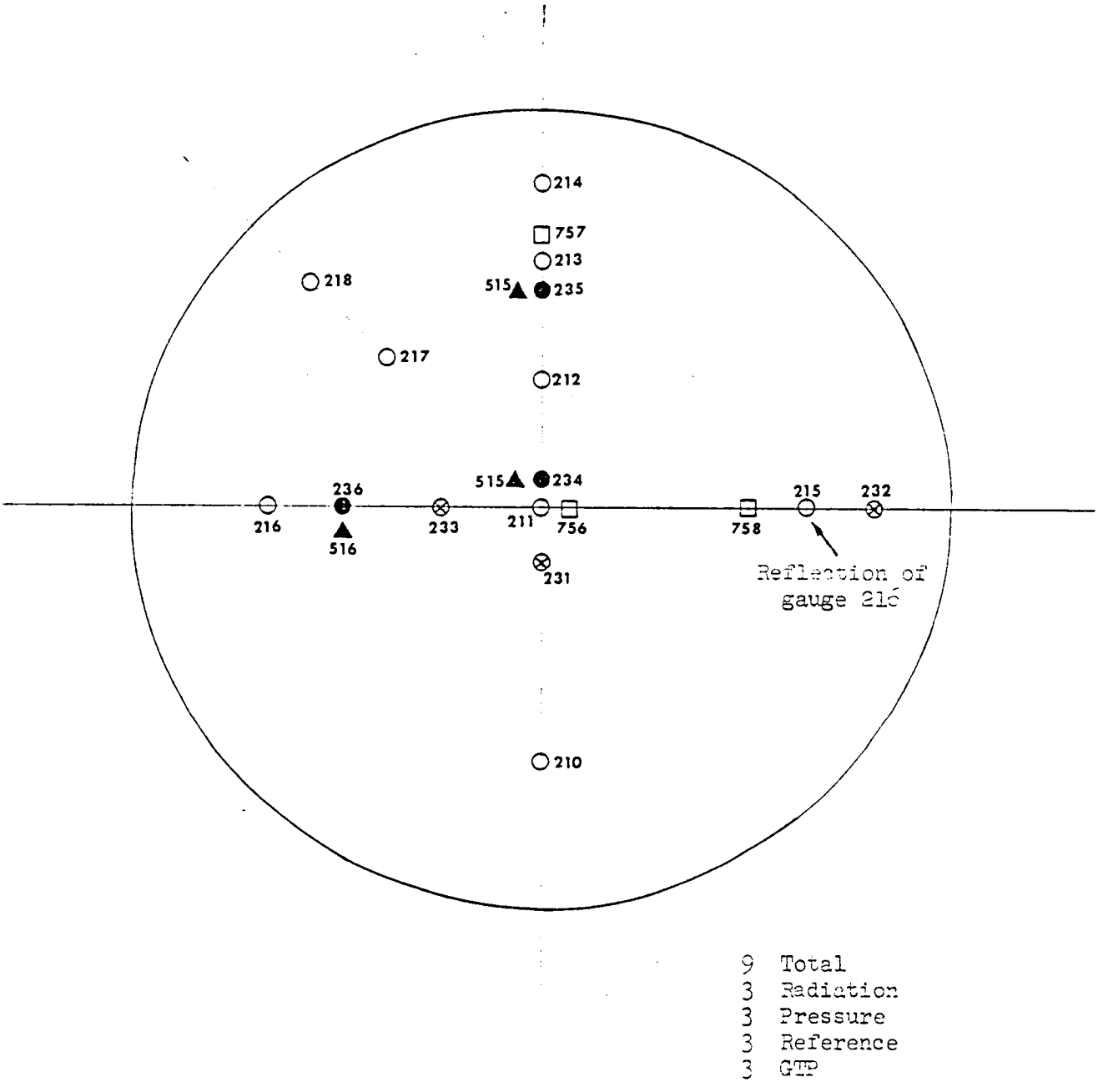

9 Total
3 Radiation
3 Pressure
3 Reference
3 GTP

p. External Tank Aft Dome
Figure 4. Continued.

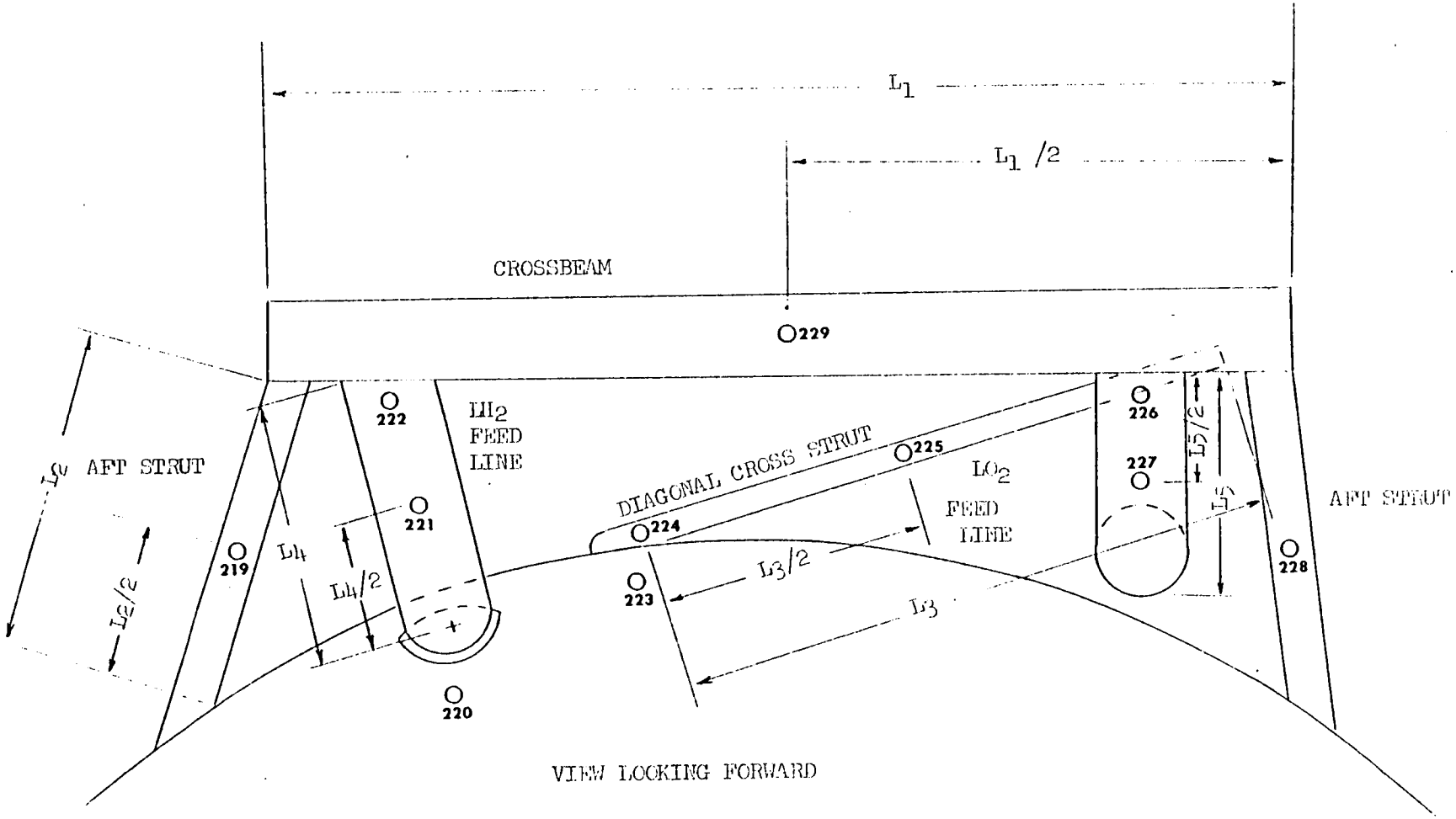

11 Total

q. External Tank Hardware
Figure 4. Continued.

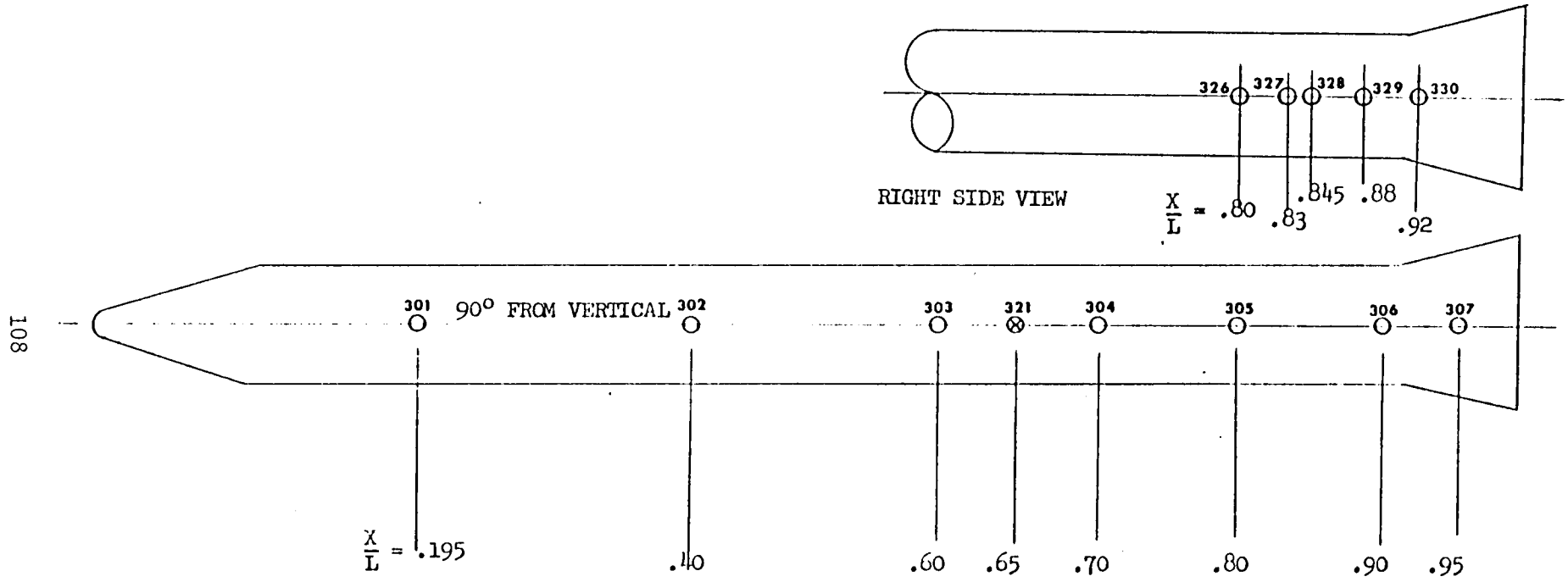

LEFT HAND ROCKET ONLY

12 Total
1 Radiation

r. Left SRB Sidewall
Figure 4. Continued.

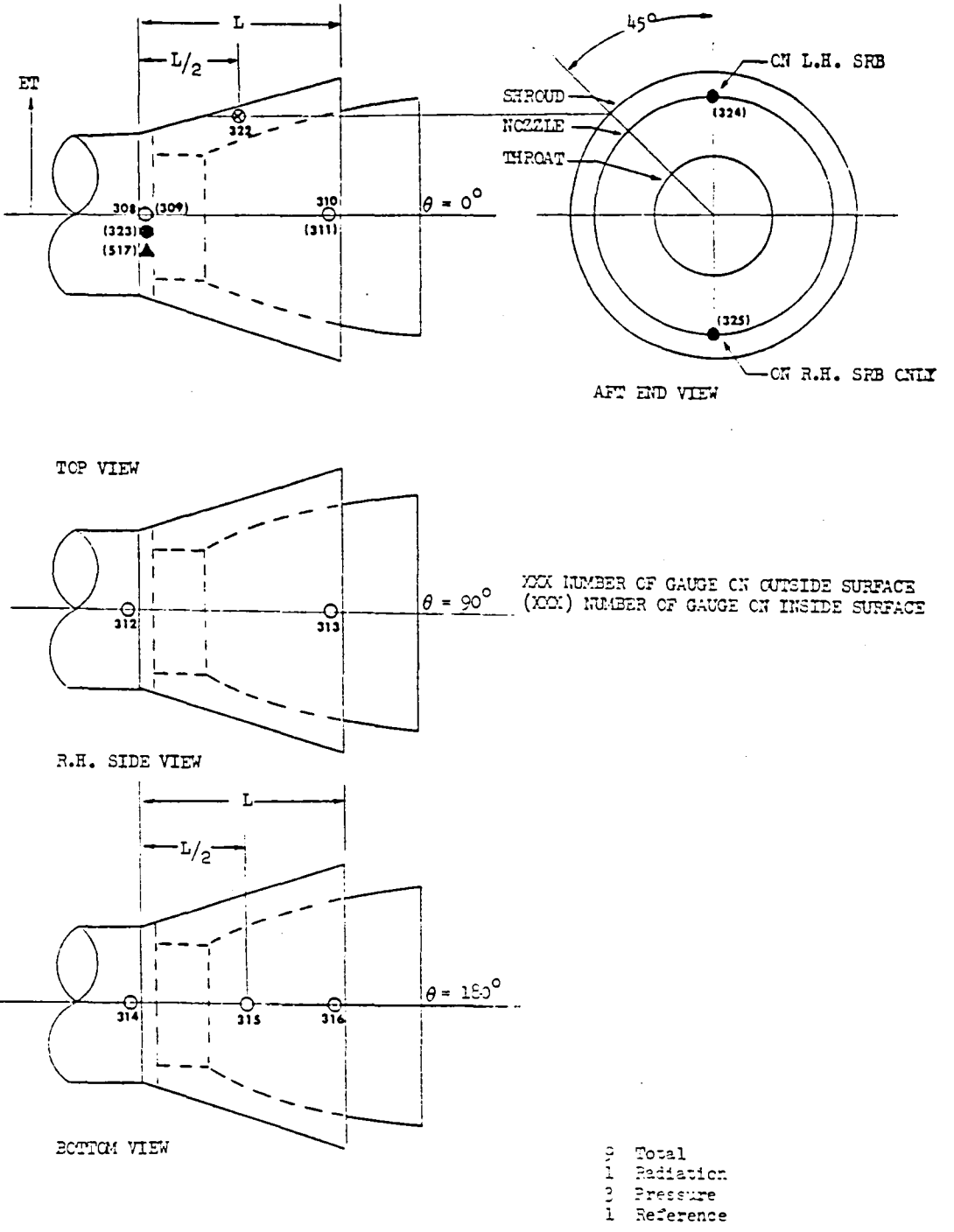

s. Left SRB Nozzle and Shroud
Figure 4. Continued.

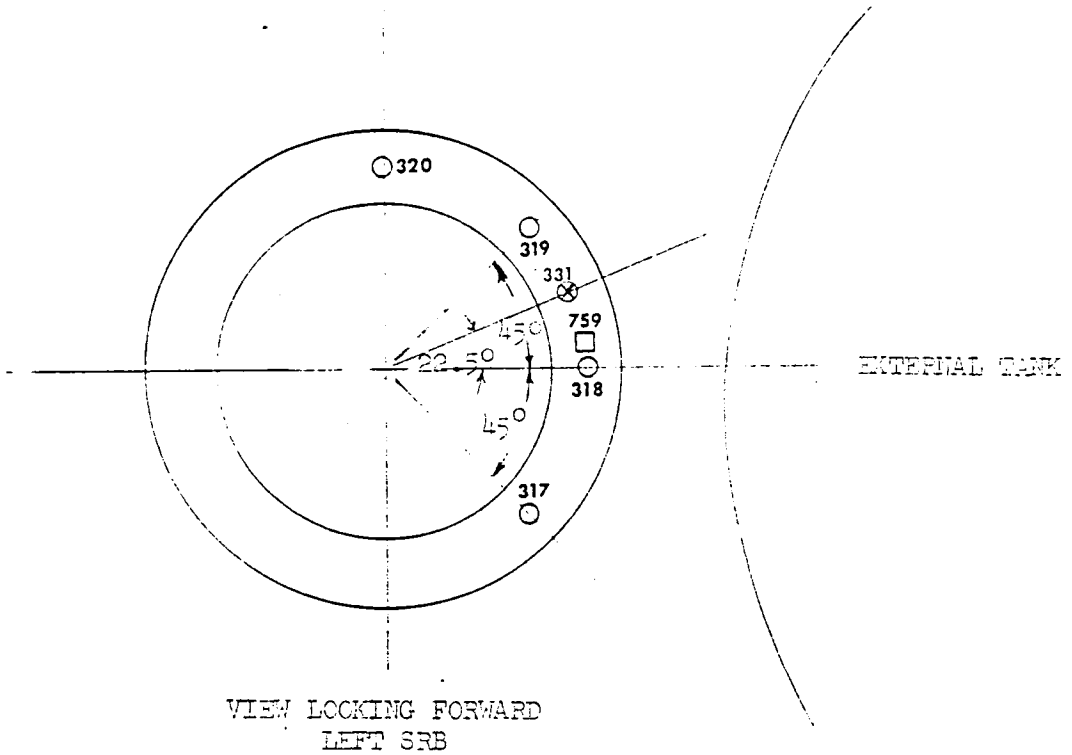

VIEW LOCKING FORWARD
LEFT SRB

4 Total
1 Radiation
1 GTP

t. Left SRB Skirt Curtain
Figure 4. Concluded.

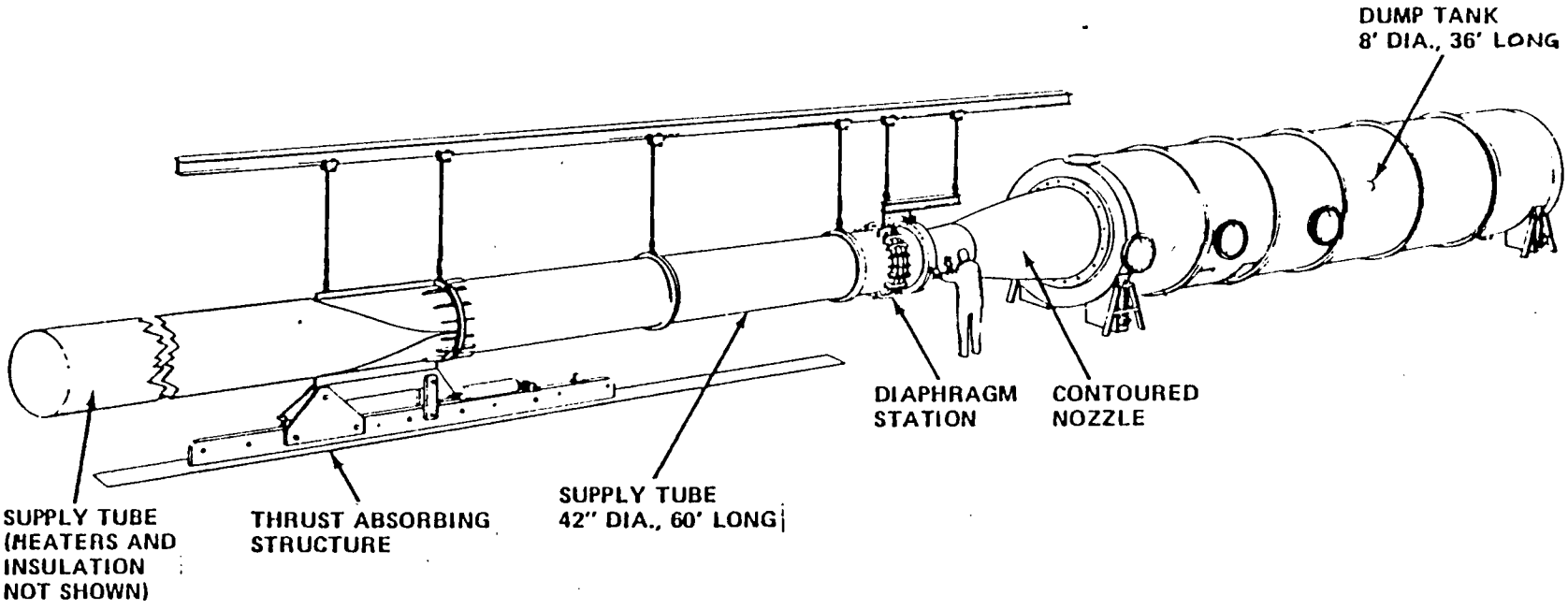

Figure 5. Short-duration Ludwieg Tube Wind Tunnel.

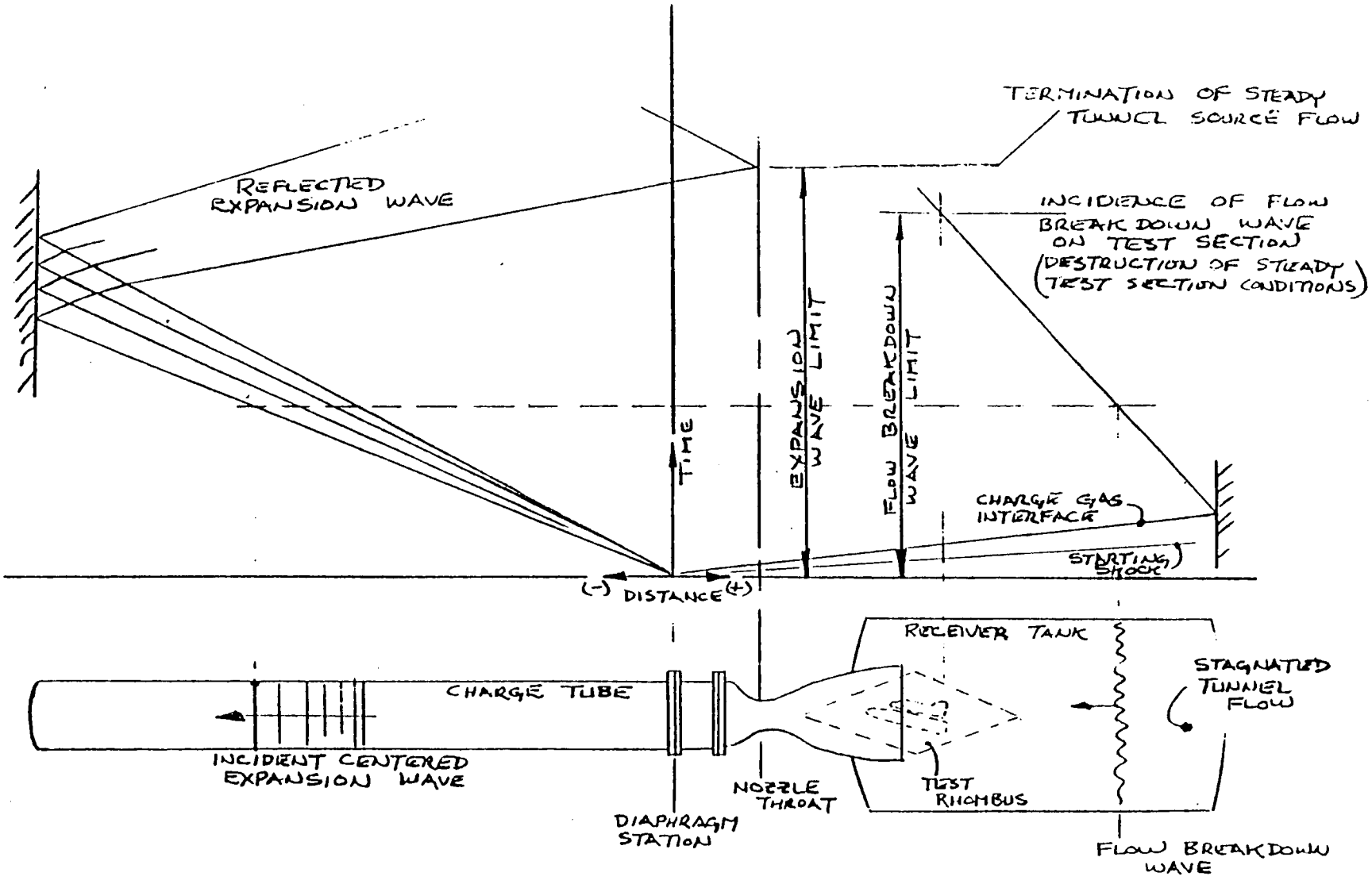

Figure 6. Wave diagram for Tube Wind Tunnel.

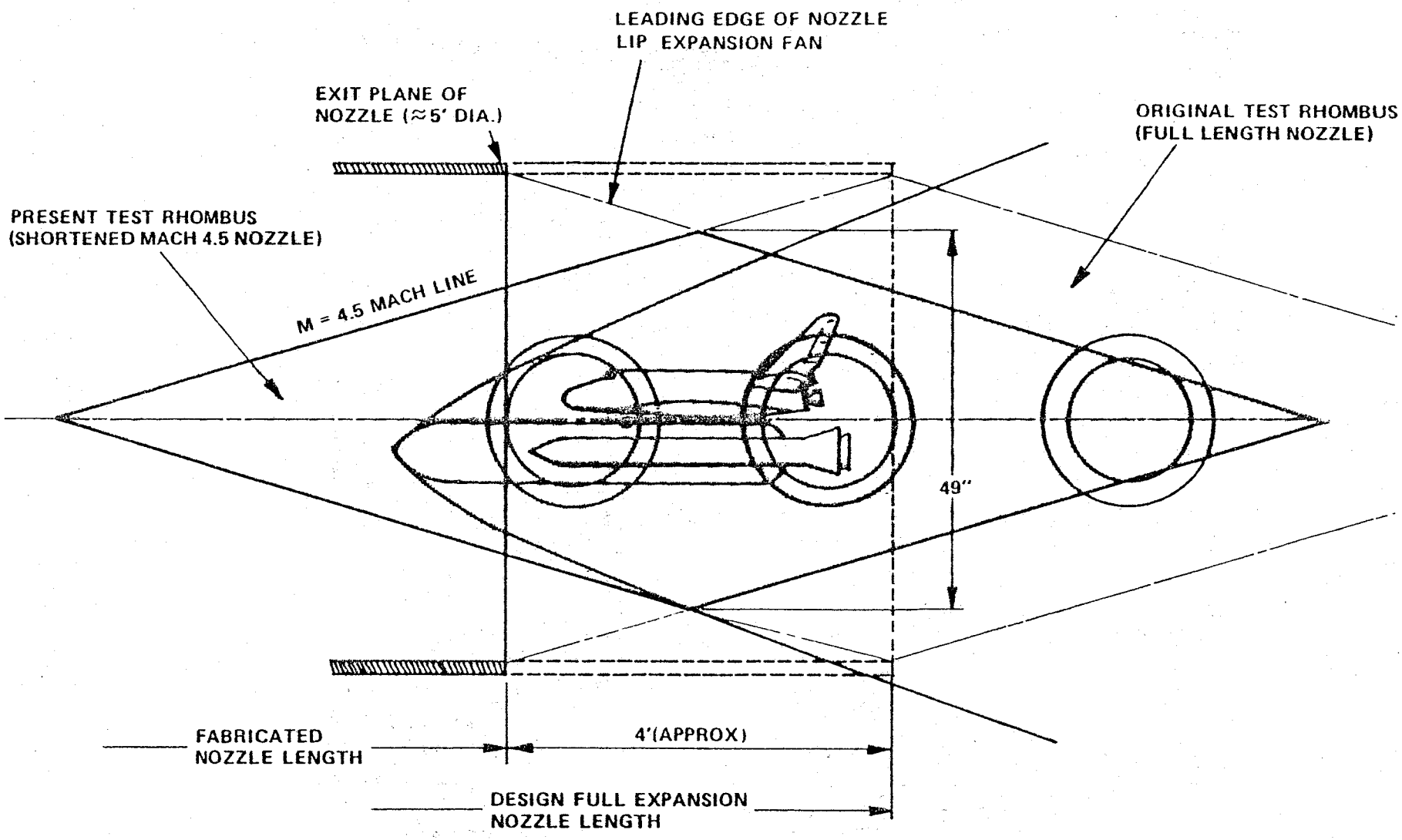

Figure 7. Ludwieg Tube Free Jet Test Rhombus for MACH 4.5 nozzle.

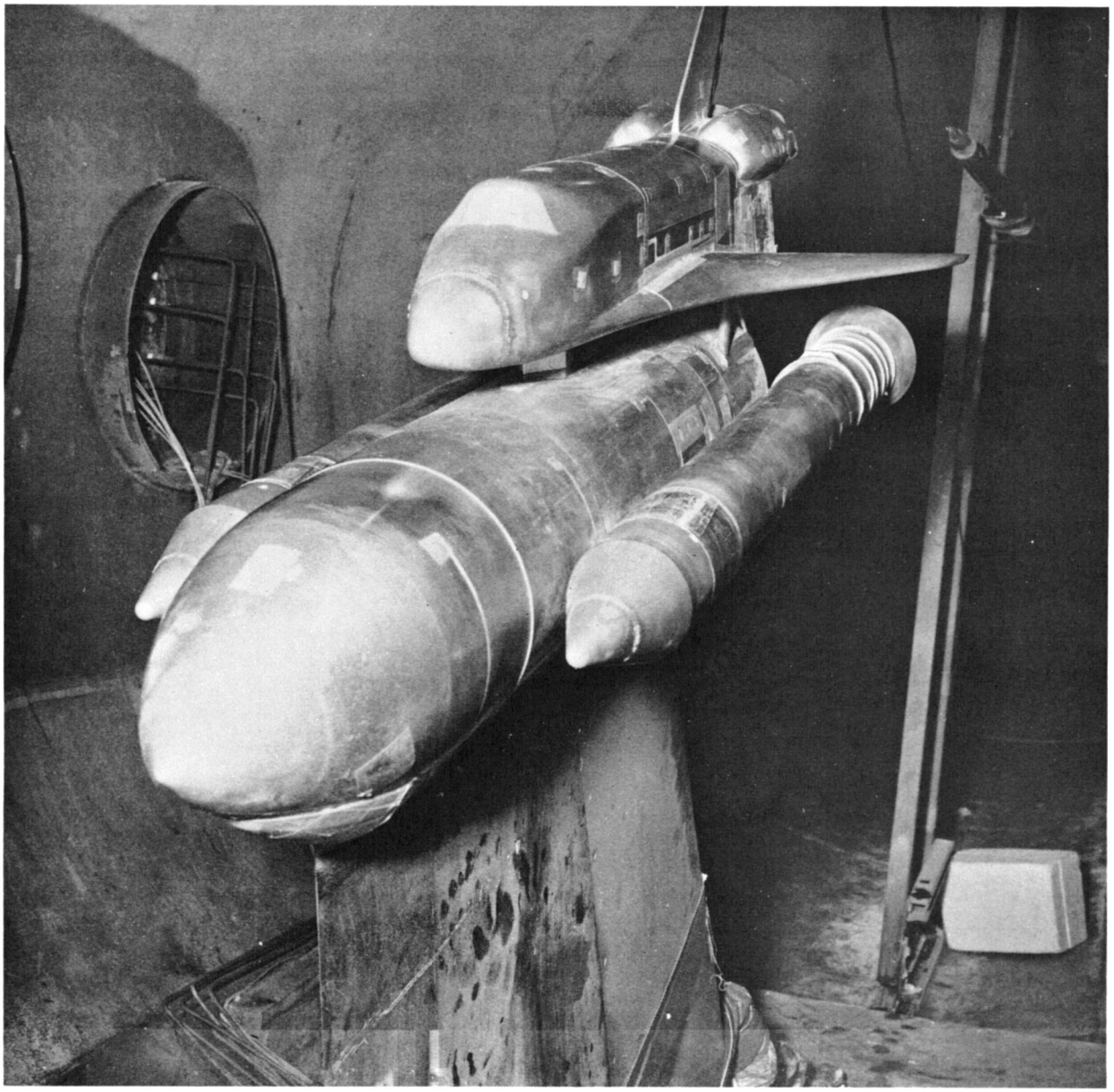

a. First Stage Configuration: Front View
Figure 8. Model 19-OTS installation in the Ludwieg Tube Wind Tunnel.

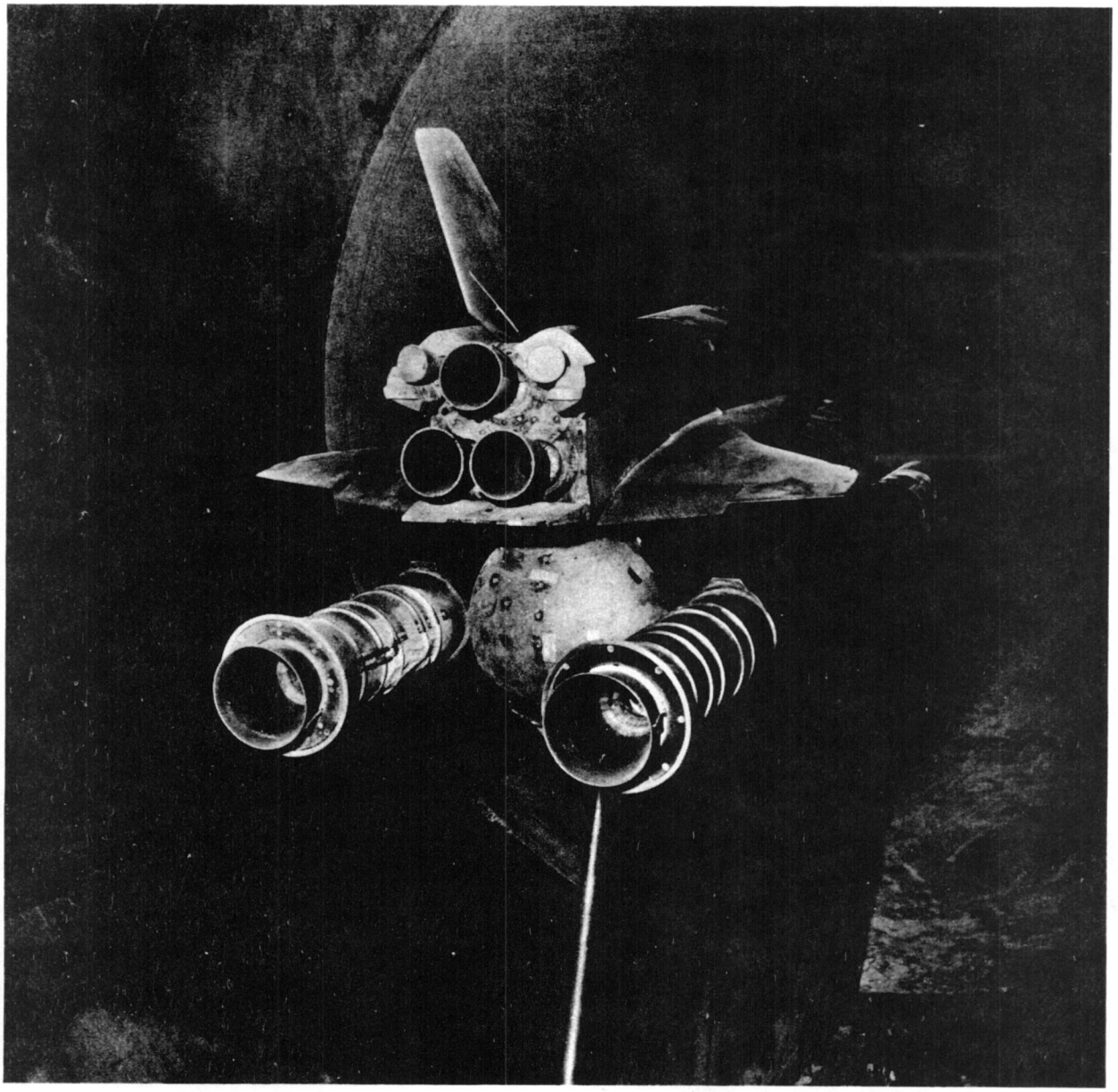

b. First Stage Configuration: Rear View
Figure 8. Continued.

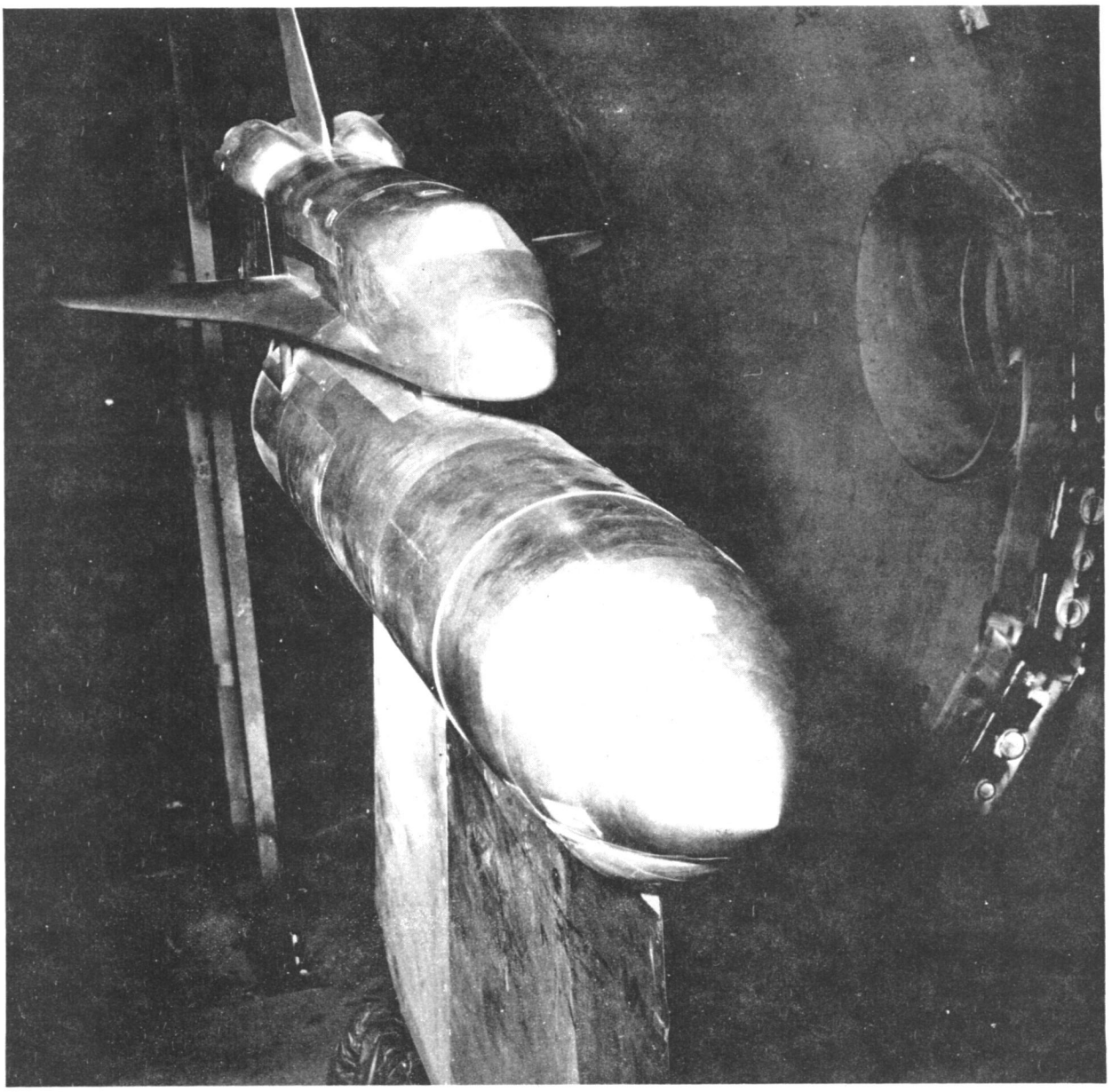

c. Second Stage Configuration: Front View
Figure 8. Continued.

d. Second Stage Configuration: Rear View
Figure 8. Concluded.

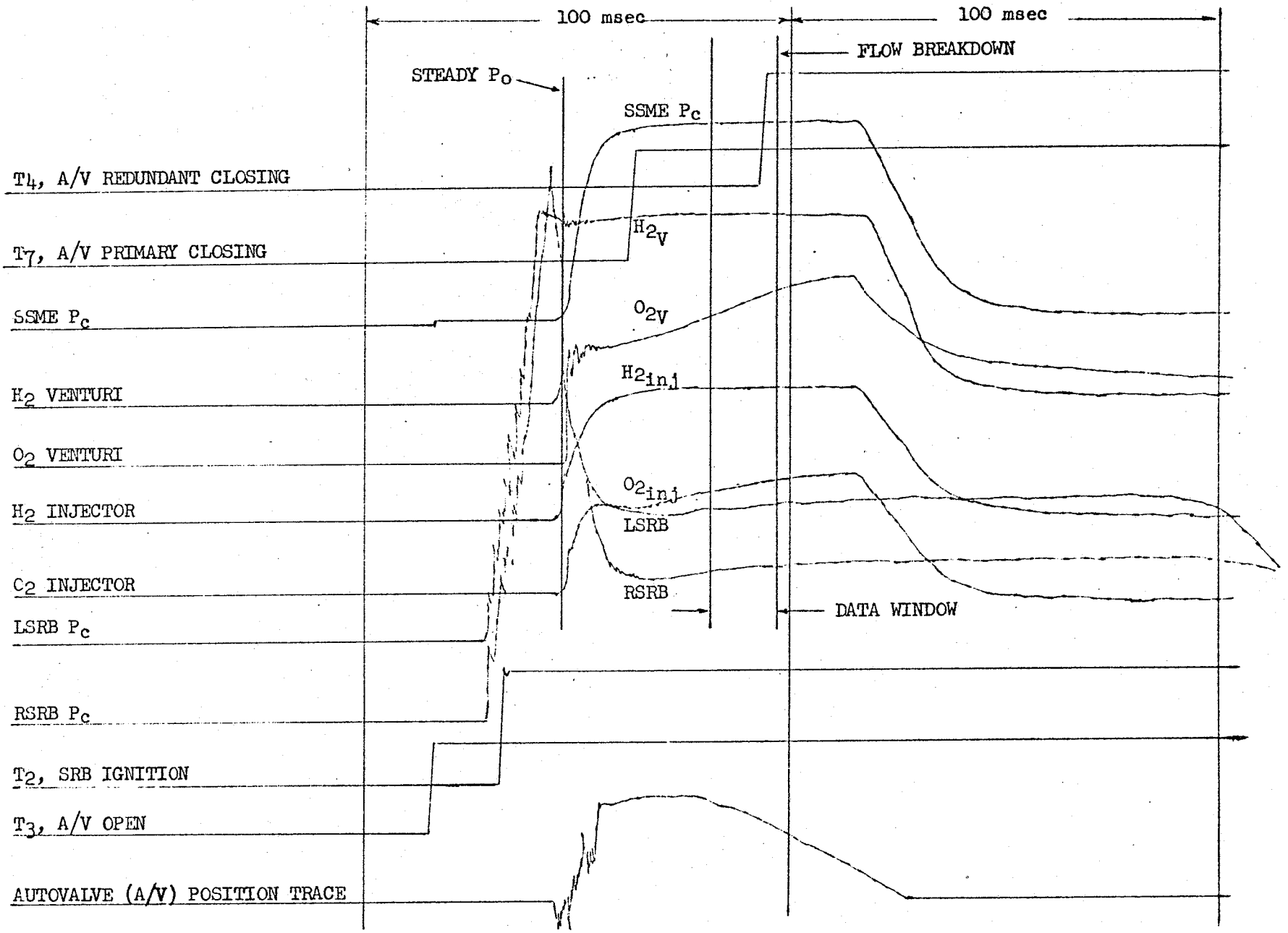

a. Model.

Figure 9. Typical operating data.

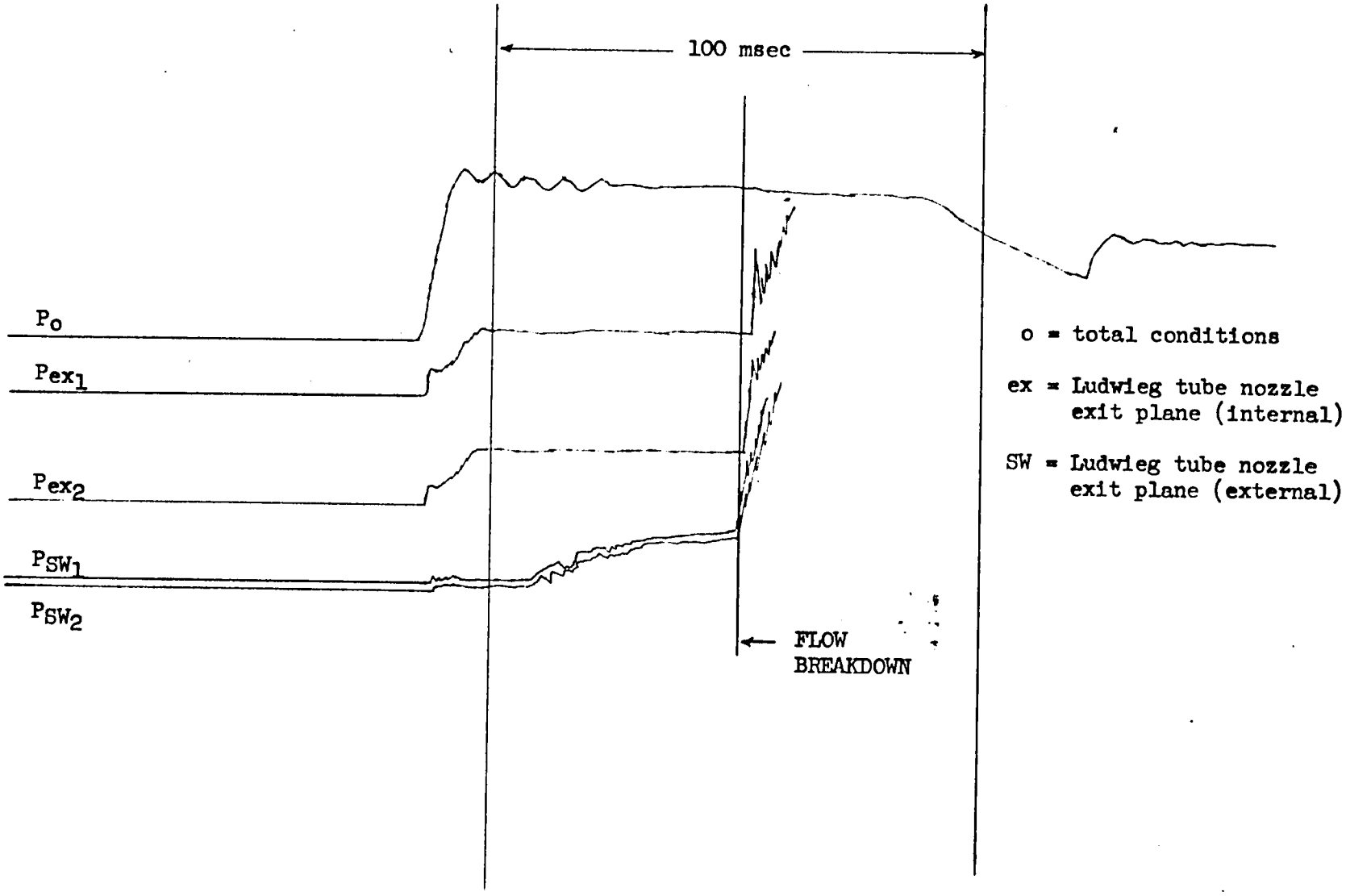

b. Tunnel

Figure 9. Concluded.

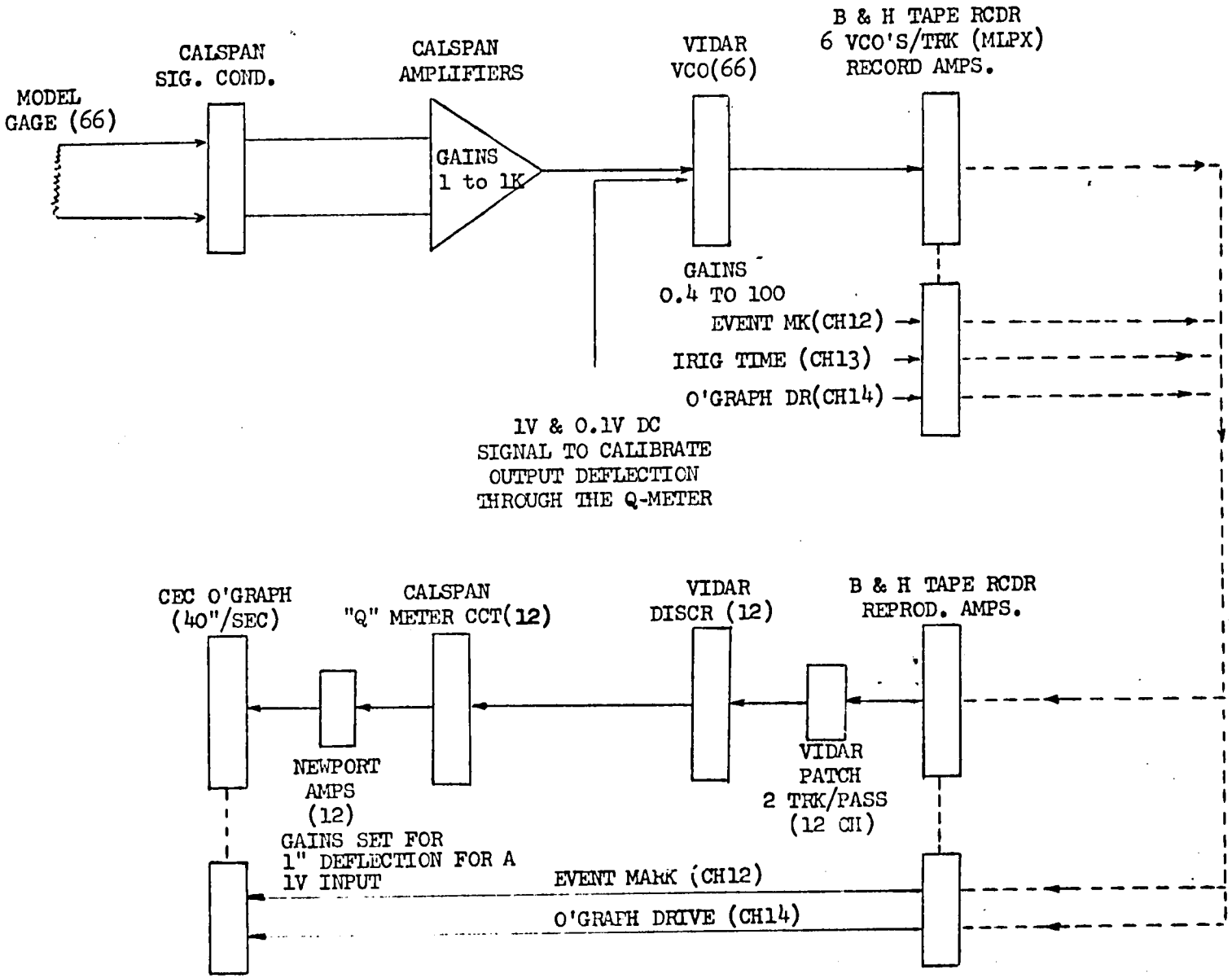

Figure 10. Vidar data acquisition and playback.

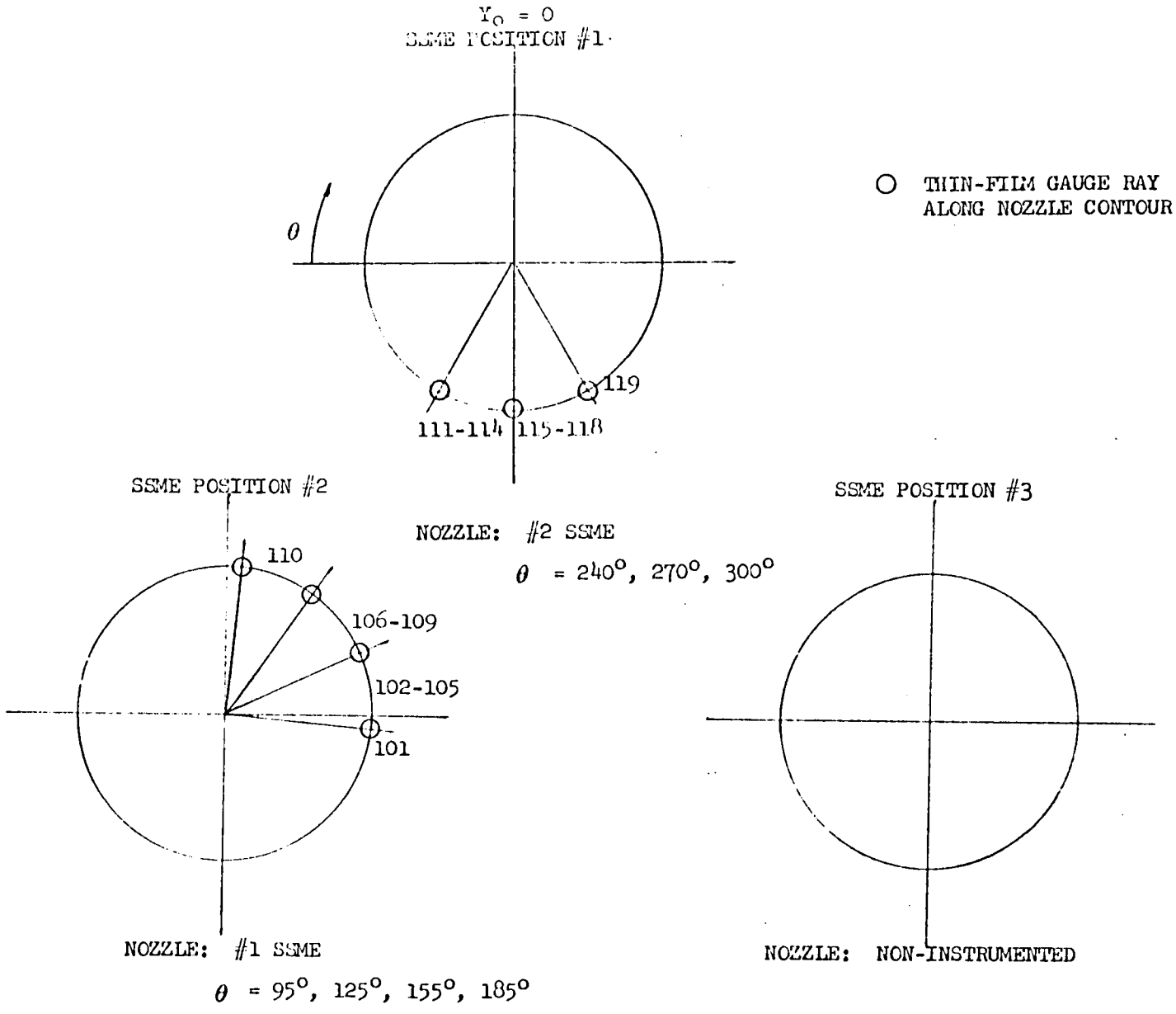

a. Without Gas Temperature Probes

Figure 11. SSME nozzle orientation.

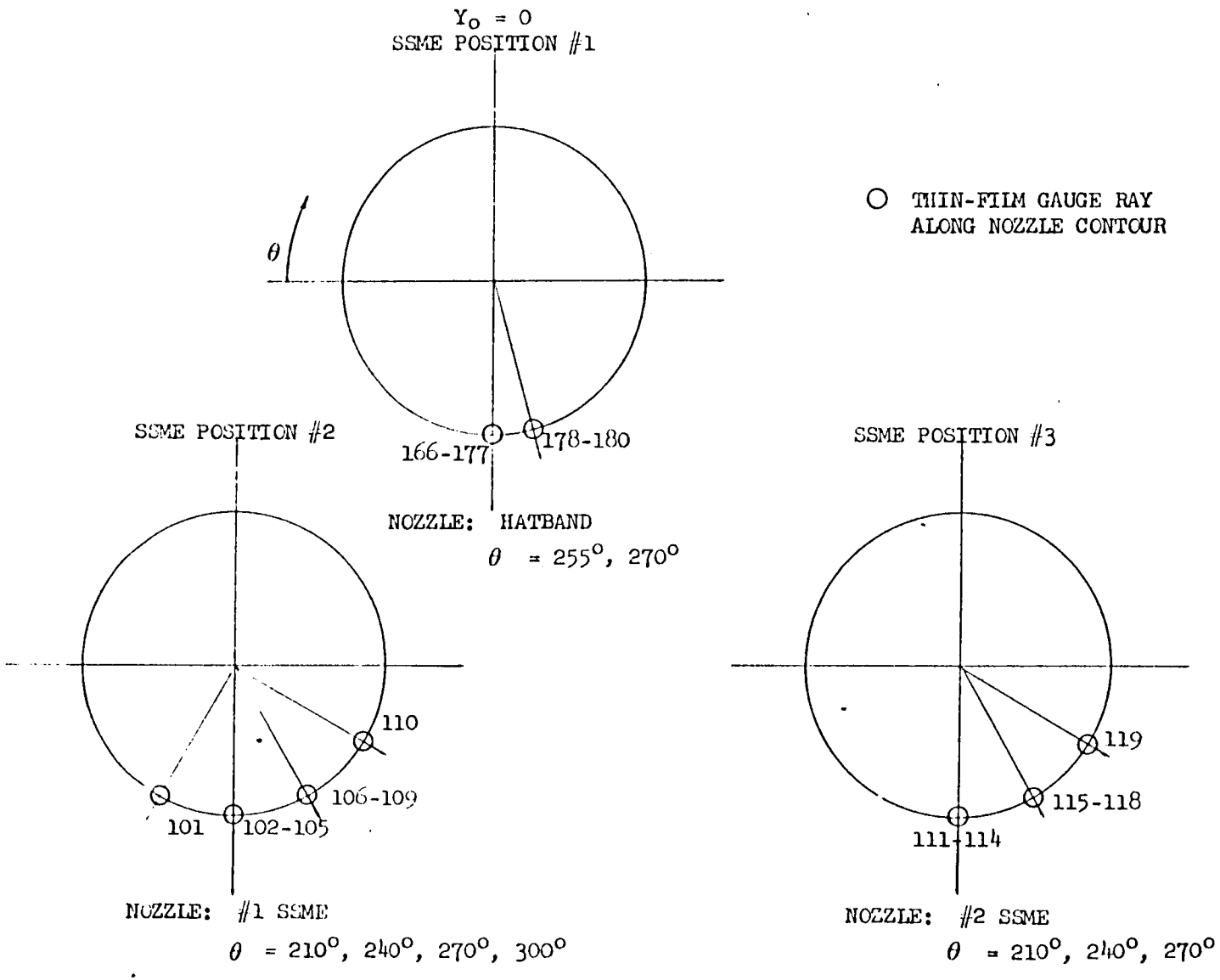

b. With Gas Temperature Probes
Figure 11. Concluded.

APPENDIX A

SOURCE DATA REFERENCES

SOURCE DATA REFERENCES

DATA	ROCKWELL INTERNATIONAL STS AERO SCIENCES DEPARTMENT	
Tabulated	Wind Tunnel Operations Group (R. S. Crowder, Supervisor)	Aeroheating Group (M. H. Harthun, Supervisor)
Oscillograph	Wind Tunnel Operations Group (R. S. Crowder, Supervisor)	Aeroheating Group (M. H. Harthun, Supervisor)

APPENDIX B

GAS RECOVERY TEMPERATURE DATA

Table B1. IH75 Data Gas Recovery Temperature (^{o}K)
Literal Data

ND - No Data

DNC - Did Not Converge

Alt. Kft.	Run #	Pos 752/155	Pos 753/146	Pos 754/148	Pos 756/234	Pos 757/235	Pos 758/236	Pos 759	Comments
130	39	DNC	2931	2890	ND	ND	ND	ND	
140	40	1544	2180	3016	ND	ND	ND	ND	
150	41	1302	1371	3419	ND	ND	ND	ND	2nd Stage Config.
160	42	1384	1192	2223	ND	ND	ND	ND	
170	43	1137	917	2027	ND	ND	ND	ND	
140	44	1440	909	1675	ND	ND	ND	ND	
140	45	511	447	701	615	ND	DNC	435	
100	46	808	829	842	863	816	948	ND	
120	47	646	684	625	1065	DNC	1373	ND	
130	48	690	617	931	DNC	558	812	ND	
140	49	453	635	818	624	529	ND	ND	
130	50	744	639	1072	735	596	1071	341	Repeat of Run 48
120	51	711	876	1023	1371	987	1870	467	
100	52	ND	882	ND	944	929	1068	583	

Literal Data

Table B2 Test IH75 Heat Transfer Coefficient (Cal/cm^2-sec-^oK)
Literal Data

BD - BAD DATA

ND - NO DATA

Alt. Kft.	Run #	Pos 752/155	Pos 753/146	Pos 754/148	Pos 756/234	Pos 757/235	Pos 758/236	Pos 759	Comments ← GTP/PRESS (POS)
130	39	1.53-03	6.97-03	4.21-03	ND	ND	ND	ND	
140	40	4.30-03	6.32-03	1.63-02	ND	ND	ND	ND	
150	41	2.18-03	6.09-03	1.06-02	ND	ND	ND	ND	2nd Stage Config.
160	42	8.98-04	5.12-03	9.17-03	ND	ND	ND	ND	
170	43	1.43-03	6.09-03	9.23-03	ND	ND	ND	ND	
140	44	2.41-03	1.14-02	7.53-03	ND	ND	ND	ND	
140	45	1.67-02	1.76-02	1.59-02	2.37-02	ND	ND	1.09-02	
100	46	4.74-02	1.66-02	1.02-02	8.58-02	4.40-02	2.09-02	ND	
120	47	5.42-02	1.55-02	1.71-02	1.66-02	ND	6.36-03	ND	
130	48	9.61-03	2.38-02	8.55-03	BD	6.02-02	7.23-03	ND	
140	49	2.26-02	1.12-02	6.63-03	2.52-02	6.75-02	ND	ND	
130	50	7.69-03	1.94-02	9.67-03	2.46-02	2.00-01	3.62-03	4.43-03	Repeat of Run 48
120	51	2.72-01	1.15-02	4.99-03	2.68-02	1.32-01	1.20-02	7.54-03	
100	52	ND	4.62-02	ND	7.67-02	7.34-01	2.79-02	1.07-01	

Table B3 IH75 Data Gas Recovery Temperature (^{o}K)
(Input Data ÷ 2)

ND - No Data

DNC - Did Not Converge

Alt. Kft.	Run #	Pos 752/155	Pos 753/146	Pos 754/148	Pos 756/234	Pos 757/235	Pos 758/236	Pos 759	Comments
130	39	1369	1093	1081	ND	ND	ND	ND	
140	40	831	967	1091	ND	ND	ND	ND	
150	41	759	772	1148	ND	ND	ND	ND	2nd Stage Config.
160	42	740	713	970	ND	ND	ND	ND	
170	43	687	603	931	ND	ND	ND	ND	
140	44	791	597	850	ND	ND	ND	ND	
140	45	421	368	500	431	ND	DNC	353	
100	46	560	565	556	549	581	593	ND	
120	47	484	485	448	648	DNC	752	ND	
130	48	476	450	605	DNC	432	525	ND	
140	49	DNC	320	472	ND	521	ND	ND	
130	50	499	469	672	507	454	701	303	Repeat of Run 48
120	51	494	587	670	755	633	893	383	
100	52	ND	590	ND	607	DNC	657	434	

Table B4. Test IH75 Heat Transfer Coefficient (Cal/cm^2-sec-^oK)
(Input Data ÷ 2)

BD - BAD DATA DNC - Did Not Converge ND - NO DATA

Alt. Kft.	Run #	Pos 752/155	Pos 753/146	Pos 754/148	Pos 756/234	Pos 757/235	Pos 758/236	Pos 759	Comments ←GTP/PRESS (POS)
130	39	2.29-03	7.81-03	4.81-03	ND	ND	ND	ND	
140	40	4.55-03	6.91-03	1.89-02	ND	ND	ND	ND	
150	41	2.33-03	6.43-03	1.22-02	ND	ND	ND	ND	2nd Stage Config.
160	42	1.14-03	5.41-03	1.01-02	ND	ND	ND	ND	
170	43	1.70-03	6.31-03	1.02-02	ND	ND	ND	ND	
140	44	2.64-03	1.16-02	8.19-03	ND	ND	ND	ND	
140	45	1.26-02	1.02-01	1.62-02	1.12-01	ND	ND	1.10-02	
100	46	3.96-02	1.54-02	1.06-02	8.32-01	3.06-02	2.84-02	ND	
120	47	3.37-02	1.57-02	2.41-02	2.25-02	ND	7.88-03	ND	
130	48	1.32-02	2,47-02	8.95-03	BD	8.31-02	1.11-02	ND	
140	49	DNC	1.47-02	1.41-03	ND	2.31-02	ND	ND	
130	50	1.14-02	1.89-02	9.89-03	3.84-02	3.76-01	3.19-03	4.52-03	Repeat of Run 48
120	51	7.88-01	1.18-02	4.82-03	3.67-02	2.28-01	1.32-02	6.85-03	
100	52	ND	4.49-02	ND	1.25-01	DNC	3.10-02	1.03-01	

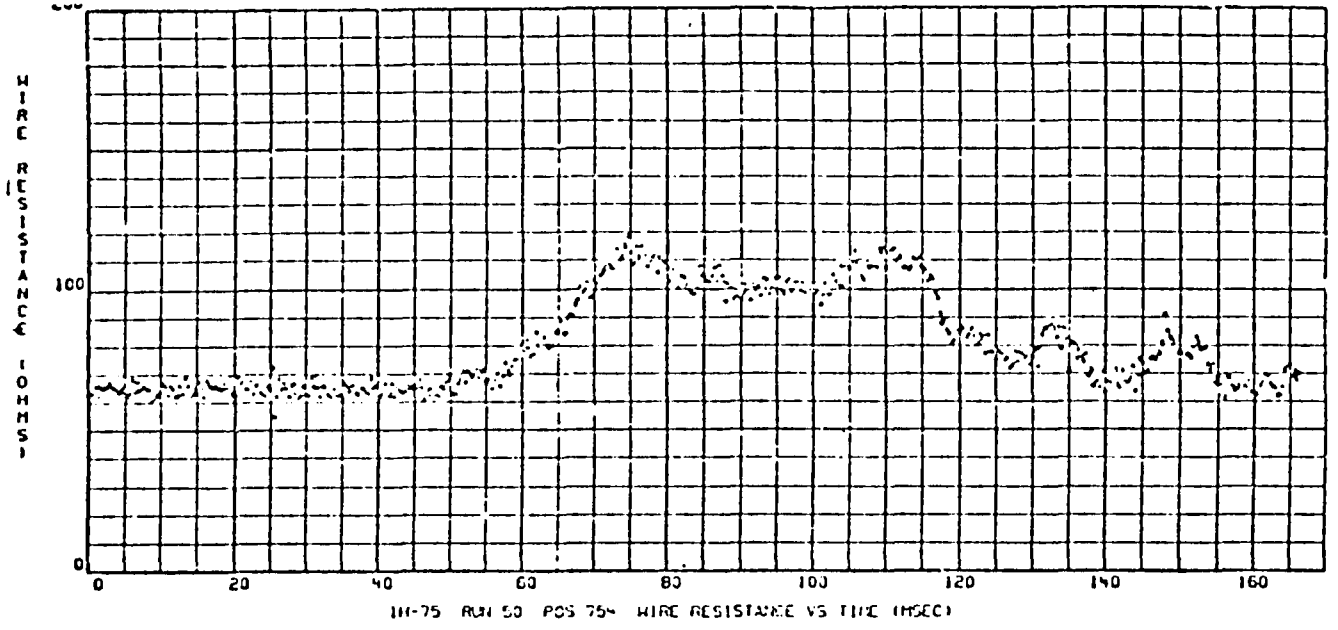

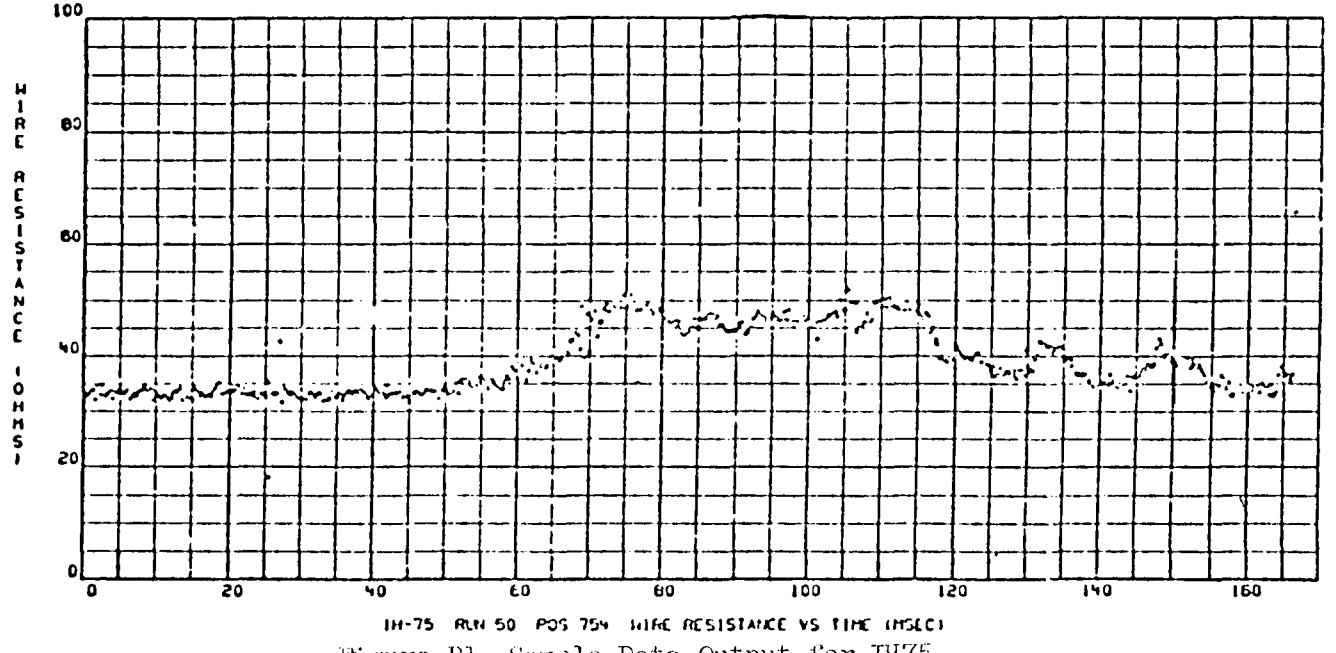

Figure B1 Sample Data Output for IH75

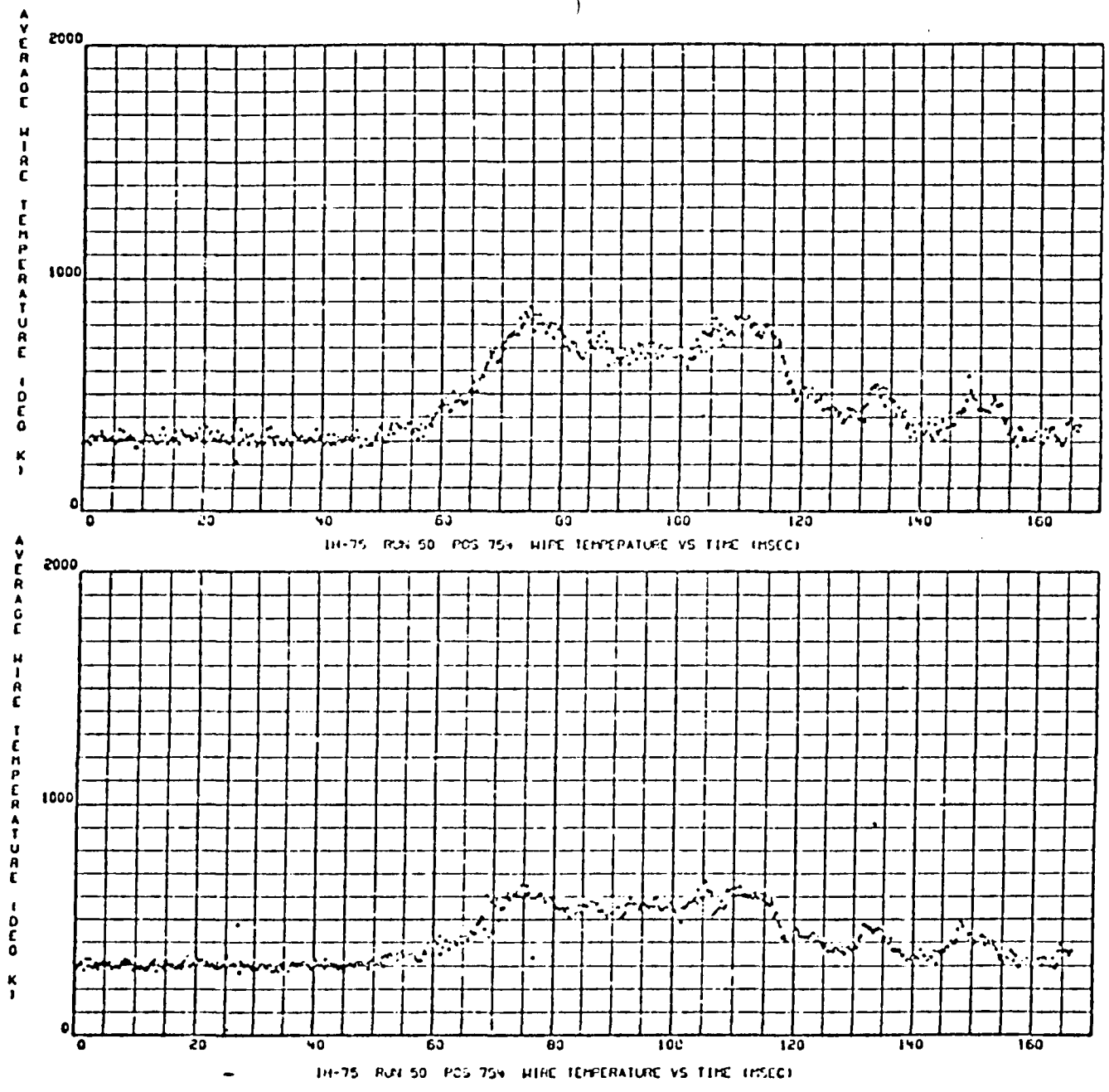

Figure B2 Sample Data Output for IH75

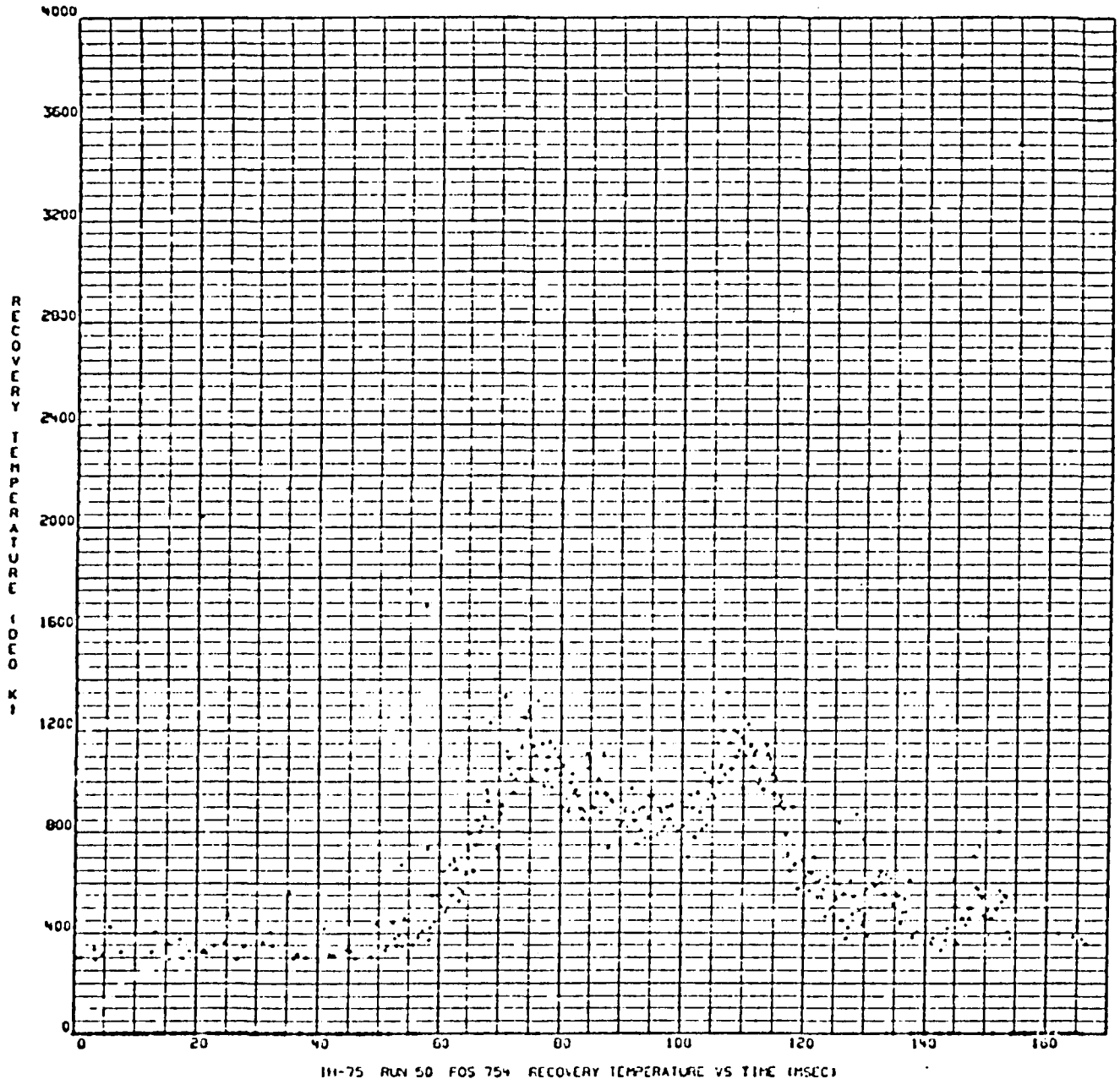

Figure B3 Sample Data Output for III75

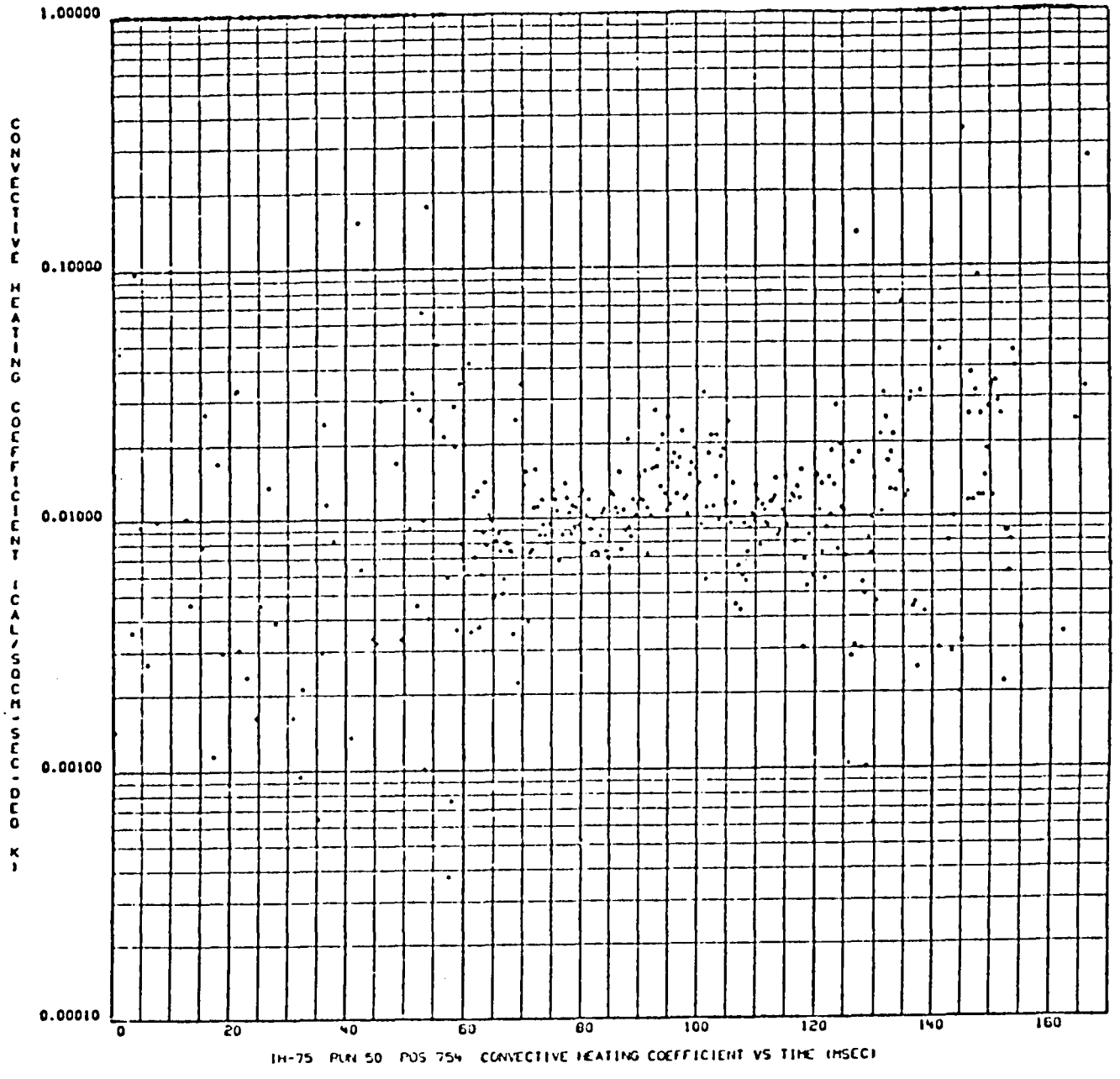

Figure B4 Sample Data Output for IH75

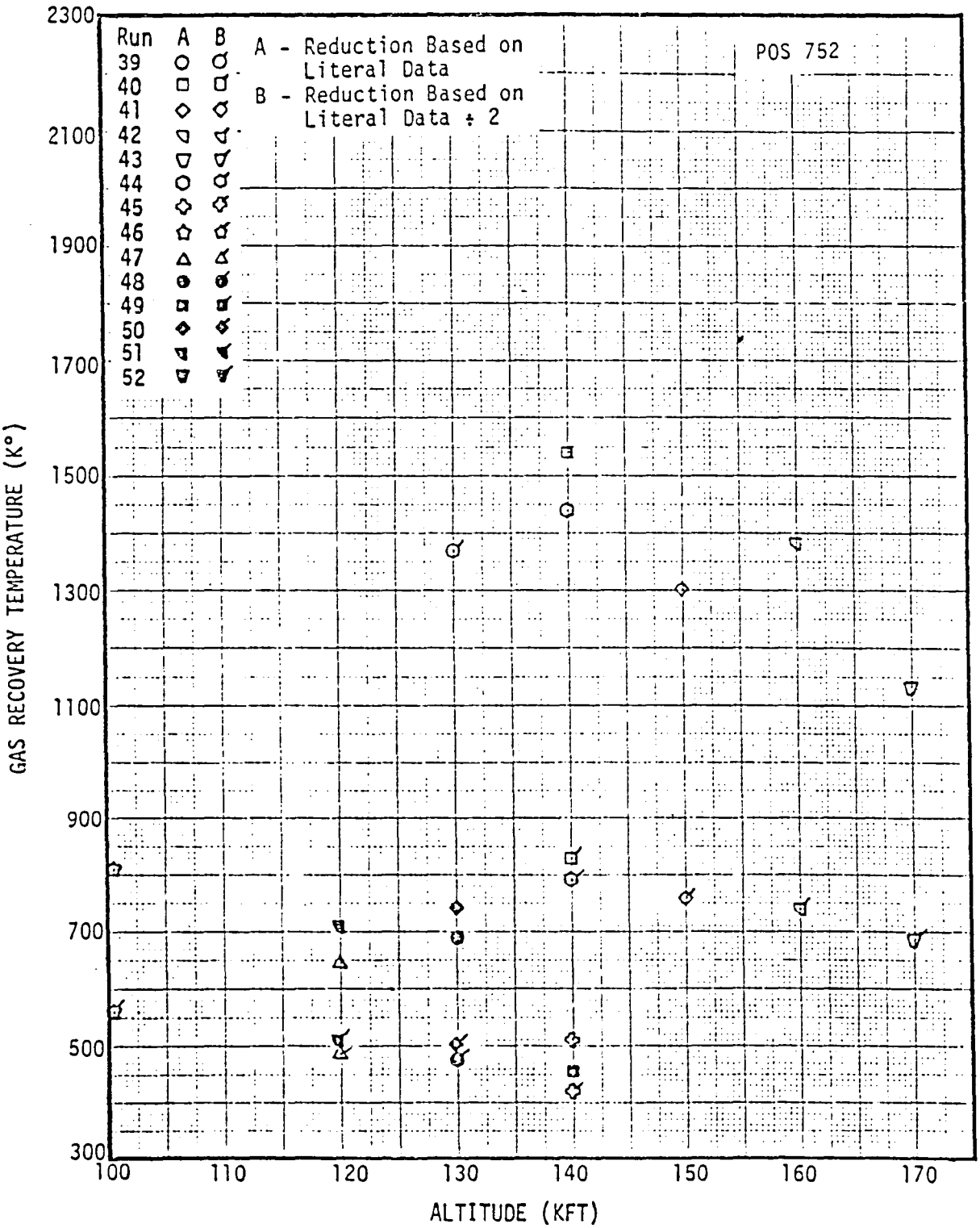

Figure B5 Test IH75 Gas Recovery Temperature Measurements on 19-OTS Space Shuttle Model at Position 752

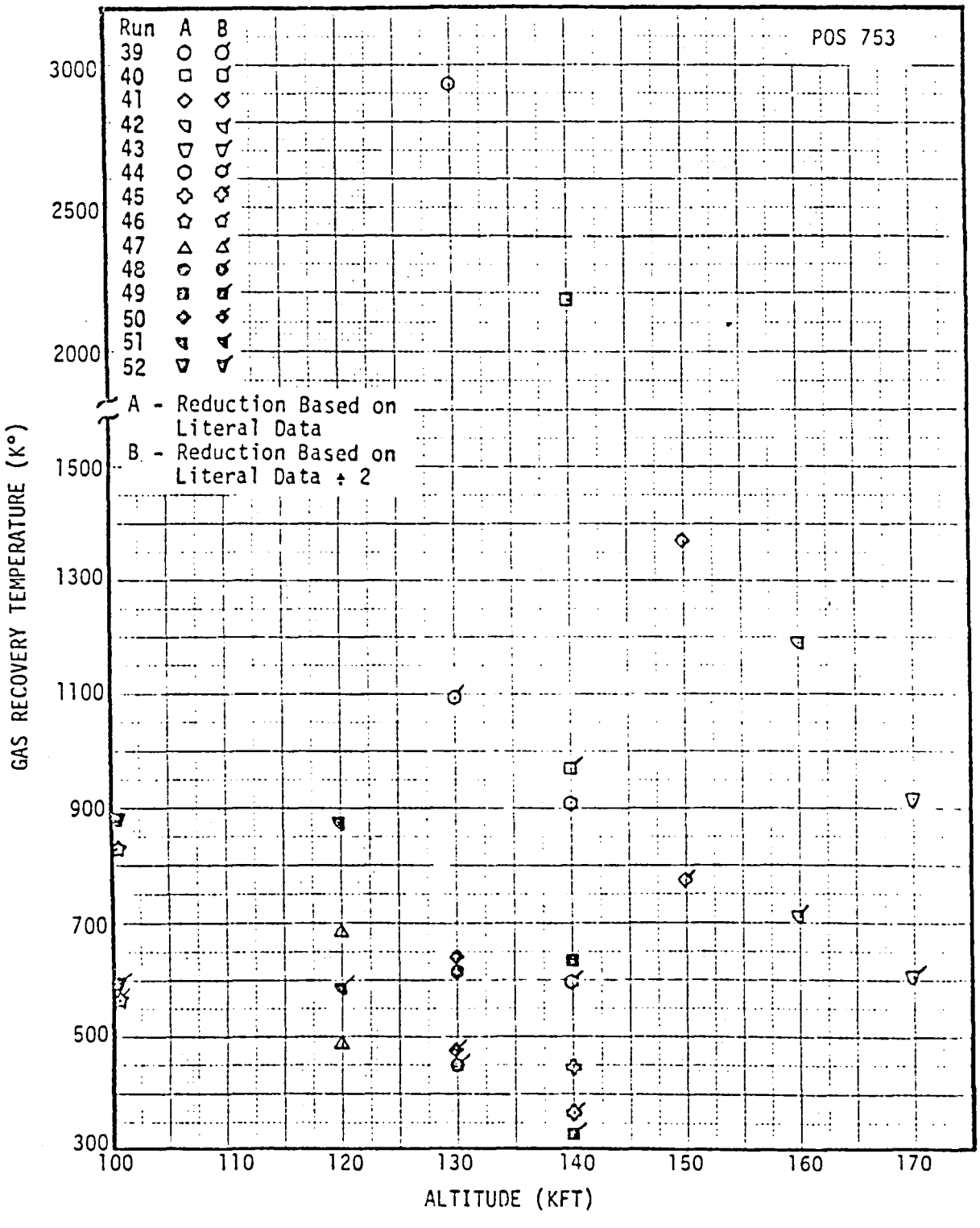

Figure B6 Test IH75 Gas Recovery Temperature Measurements on 19-OTS Space Shuttle Model at Position 753

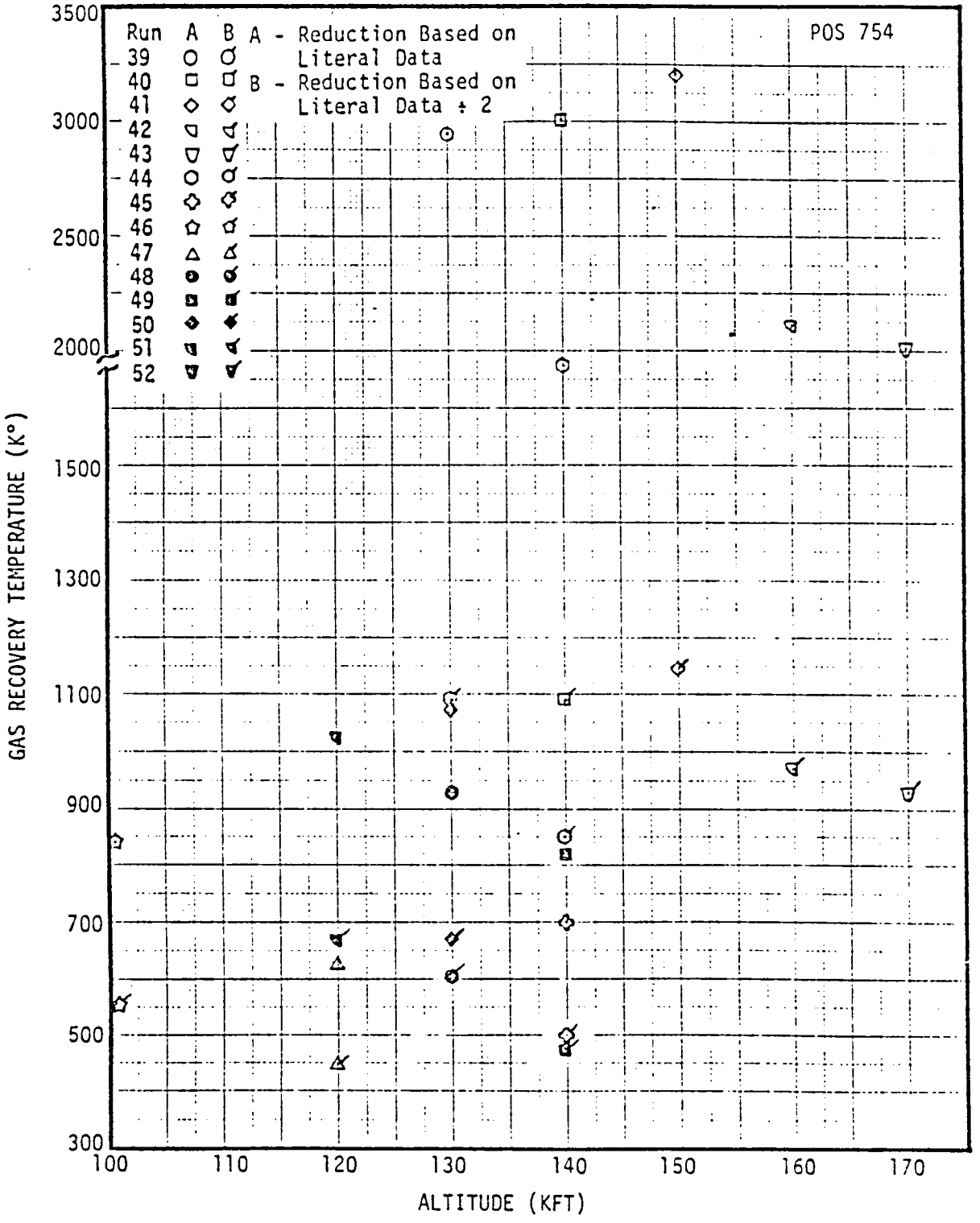

Figure B7 Test IH75 Gas Recovery Temperature Measurements on 19-OTS Space Shuttle Model at Position 754

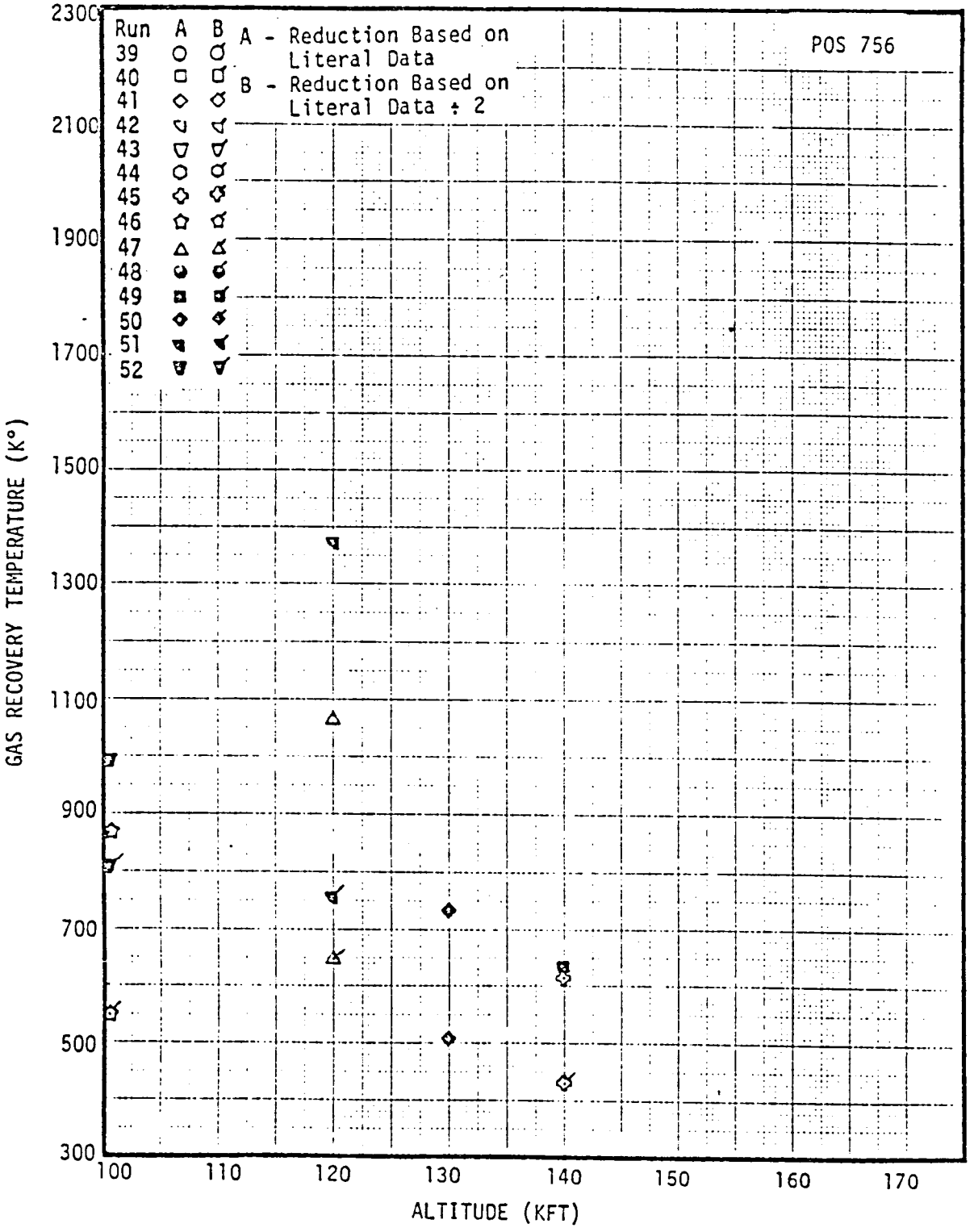

Figure B8 Test IH75 Gas Recovery Temperature Measurements on 19-OTS Space Shuttle Model at Position 756

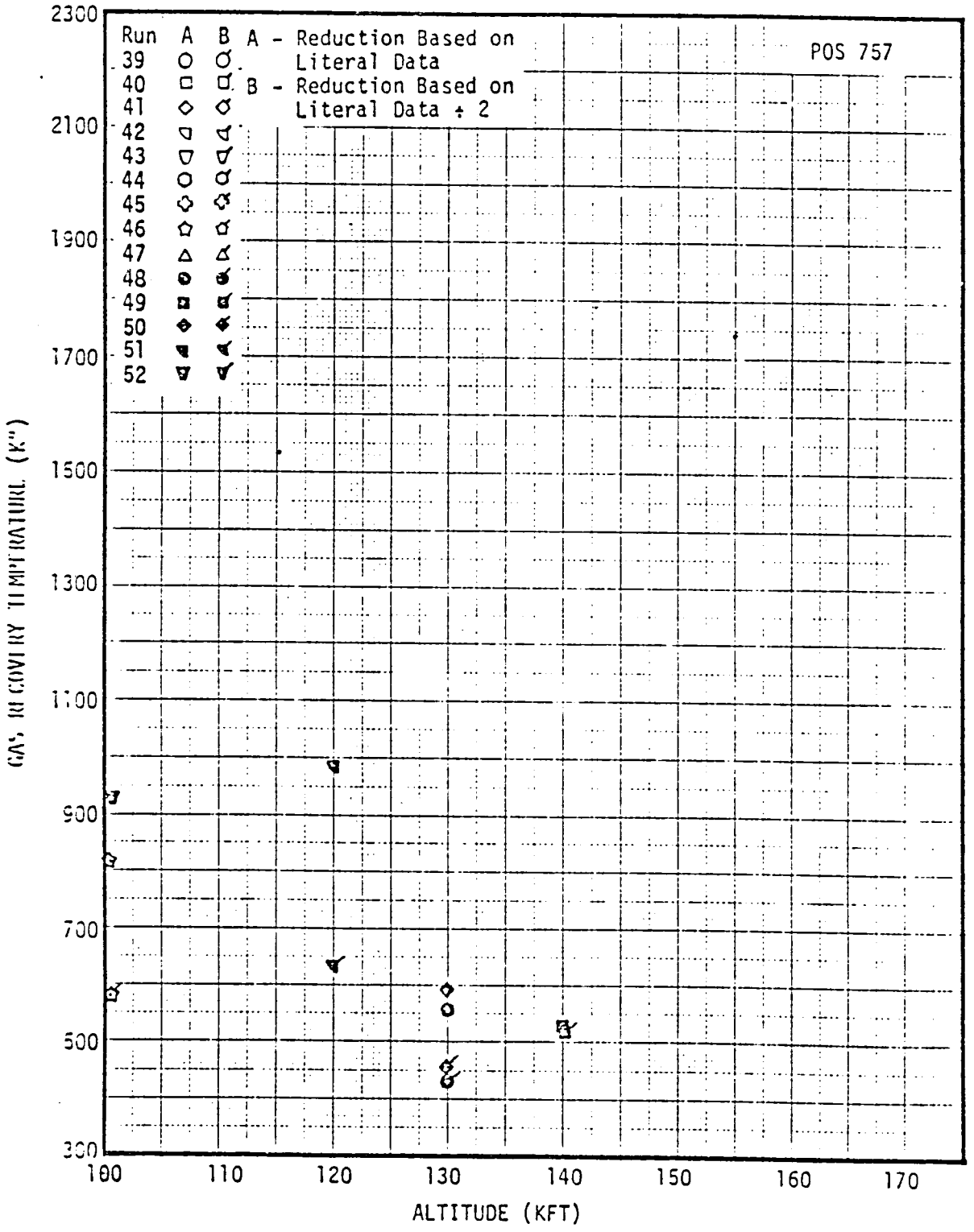

Figure B9 Test IH75 Gas Recovery Temperature Measurements on 19-OTS Space Shuttle Model at Position 757

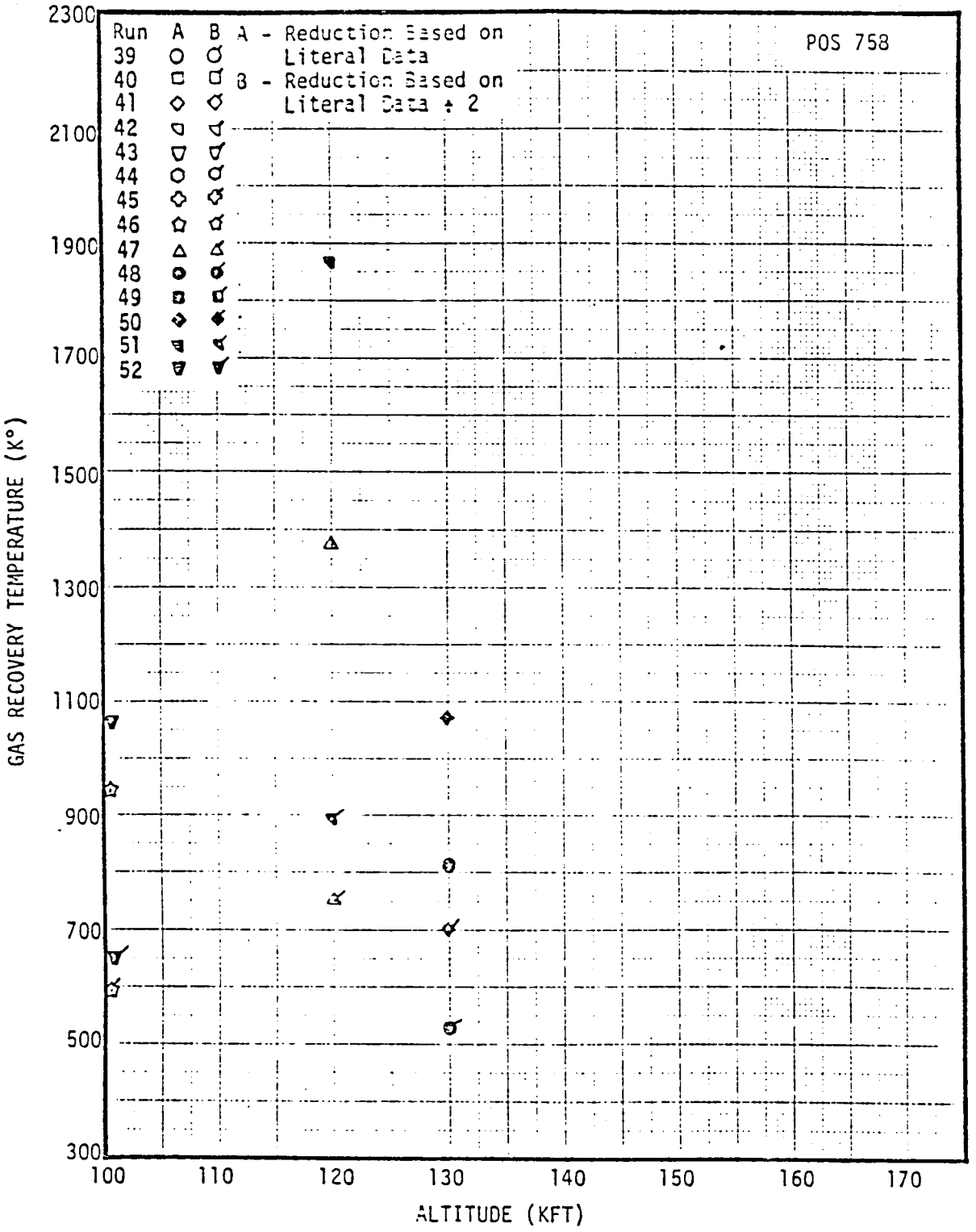

Figure B10 Test IH75 Gas Recovery Temperature Measurements on 19-OTS Space Shuttle Model at Position 758

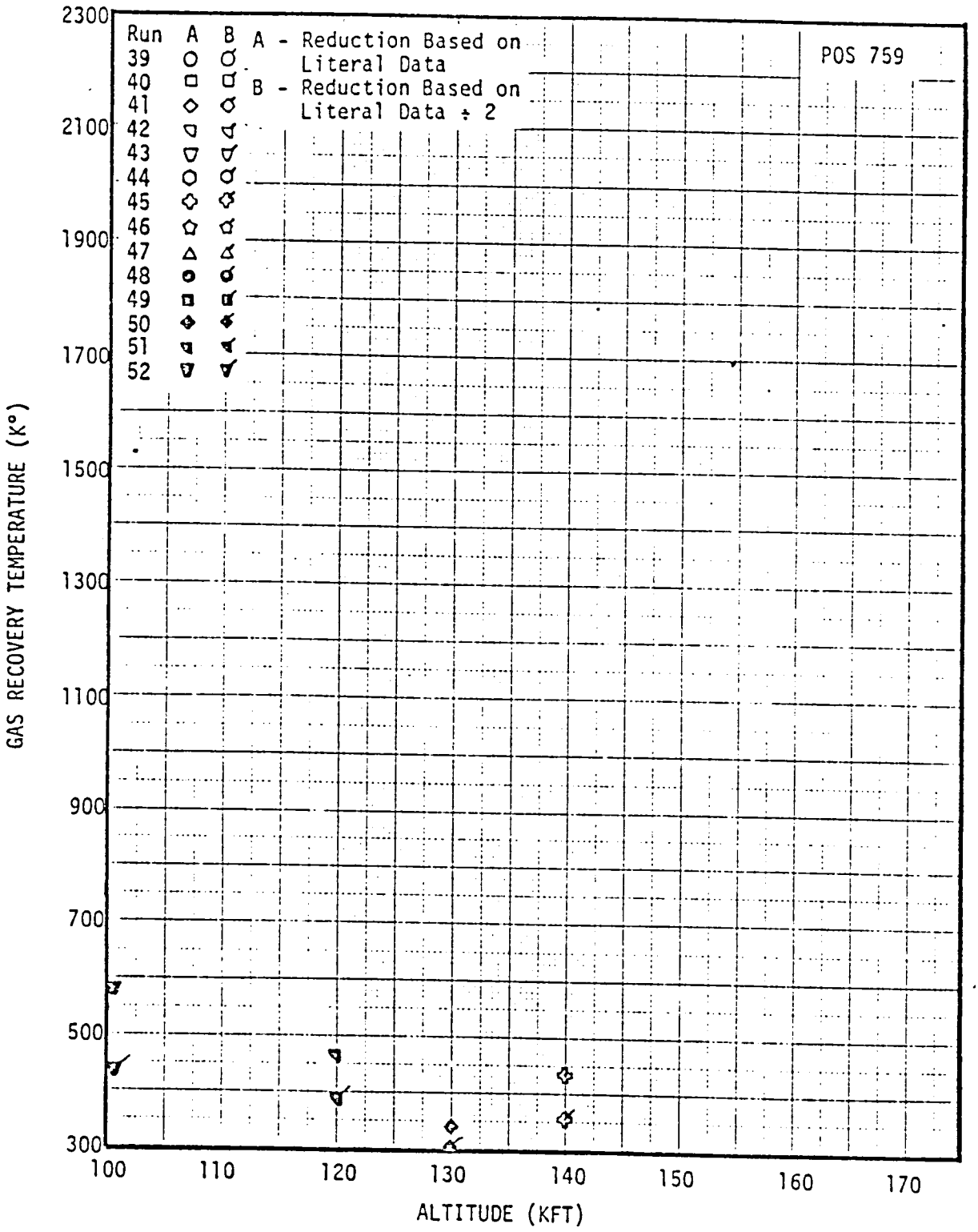

Figure B11 Test IH75 Gas Recovery Temperature Measurements on 19-OTS Space Shuttle Model at Position 759

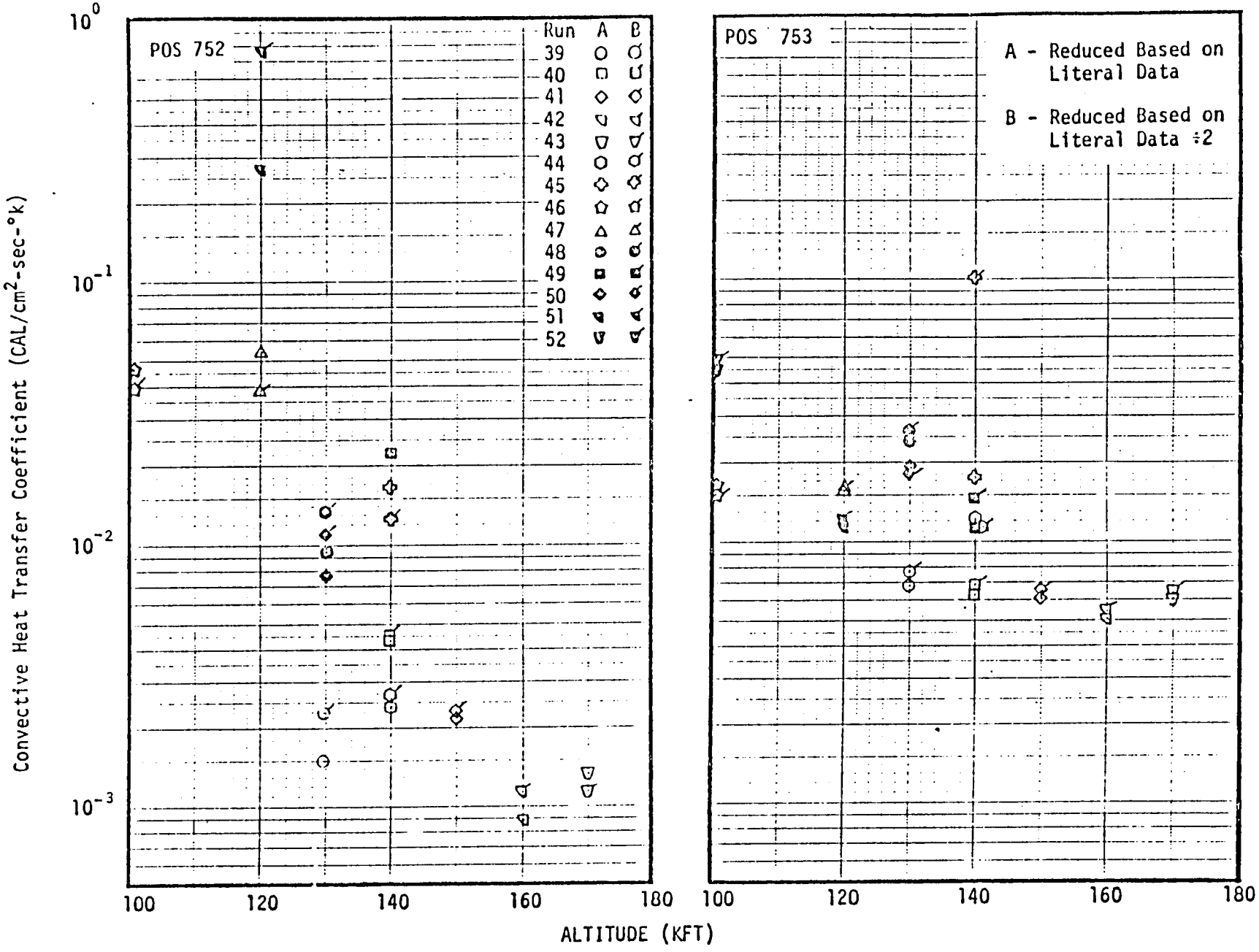

Figure B12 Test IH75 Convective Heat Transfer Coefficient Measurements on 19-OTS Space Shuttle Model

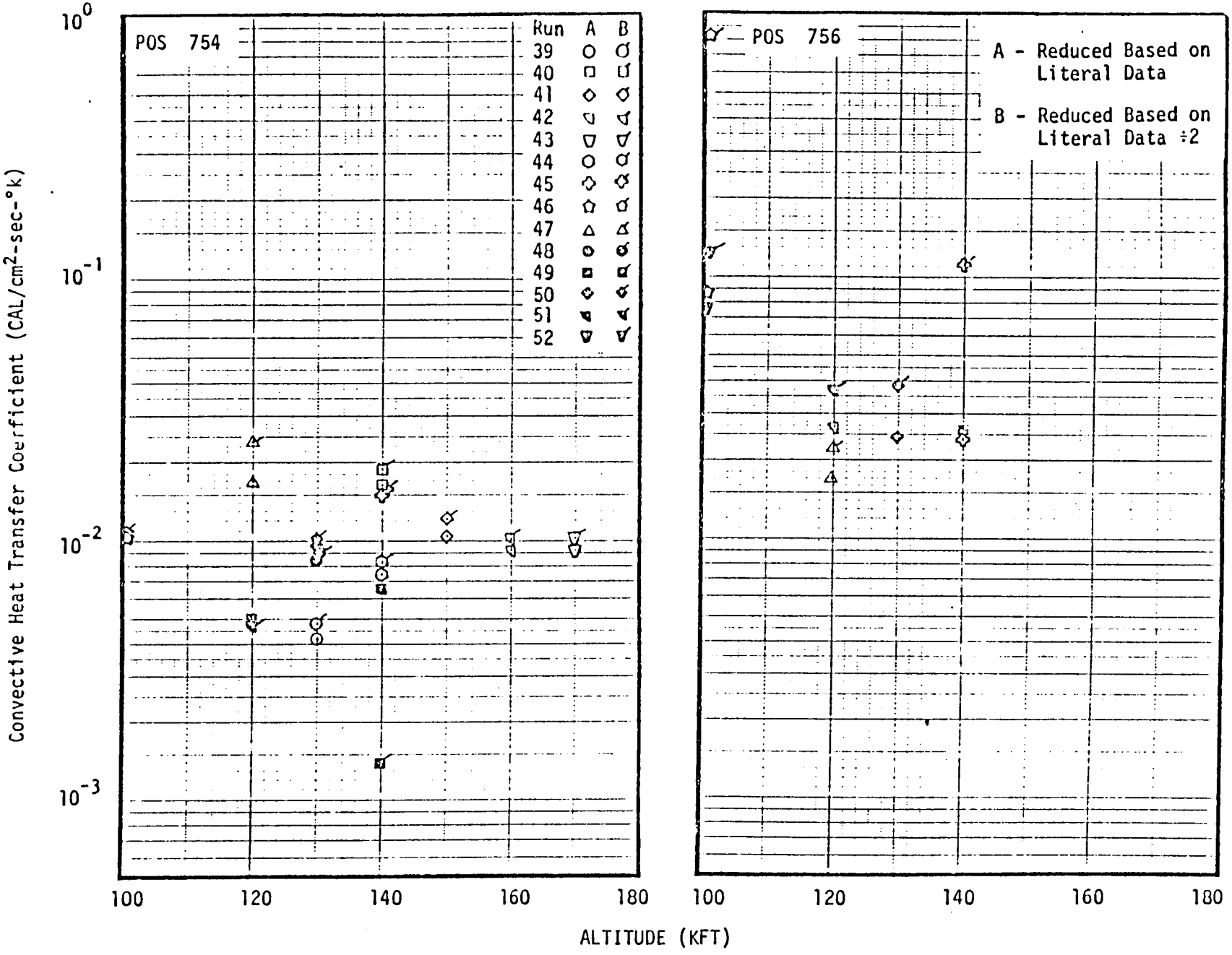

Figure B13 Test IH75 Convective Heat Transfer Measurements on 19-OTS Space Shuttle Model

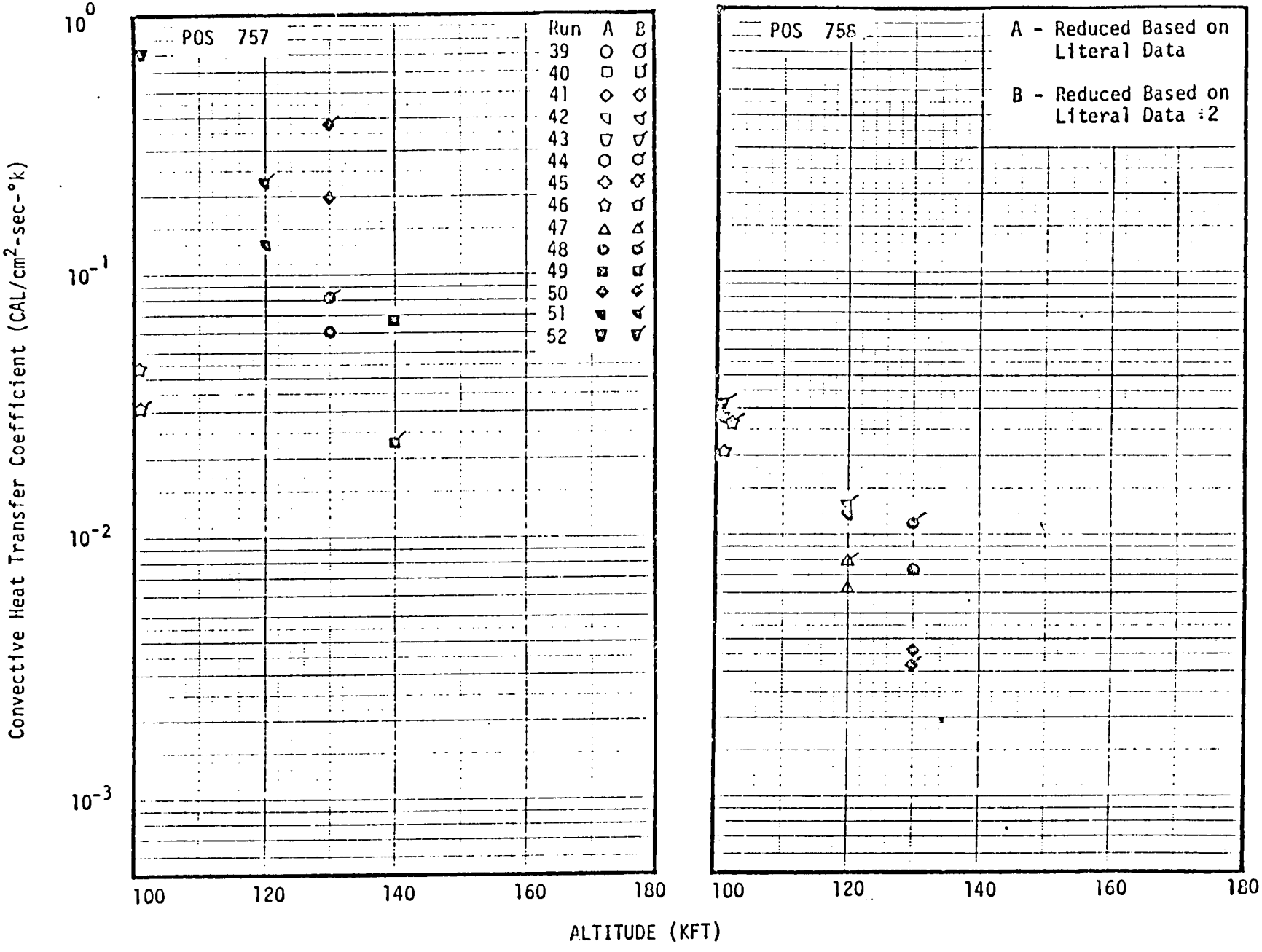

Figure B14 Test IH75 Convective Heat Transfer Coefficient Measurements on 19-OTS Space Shuttle Model

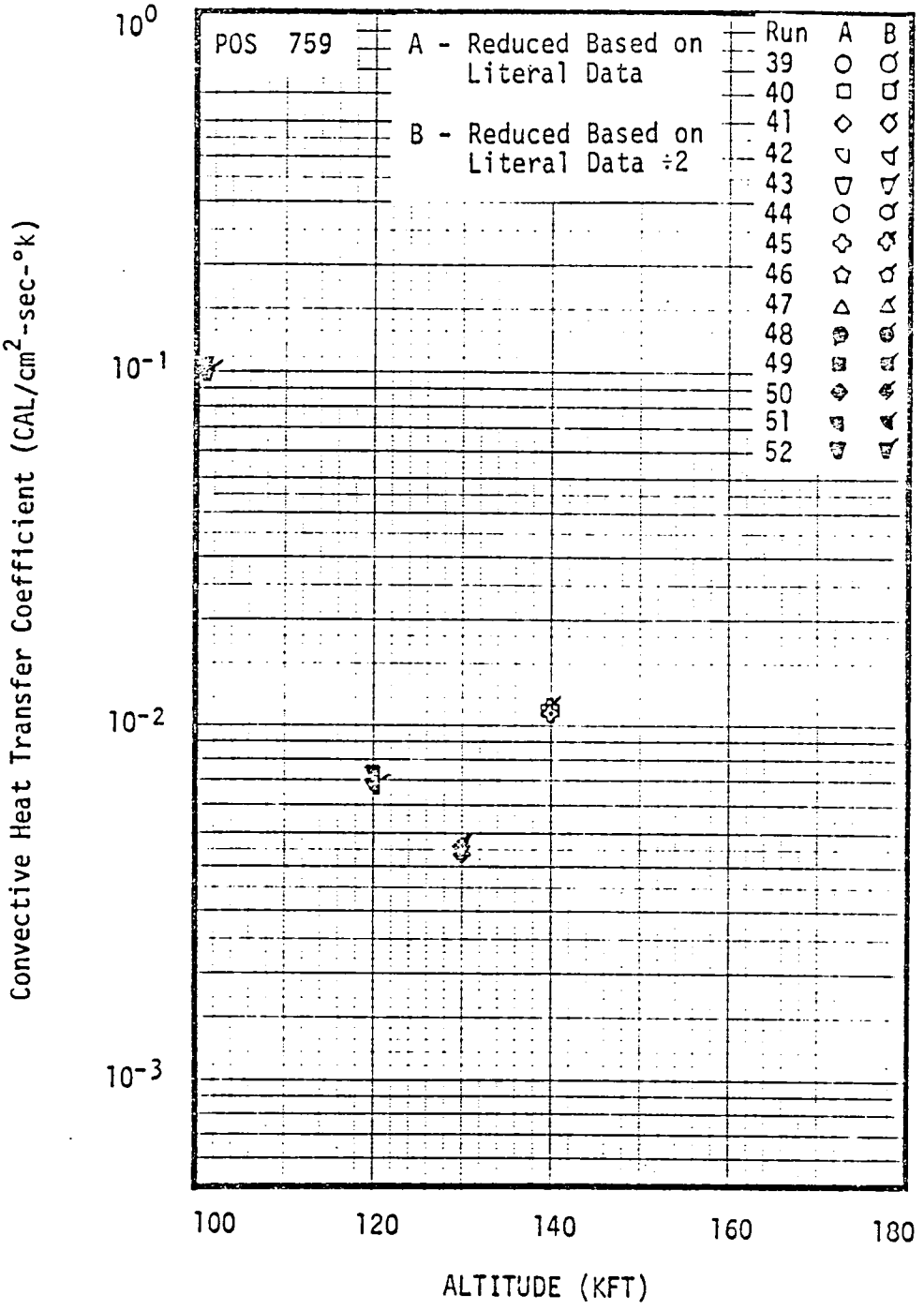

Figure B15 Test IH75 Convective Heat Transfer Coefficient Measurements on 19-OTS Space Shuttle Model

APPENDIX C

FM DATA TAPE CORRECTION

FM TAPE DATA CORRECTION

The Rockwell-supplied FM-Multiplex Tape Recorder System was used to record heat-transfer gauge and gas temperature probe data. The outputs of the thin-film heat transfer gauges (which are proportional to the surface temperature of the gauge) were recorded on the FM tape. After a test run, the tape was played back through an analog $\dot{q}$-meter and the signals proportional to heat transfer rate were recorded on an oscillograph. It was noted, that the heat transfer data exhibited a droop that implied a severely limited DC response of the system. Only after a careful review of the entire data acquisition system was it discovered that the cause of the droop was not in the cabling, the amplifiers or the FM Multiplex system, but rather in the circuitry powering the heat transfer gauges being recorded on FM tape.

The particular bank of heat transfer gauge conditioning circuits used with the FM tape system were originally intended for use with the Ludwieg tube tunnel. However, they were first used on Test OH-66 in the Calspan Hypersonic Shock Tunnel. The circuits have a 1 μfd coupling capacitor in the output and were intended to be used with the amplifiers having a 1 Megohm input impedance. This would yield a time constant of 1 second, which would have been adequate. However, in order to meet the data acquisition requirements of Test IH-75, a large number of amplifiers were borrowed from the hypersonic shock tunnel. These amplifiers had an imput impedance of 100 Kohms and resulted in a system time constant of 0.10 seconds.

An analysis of the circuit response for a constant heat transfer rate has been made in order to determine the corrections to be applied to the data. For a constant heating rate $\dot{q}$, the thin film gauge surface temperature is

$$T(t) = \frac{2\dot{q}}{\sqrt{\pi \rho c k}} \sqrt{t}$$

* Seymour, D.C., "IH-75 Shuttle Base Heating Test Analysis," NASA MSFC Memorandum ED 33-78-16, May 5, 1978.

Analysis of the RC circuit to such an input was made using Laplace transforms. The output (as recorded on FM tape) was found to be

$$T_o(t) = \frac{2\dot{q}\sqrt{\tau}}{\sqrt{\pi\rho c k}} e^{-t/\tau} \int_0^{\sqrt{t/\tau}} e^{\lambda^2} d\lambda$$

where τ = RC, the time constant, and $e^{-t/\tau} \int_0^{\sqrt{t/\tau}} e^{\lambda^2} d\lambda$ is Dawson's Integral and is tabulated.*

The correction factors for the recorded heat transfer rate were found from the general relationship between $\dot{q}_o$ and surface temperature T_o (t).

$$\dot{q}_o(t) = \sqrt{\frac{\rho c k}{\pi}} \left[\frac{T_o(t)}{\sqrt{\tau}} + \frac{1}{2} \int_0^t \frac{T_o(t) - T_o(\lambda)}{(t-\lambda)^{3/2}} d\lambda \right]$$

This integral relation has been evaluated numerically, using the technique of Cook and Felderman**. The relationship can be expressed as

$$\dot{q}_o(t_n) = 2\sqrt{\frac{\rho c k}{\pi}} \sum_{i=1}^{n} \frac{T_o(t_i) - T_o(t_{i-1})}{(t_n - t_i)^{1/2} + (t_n - t_{i-1})^{1/2}}$$

Since $\dot{q}_o$ represents the recorded heat transfer rate, whereas $\dot{q}$ is the true heat transfer rate, the correction factor $\dot{q}/\dot{q}_o$ has been evaluated for $0 \leq t/\tau \leq 0.8$ (or $0 \leq t \leq 80$ msec). the enclosed figures show T_o/T and $\dot{q}/\dot{q}_o$ as functions of t/τ. The curve for T_o/T compares very well with that given by Seymour; however, the correction $\dot{q}/\dot{q}_o$ found here is significantly different than obtained by Seymour using a linear approximation to the T_o/T curve. Seymour's correction is also shown.

---

* Gautschi, W. "Error Function and Fresnel Integrals," Chap. 7, Handbook of Mathematical Functions, NBS Appl. Math Series 55, June 1964.

** Cook, W.J. and Felderman, E.J., "Reduction of Data from Thin-Film Heat-Transfer Gages: A Concise Numerical Technique," AIAA Journal Vol. 4, No. 3, pp. 561, 562, March 1966.

During Test IH-75, the Calspan amplifiers were used with Channels 1 thru 41 for the FM-Multiplex Tape Recorder System. Incor amplifiers having an input impedance of 1 Megohm were used for Channels 42 thru 66. The latter channels have a time constant of 1 sec. The heat transfer data correction factors for each group of channels are listed in the following table, along with the time during which the data were read on each run.

Heat Transfer Rate Correction Factors.

RUN NO.	TIME (Msec)	CHANNELS 1-41	CHANNELS 42-66
4	67	1.94	1.06
5	58	1.77	1.05
6	50	1.64	1.05
7	60	1.81	1.05
8	60	1.81	1.05
9	48	1.61	1.04
10	45	1.56	1.04
11	50	1.64	1.05
12	70	2.00	1.06
13	60	1.81	1.05
14	63	1.86	1.06
15	63	1.86	1.06
16	63	1.86	1.06
17	59	1.79	1.05
18	68	1.96	1.06
19	66	1.92	1.06
20	69	1.98	1.06
21	67	1.94	1.06
22	63	1.86	1.06
23	63	1.86	1.06
24	60	1.81	1.05
25	58	1.77	1.05
26	54	1.70	1.05
27	54	1.70	1.05
28	66	1.92	1.06
29	70	2.00	1.06
30	70	2.00	1.06
31	75	2.10	1.07
32	71	2.02	1.07
33	66	1.92	1.06
34	66	1.92	1.06
35	70	2.00	1.06
36	72	2.04	1.07
37	70	2.00	1.06
38	76	2.13	1.07
39	76	2.13	1.07
40	76	2.13	1.07
41	73	2.06	1.07
42	70	2.00	1.06
43	70	2.00	1.06
44	79	2.19	1.07
45	66	1.92	1.06
46	66	1.92	1.06

Cont'd. Heat Transfer Rate Correction Factors.

RUN NO.	TIME (Msec)	CHANNELS 1-41	CHANNELS 42-66
47	64	1.88	1.06
48	73	2.06	1.07
49	73	2.06	1.07
50	72	2.04	1.07
51	58	1.77	1.05
52	64	1.88	1.06
53	52	1.67	1.05

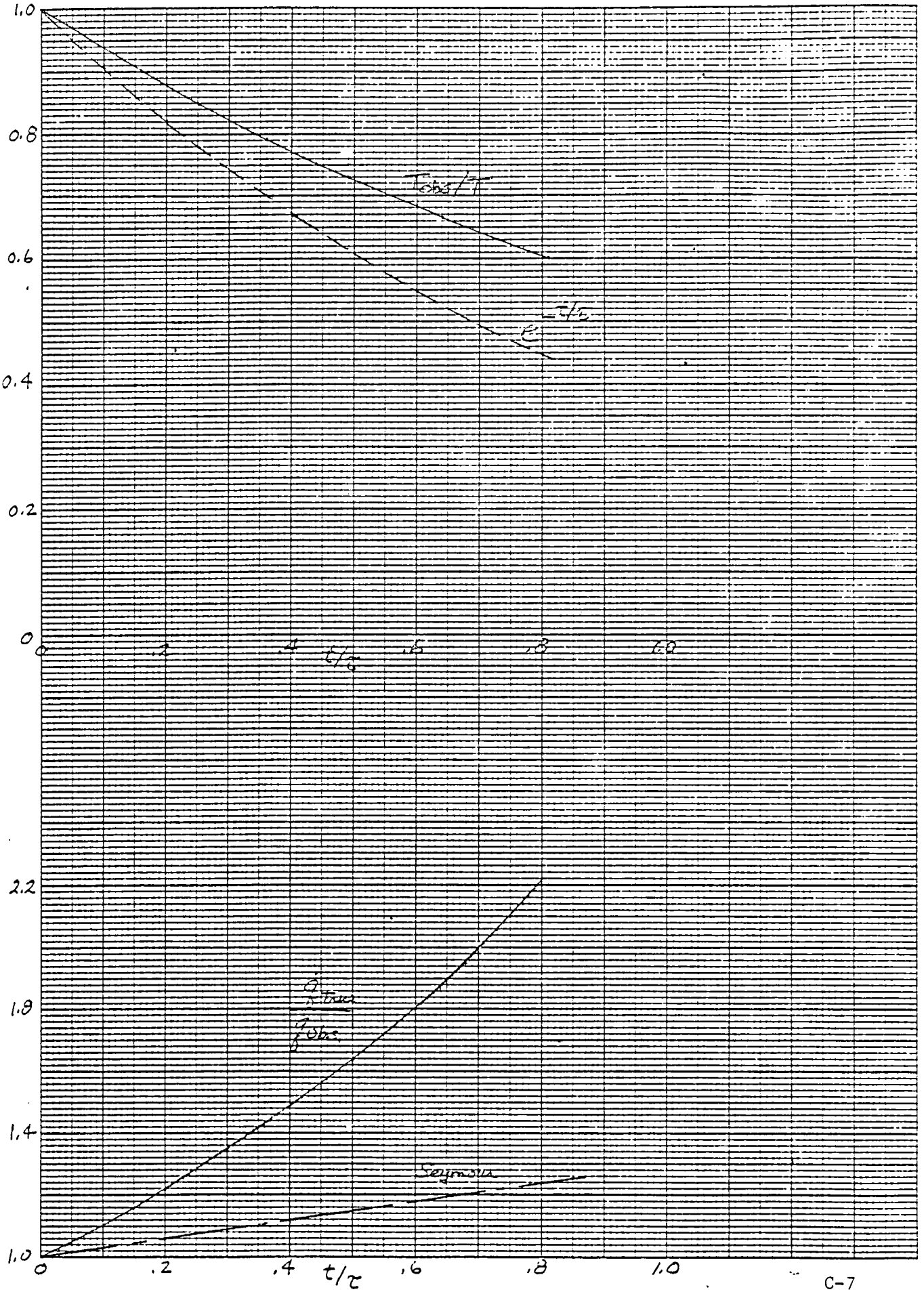

APPENDIX D

FLOW CALIBRATION OF MACH 3.5 FIBERGLASS NOZZLE IN NASA/CALSPAN LUDWIEG TUBE TUNNEL

FLOW CALIBRATION OF MACH 3.5 FIBERGLASS NOZZLE IN NASA/CALSPAN LUDWIEG TUBE TUNNEL

Summary

A series of calibration tests were performed prior to Space Shuttle Test IH75 to determine the airflow characteristics of the contoured Mach 3.5 fiberglass nozzle for the NASA/Calspan Ludwieg Tube Wind Tunnel. Supply tube operating conditions consisted of heated nitrogen (nominally 300°F) at pressures (P_o) approximating the range required during the IH75 test program of the 19-OTS Space Shuttle model.

The average value of the Mach number determined from the calibration tests is 3.484. There was no discernible variation in Mach number with Reynolds number over the range of the tests.

Apparatus

A three-armed rake instrumented with pitot-pressure probes was used to survey the flow. Figure D1 depicts the rake configuration and defines the probe positions. The flow surveys were made with the probes located at the exit plane of the nozzle, at a location 12 inches into the nozzle, and 12 inches downstream of the nozzle exit. In addition, at the nozzle exit plane location, the rake was rotated $\pm 90^{\circ}$ from its nominal position to check flow symmetry.

The pitot-pressure probes were instrumented with Calspan PCB-37-21 pressure transducers having a nominal sensitivity of 1.5 v/psi and a range of 0-3 psi. The nozzle flow stagnation pressure was measured with two probes instrumented with PZT-37-23 transducers that have a nominal sensitivity of 50 mv/psi and a range 0-100 psi. All transducers were

calibrated before and after nozzle flow calibrations.

Calibration Tests

The nominal test conditions for the calibrations were a stagnation temperature of 300°F and a nozzle exit static pressure equal to 1/2 the ambient pressure at altitudes of 100, 110, 130 and 140 KFT. Most of the calibration tests were made at the highest and lowest altitude conditions with only one run at each of the two intermediate altitudes. The test conditions for all runs are summarized in Table DI.

The calibration results for the lowest altitude condition are summarized in Figure D2, which shows the radial distribution of both pitot pressure normalized by stagnation pressure and Mach number. Because no flow asymmetry was detectable, the data from all three arms of the rake are plotted versus radial distance from the centerline. The identification numbers of the probes are shown along the radial distance scale.

The calibrations for the highest altitude are summarized in Figure D3. The presentation of the data is the same as in Figure D2. The average Mach number of all the data shown in Figure D3 is 3.493, whereas the average value for the data in Figure D2 is 3.477. Because the difference is much less than the scatter of the data, a variation with altitude (or Reynolds number) can not be detected. This is also evident in Figures D4 through D8. Figure D4 shows data at each of the four test conditions with the rake in fixed position. Figures D5 through D8 compare data at the two extreme altitudes for various rake orientations and

locations.

The degree of flow symmetry is best seen in Figures D9 and D10, which present data for the various orientations of the rake at the nozzle exit plane. Figure D9, which is for the lowest altitude test condition, shows exceptionally little scatter. Figure D10 is for the highest altitude. The scatter in the data measured by a given probe as the rake is rotated is much less than the variation with radial distance.

The data from the individual runs are shown in Figures D11 through D25.

TABLE DI

SUMMARY OF CALIBRATION TESTS

M = 3.5 NOZZLE, NITROGEN

Run Number	P_4 (psia)	T_4 (°F)	Rake X (in.)	Position #1 Arm	$\bar{P}_o$ (psia)	T_o (°F)
1 B	7.80	358	0	Up	5.95	329
2	4.25	363	0	Up	3.37	314
3	2.18	362	0	Up	1.76	313
4	7.70	354	0	South	5.99	317
6	7.83	362	0	North	6.12	328
7	1.50	353	0	North	1.24	308
8	1.40	356	0	Up	1.23	308
9	1.38	362	0	South	1.17	303
10	7.95	349	+12	Up	6.19	322
11	1.56	317	+12	Up	1.29	280
12	7.78	319	-12	Up	6.06	298
13	1.38	311	-12	Up	1.15	271
14	7.70	325	0	Up	5.88	301
15	7.68	320	0	Up	5.87	300
16	1.38	341	0	Up	1.13	280

1. P_4 and T_4 are static conditions in the supply tube prior to diaphragm rupture.
2. X = +12" is into the nozzle, X = -12" is downstream of the nozzle exit.
3. #1 Arm of the rake is identified in Figure D1.
4. No data were obtained on Run 5 because of a premature diaphragm rupture.

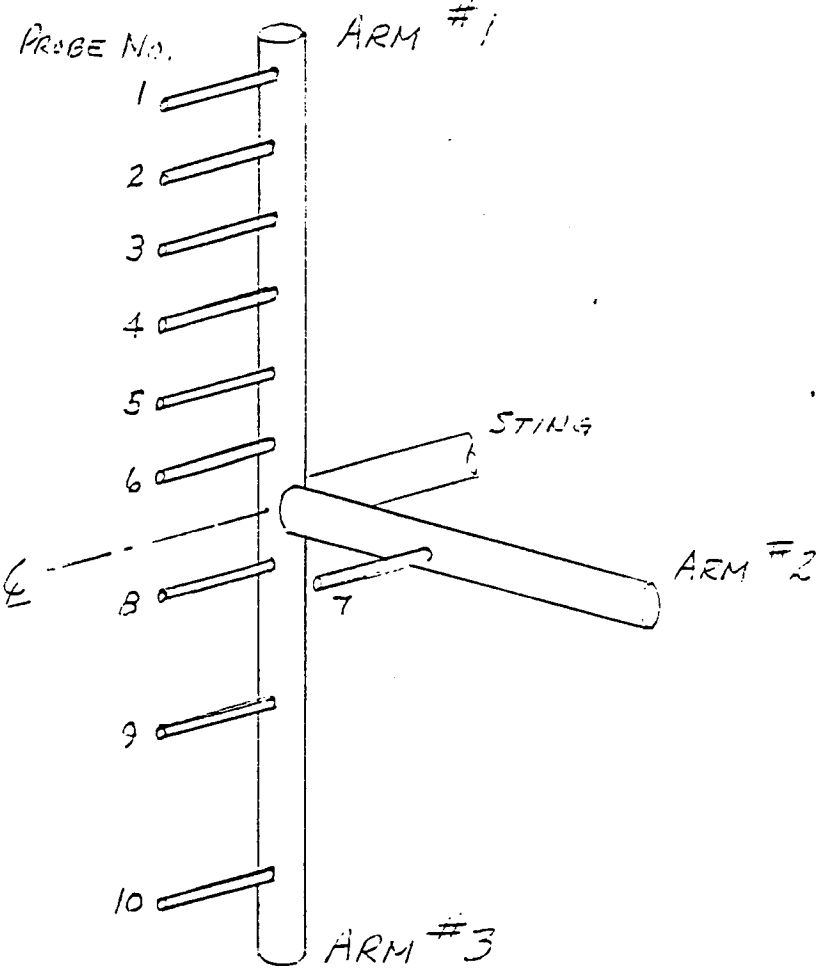

PITOT PROBE	ARM NO.	RADIAL DIST. (IN)
1	1	27.5
2	1	27.0
3	1	18.5
4	1	14.0
5	1	9.0
6	1	4.5
7	2	9.0
8	3	3.0
9	3	12.0
10	3	22.5

Figure D1. Rake Configuration.

SYM	RUN	P_4 DS1Q	P_0 DS1Q	P_T μ Hg	RAKE LOCAT. FACE	RAKE LOCAT. AX. DIS
○	18	7.8	5.95	400	UP	0"
△	4	7.7	5.98	130	S	0"
⬭	6	7.83	6.12	95	N	0"
⊡	10	7.95	6.19	90	UP	+12"
◇	12	7.78	6.06	100	UP	−12"
◇	14	7.70	5.88	110	UP	0"
◁	15	7.68	5.87	110	UP	0"

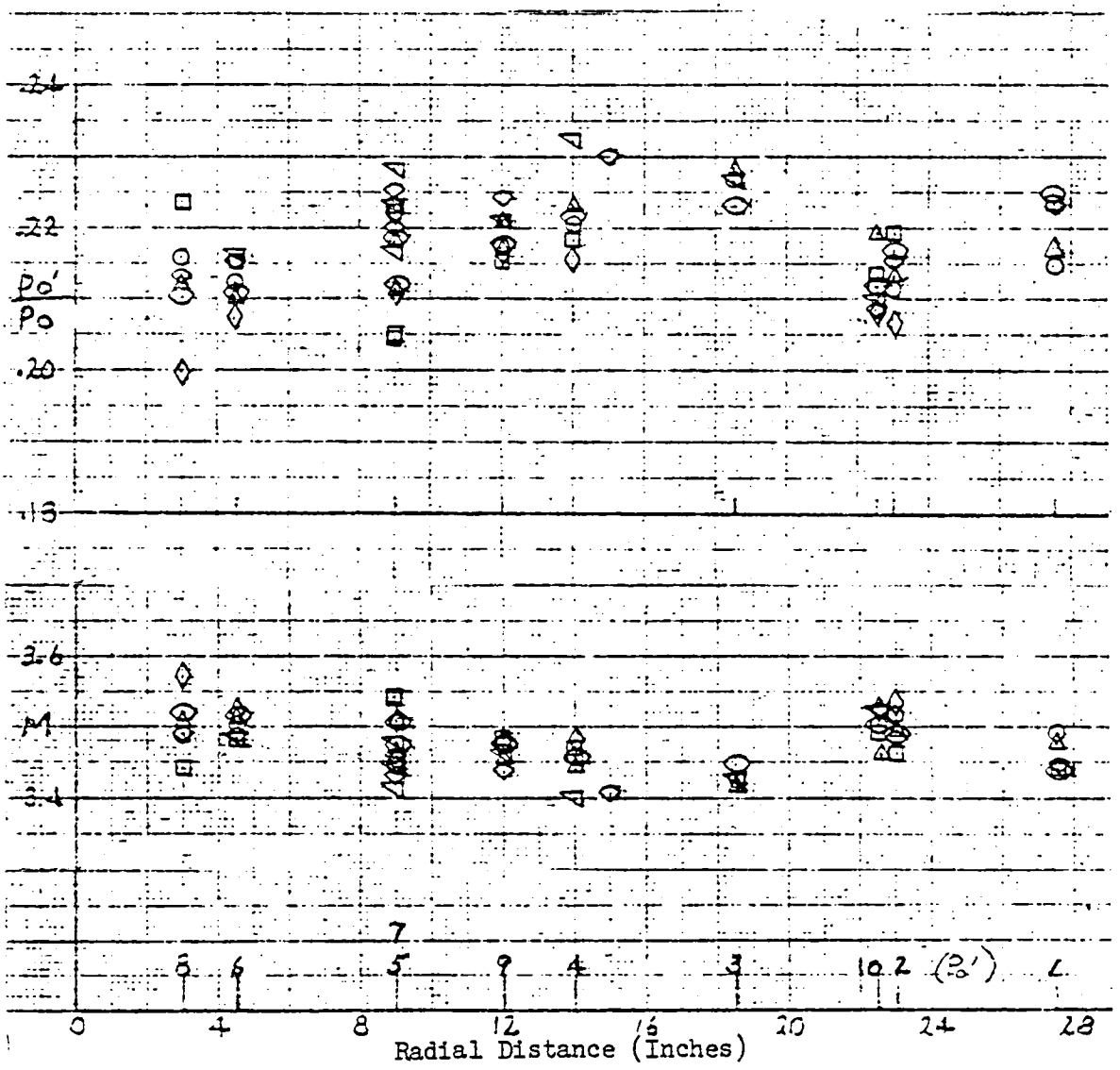

Figure D2. 100K Foot Altitude Calibration Data at Various Rake Positions.

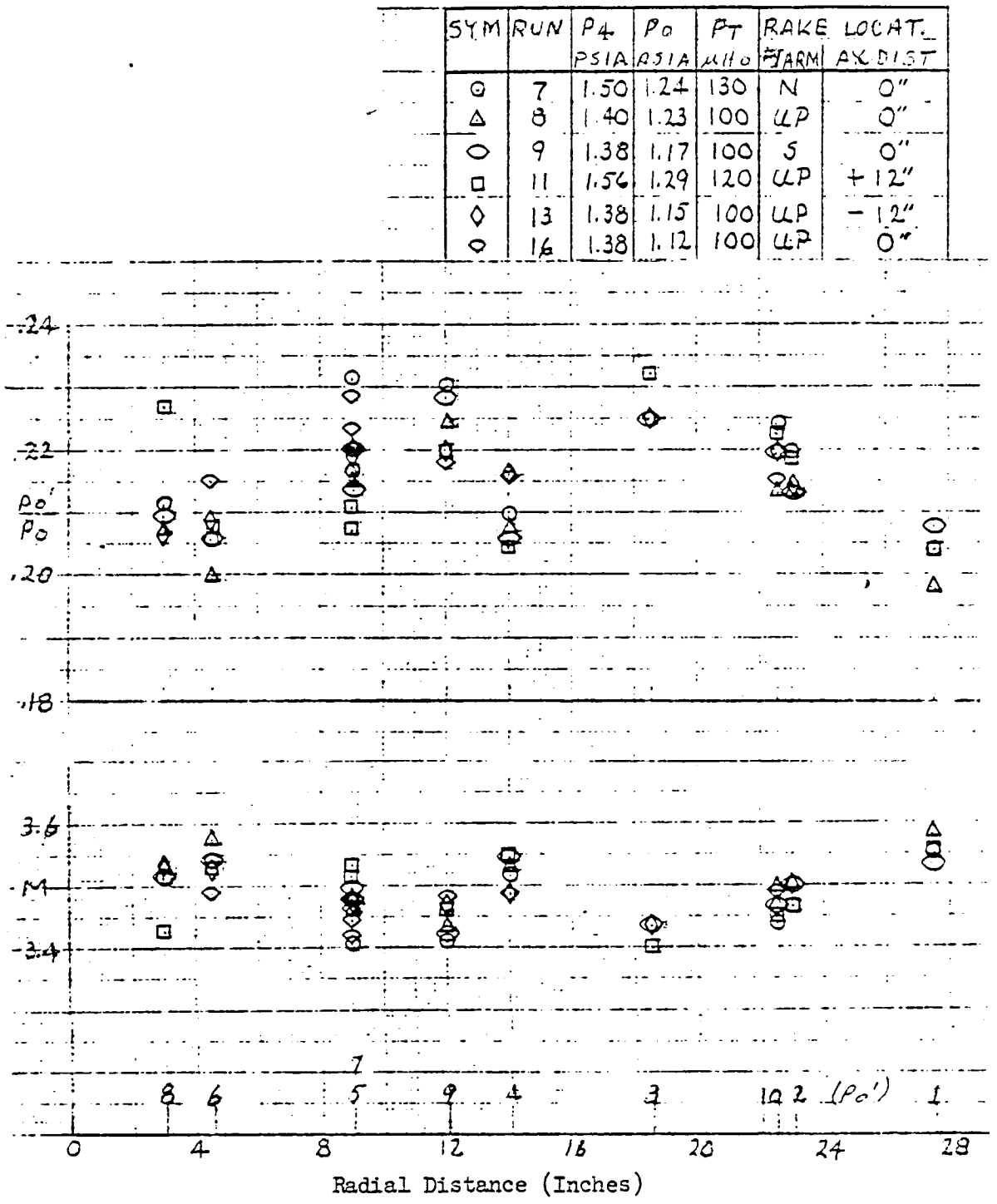

Figure D3. 140K Foot Altitude Calibration Data at Various Rake Positions.

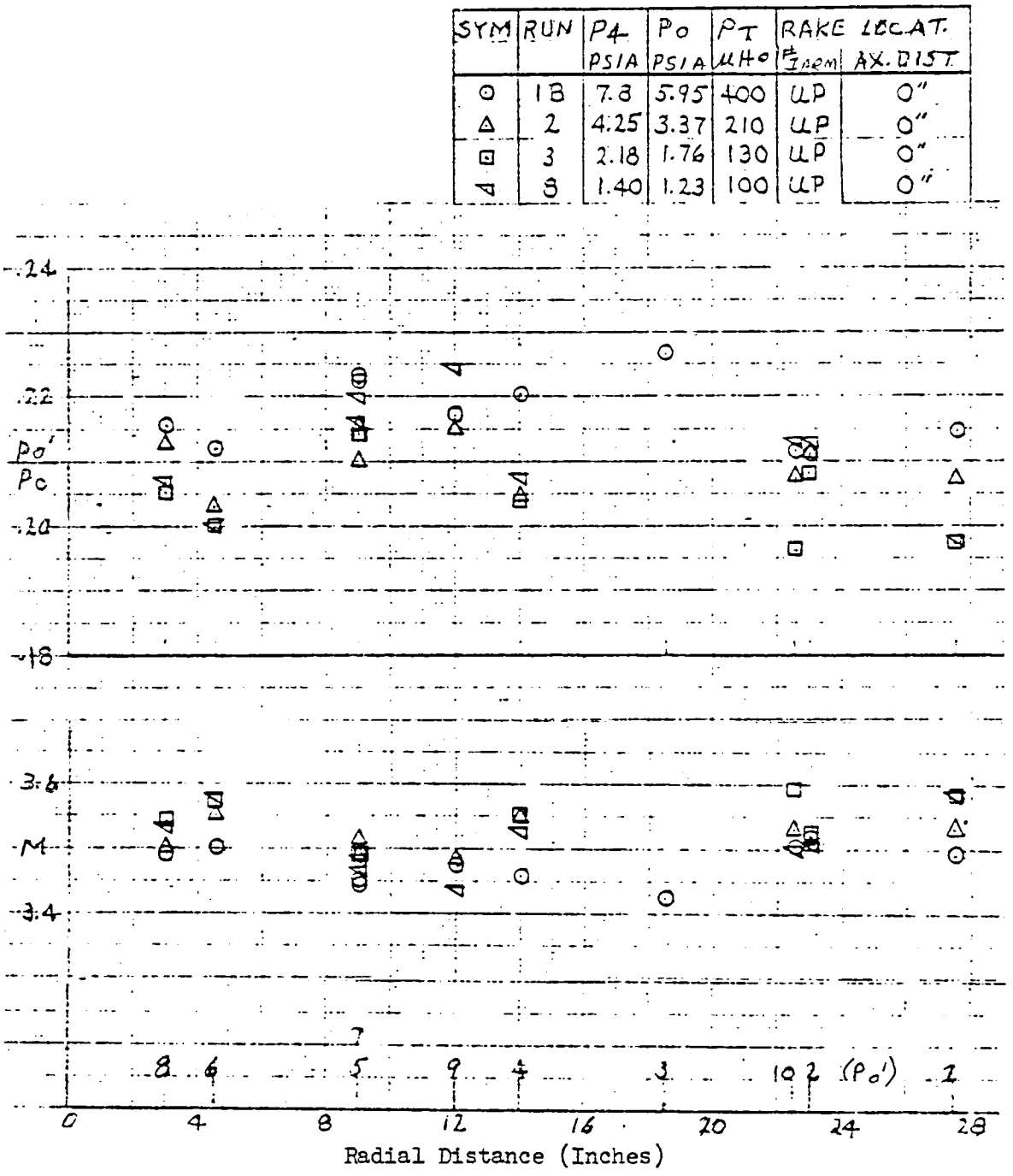

Figure D4. Calibration Data at Each Altitude with a Fixed Rake Position.

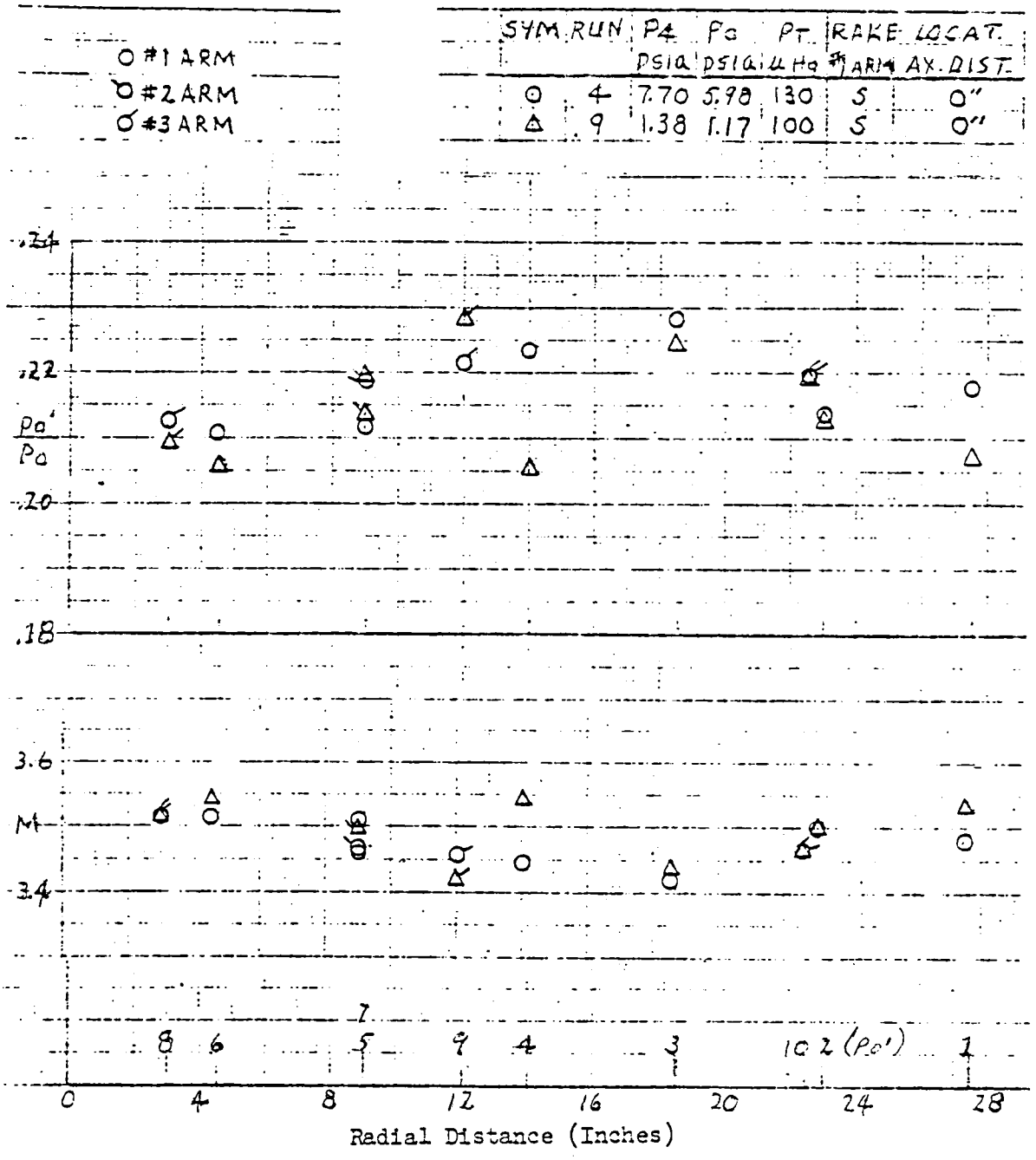

Figure D5. High and Low Altitude Calibration Data at a Fixed Rake Position.

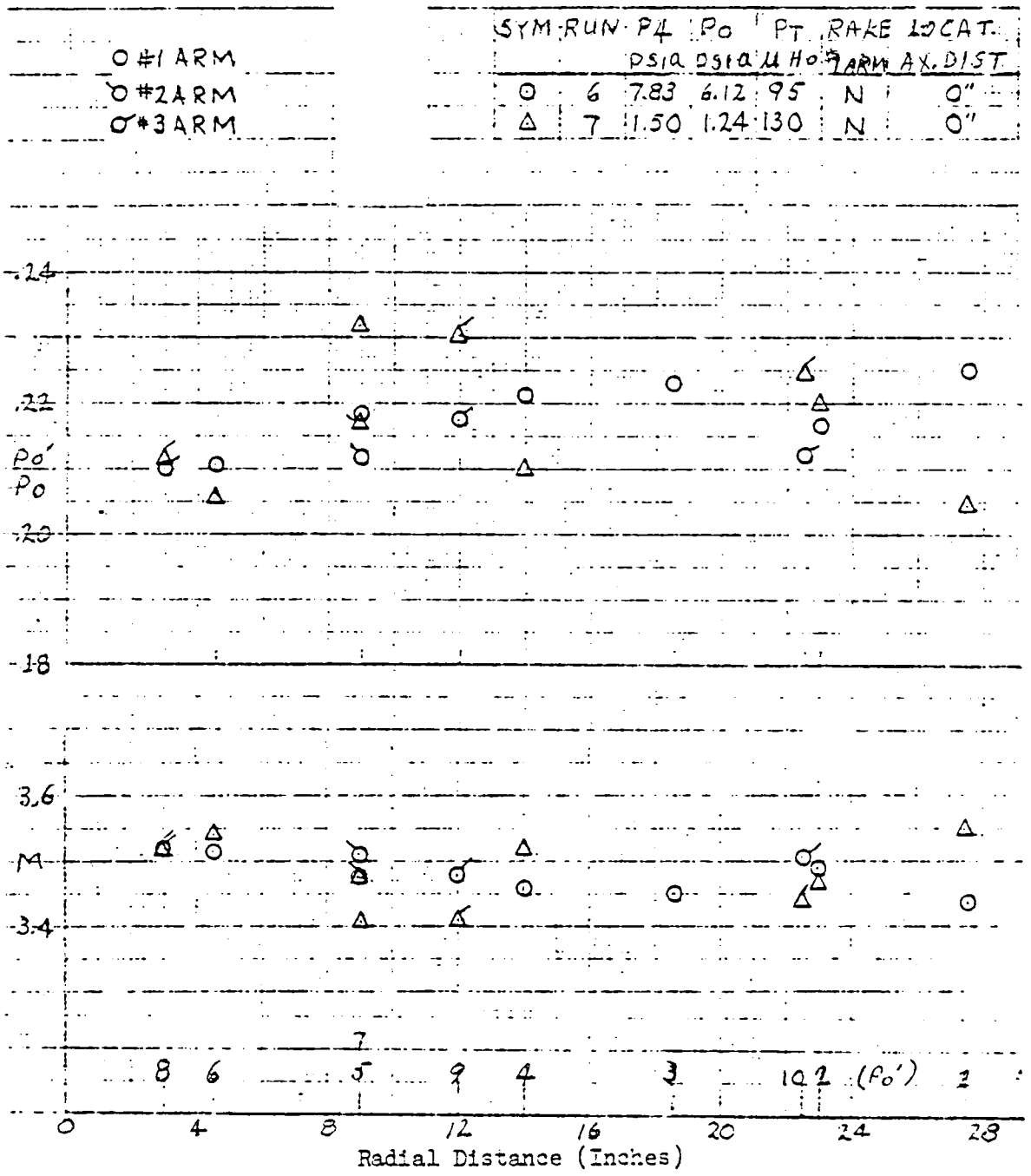

Figure D6. High and Low Altitude Calibration Data at a Fixed Rake Position.

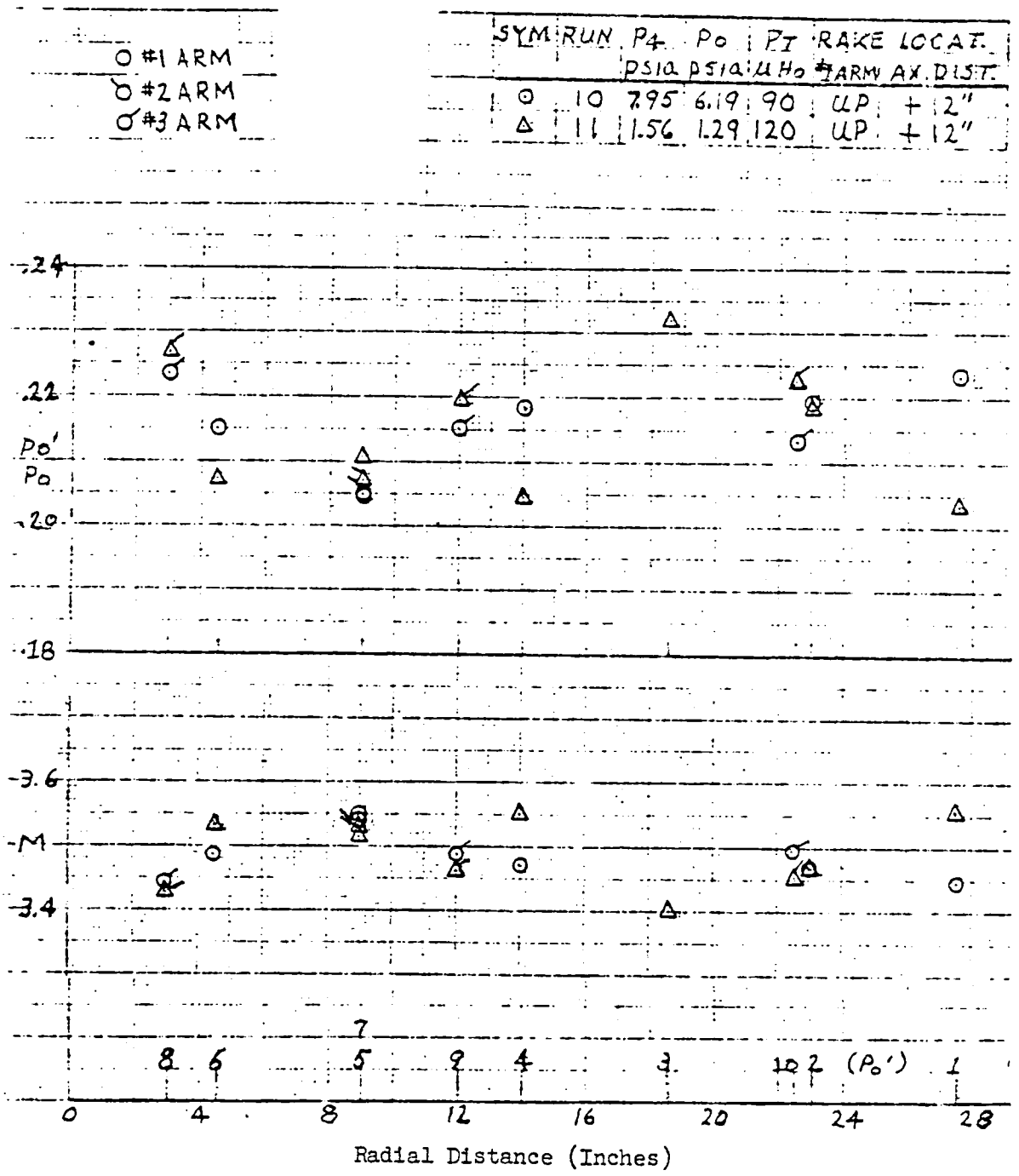

Figure D7. High and Low Altitude Calibration Data at a Fixed Rake Position.

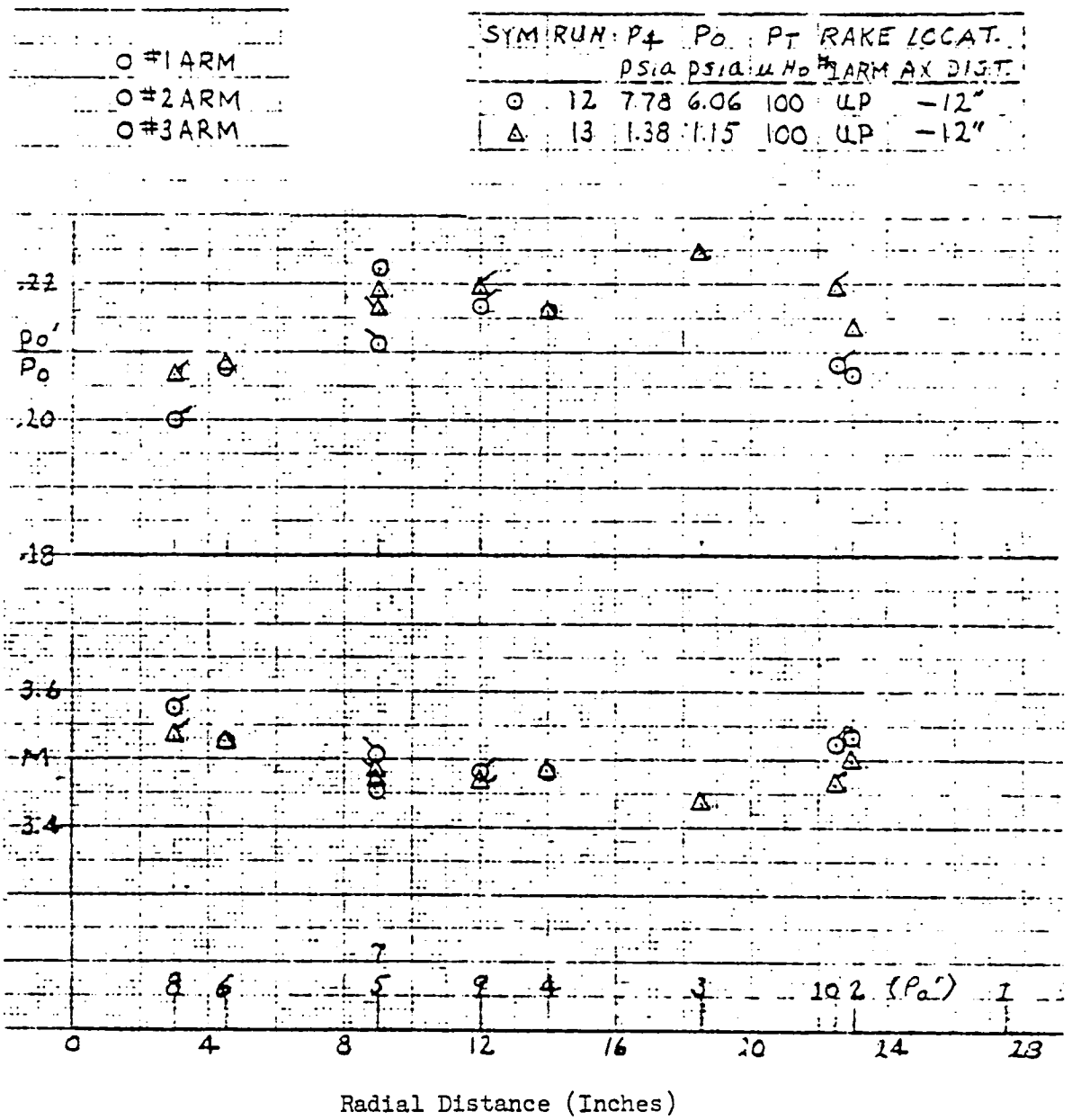

Figure D8. High and Low Altitude Calibration Data at a Fixed Rake Position.

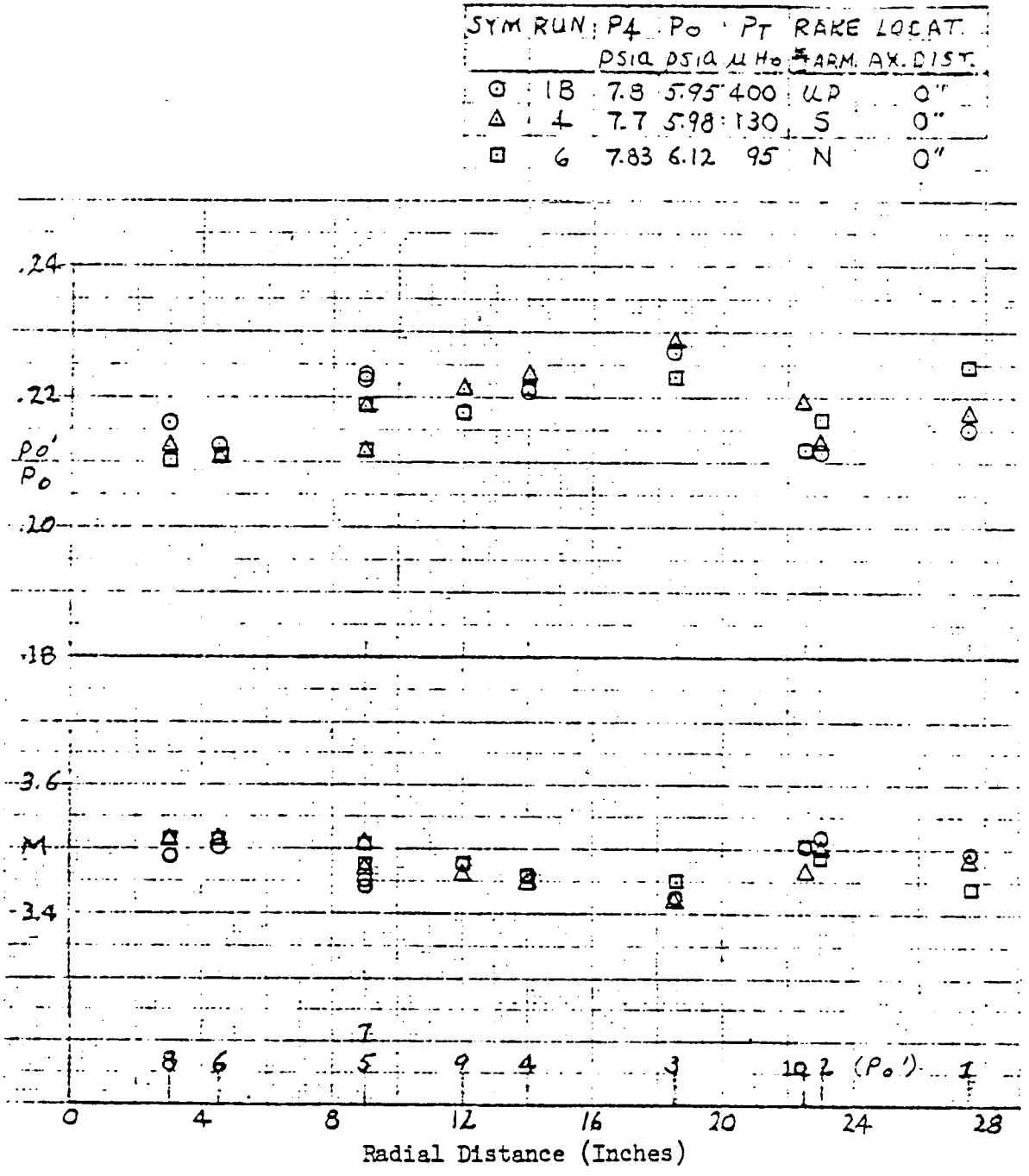

Figure D9. Flow Symmetry at 100K Foot Altitude.

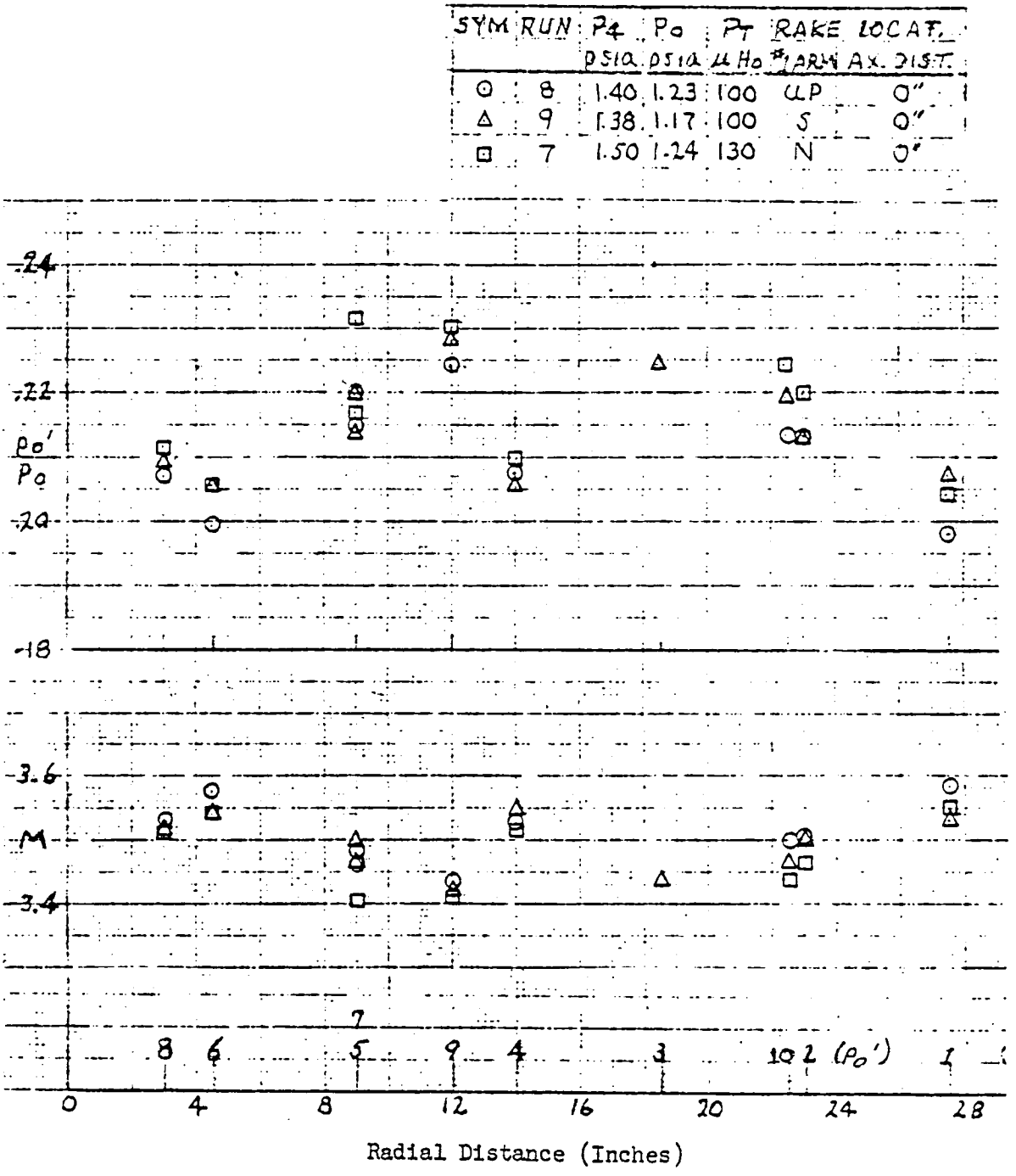

Figure D10. Flow Symmetry at 140K Foot Altitude.

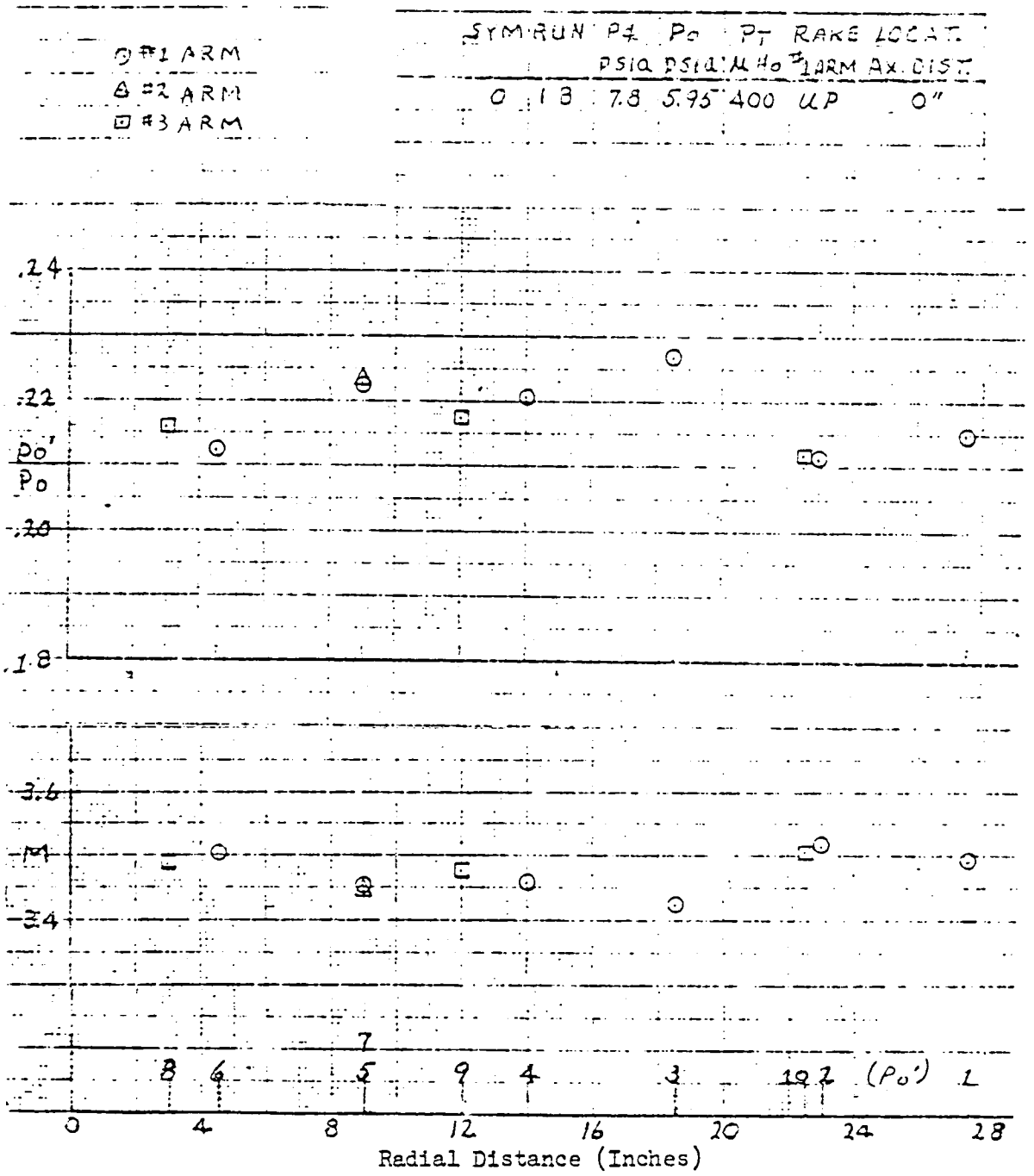

Figure D11. Run 1B Calibration Data.

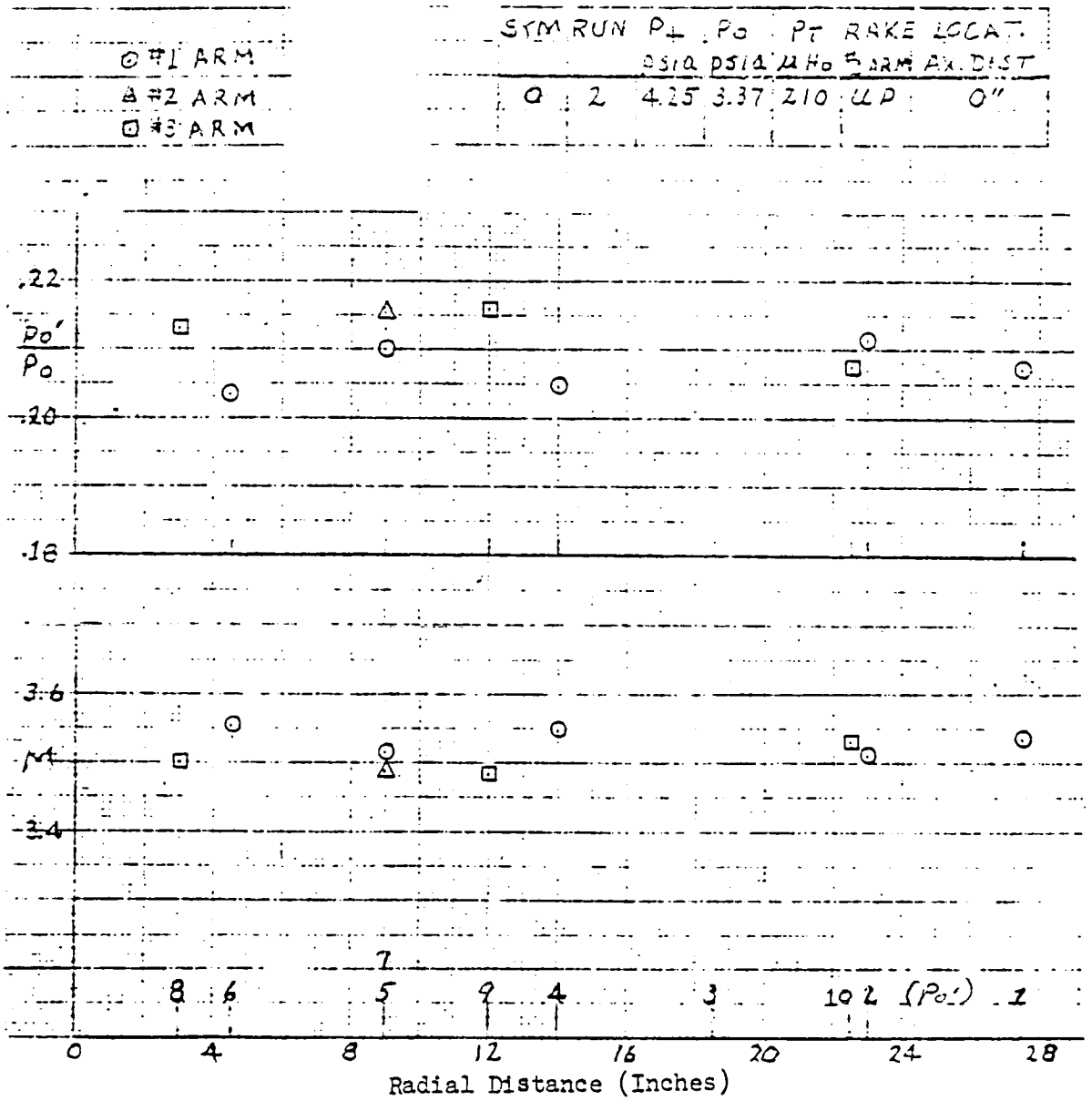

Figure D12. Run 2 Calibration Data.

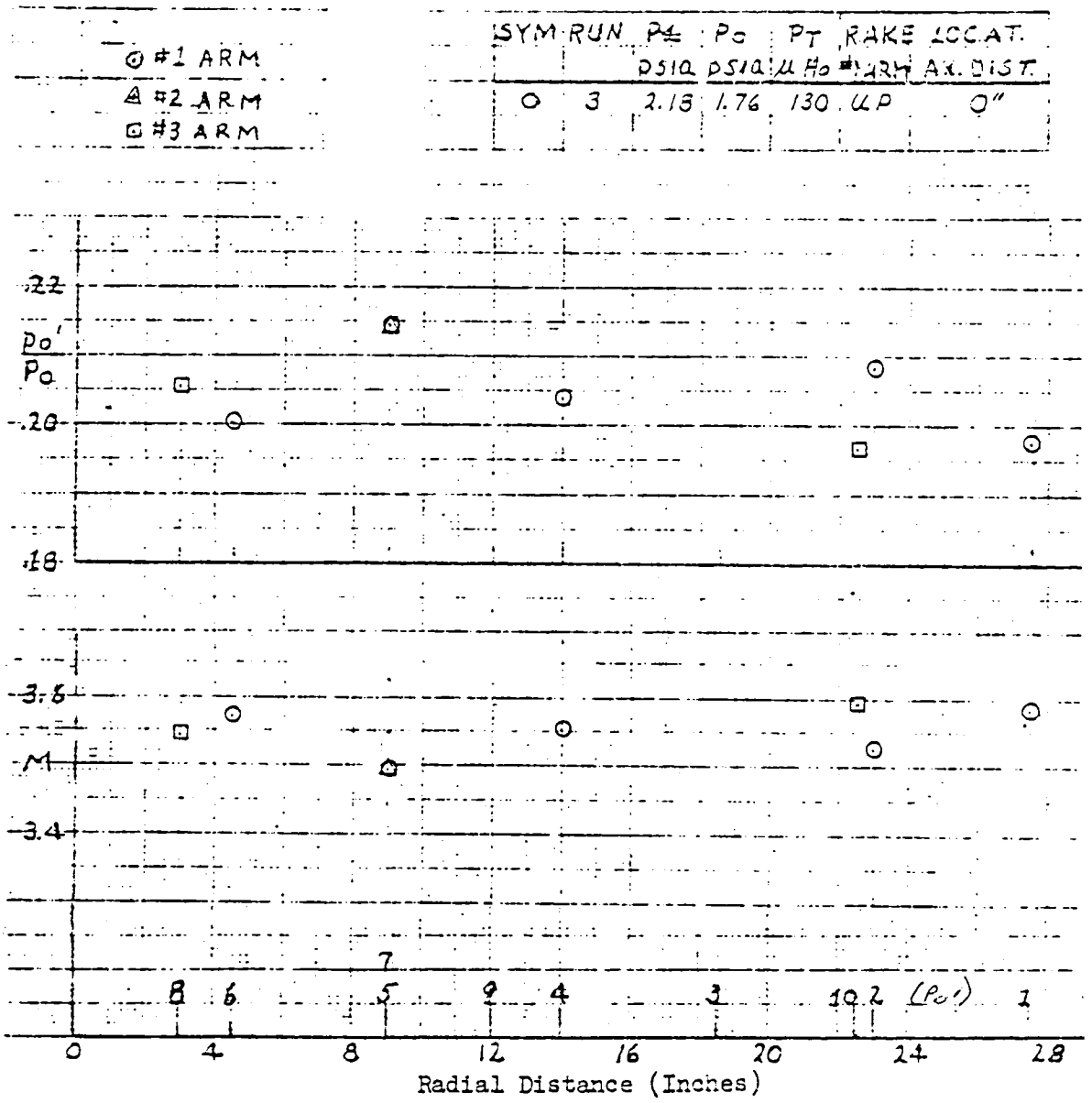

Figure D13. Run 3 Calibration Data.

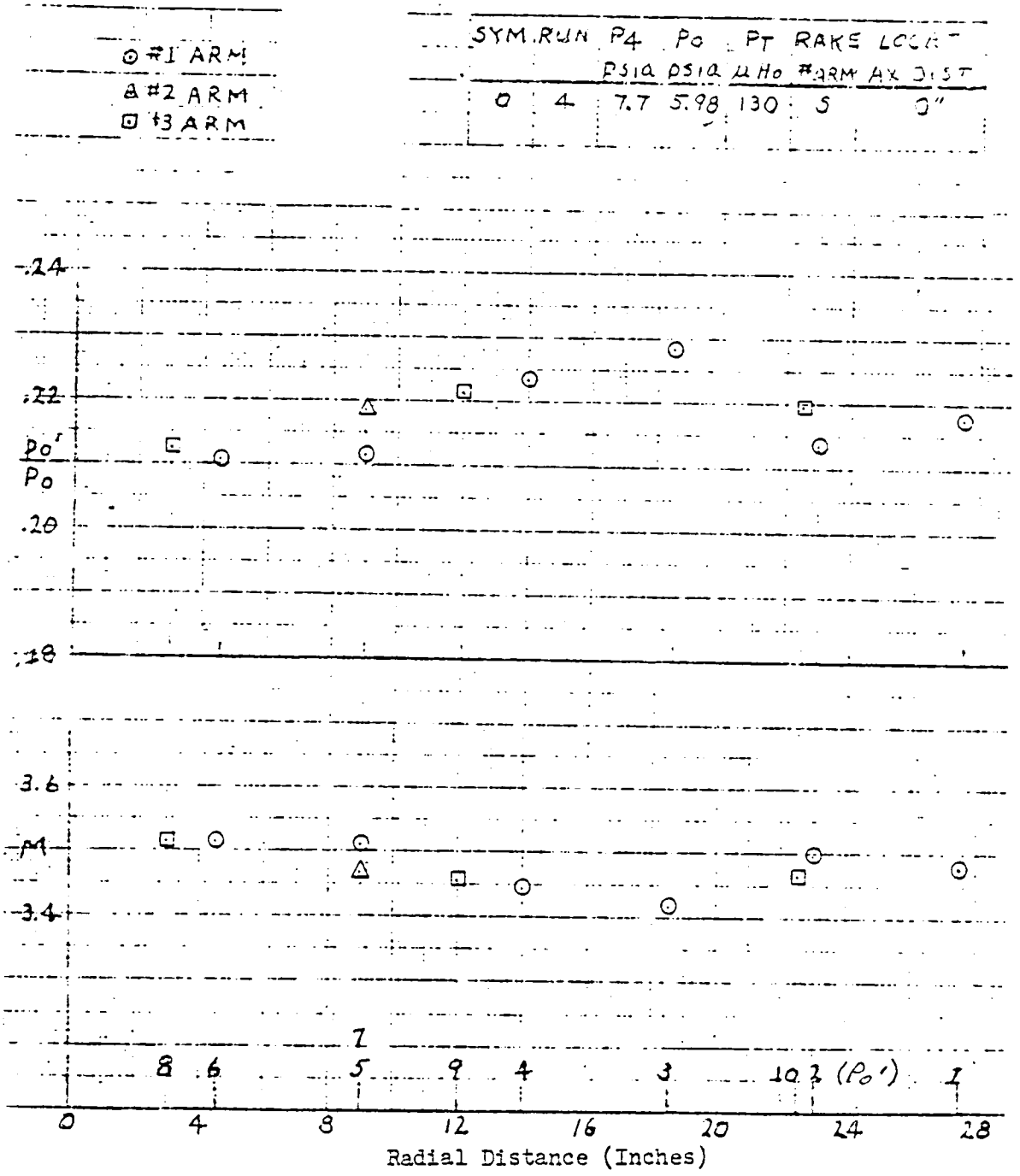

Figure D14. Run 4 Calibration Data.

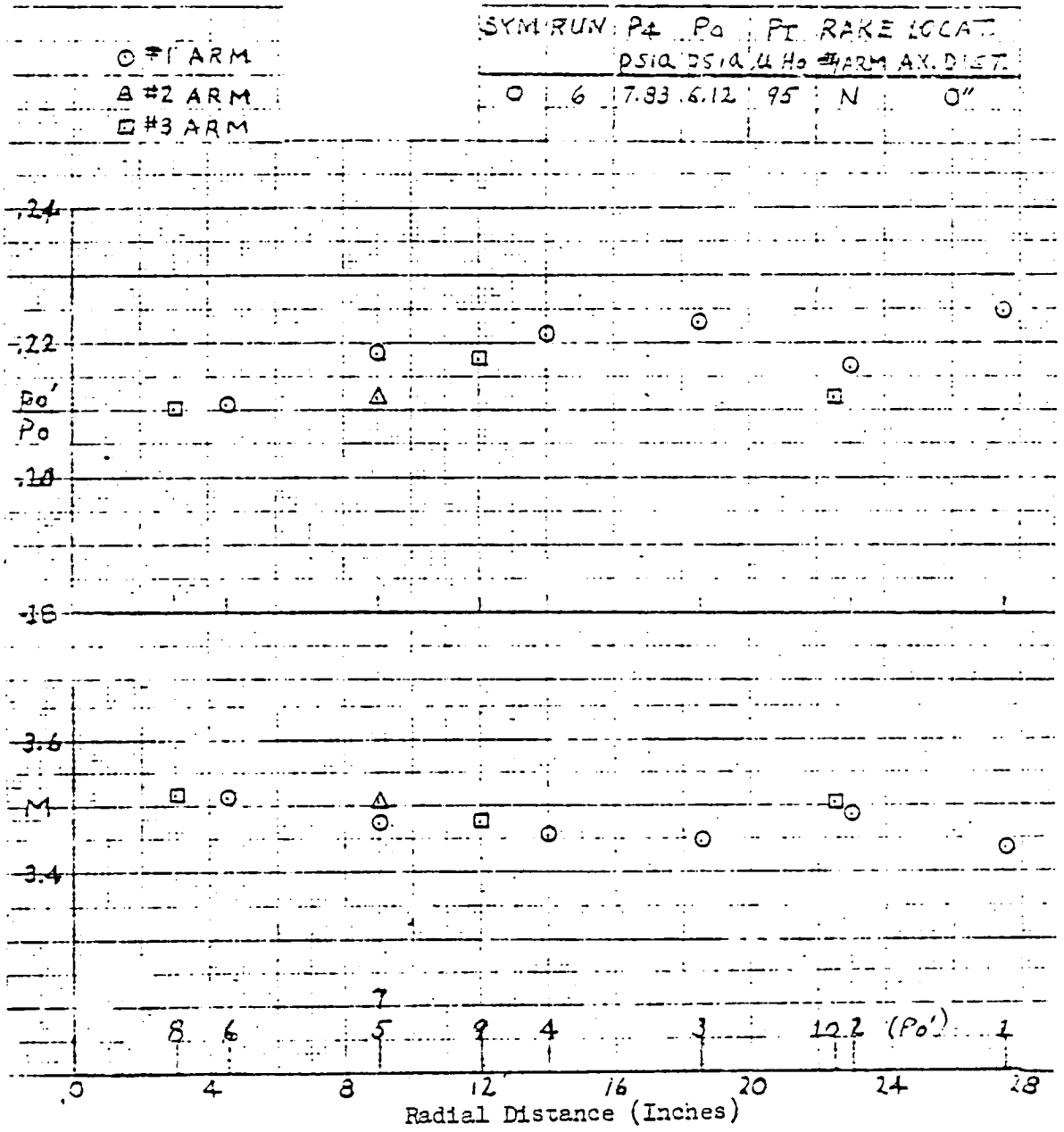

Figure D15. Calibration Data.

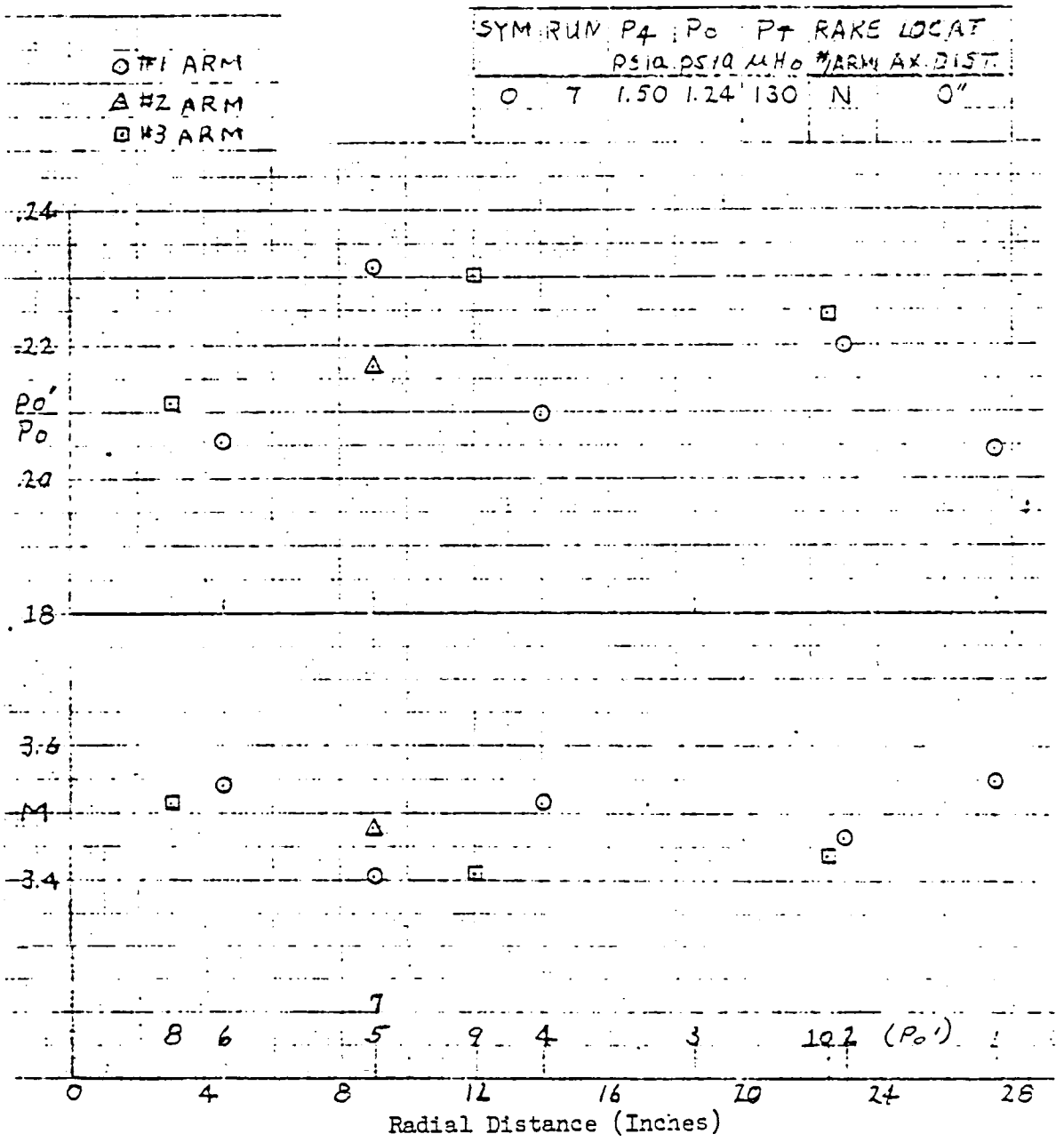

Figure D16. Calibration Data.

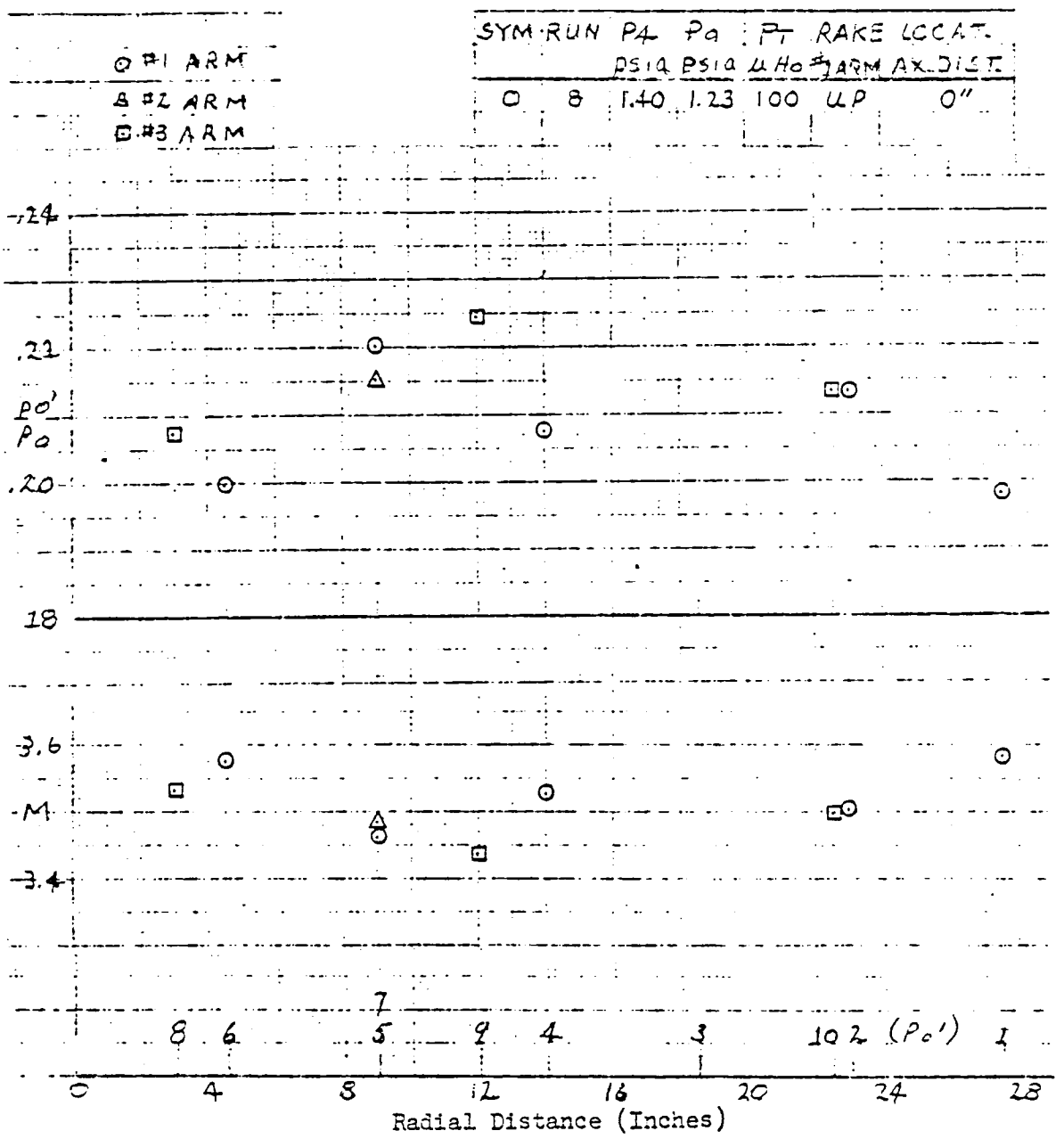

Figure D17. Calibration Data.

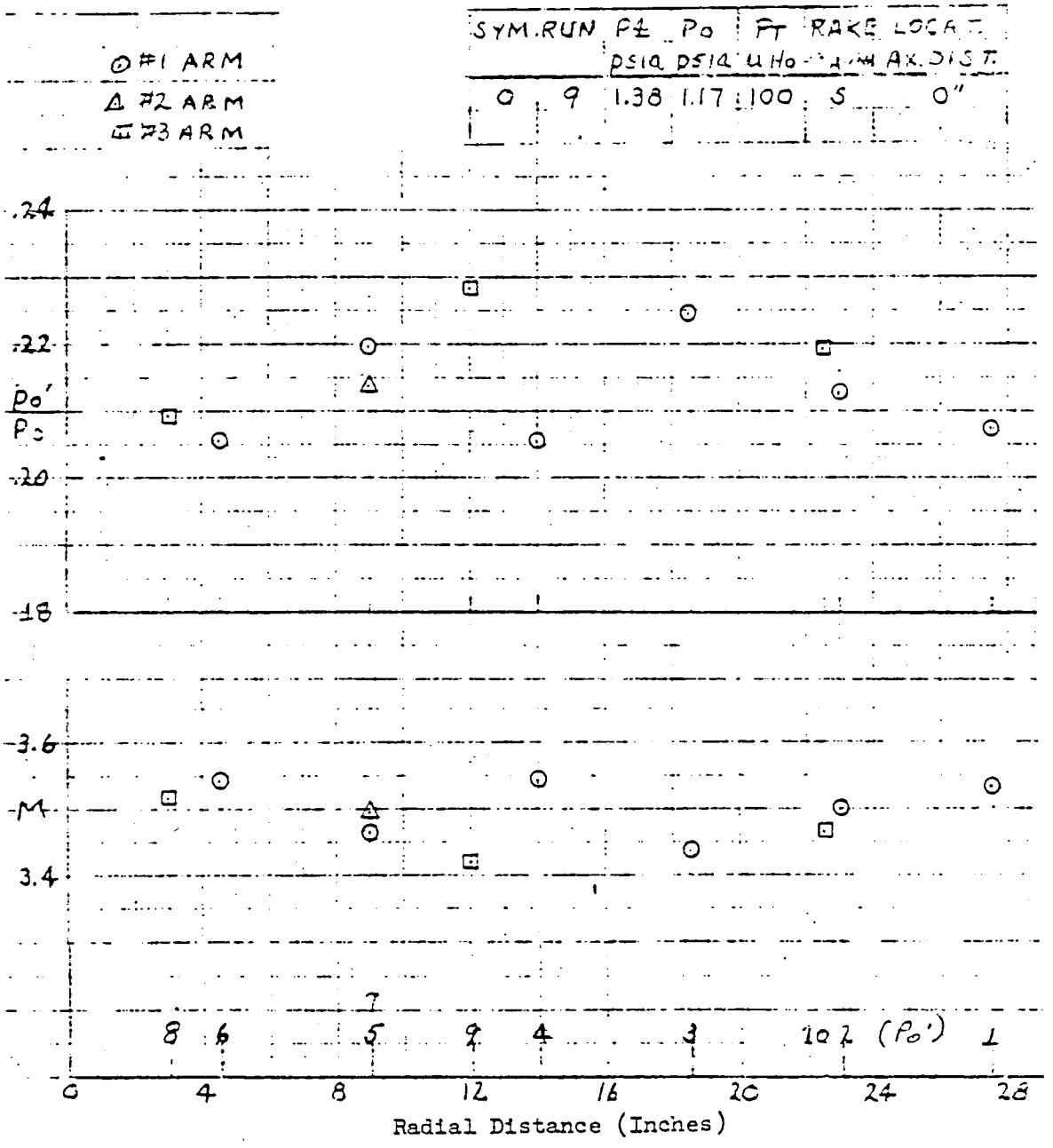

Figure D18. Calibration Data.

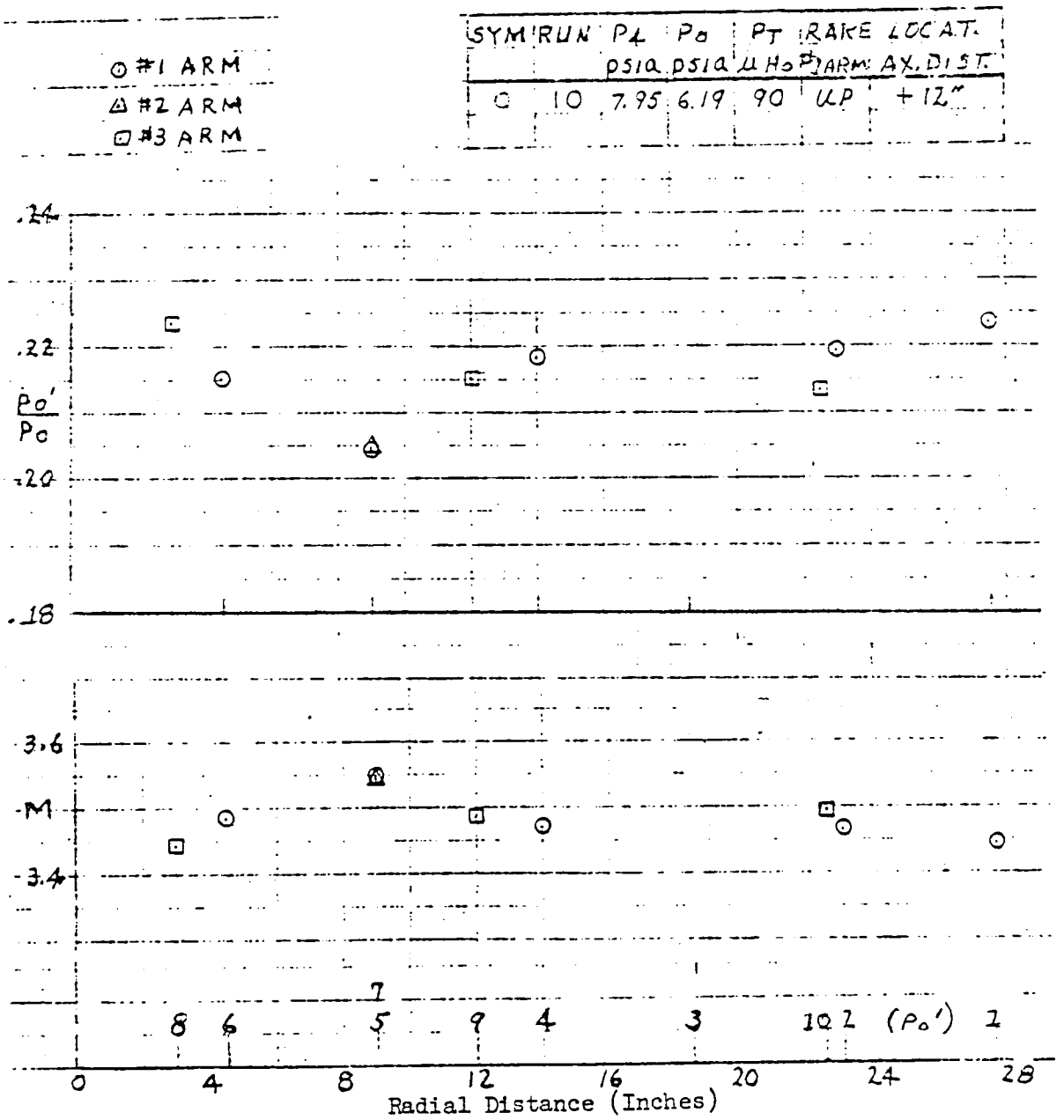

Figure D19. Run 10 Calibration Data

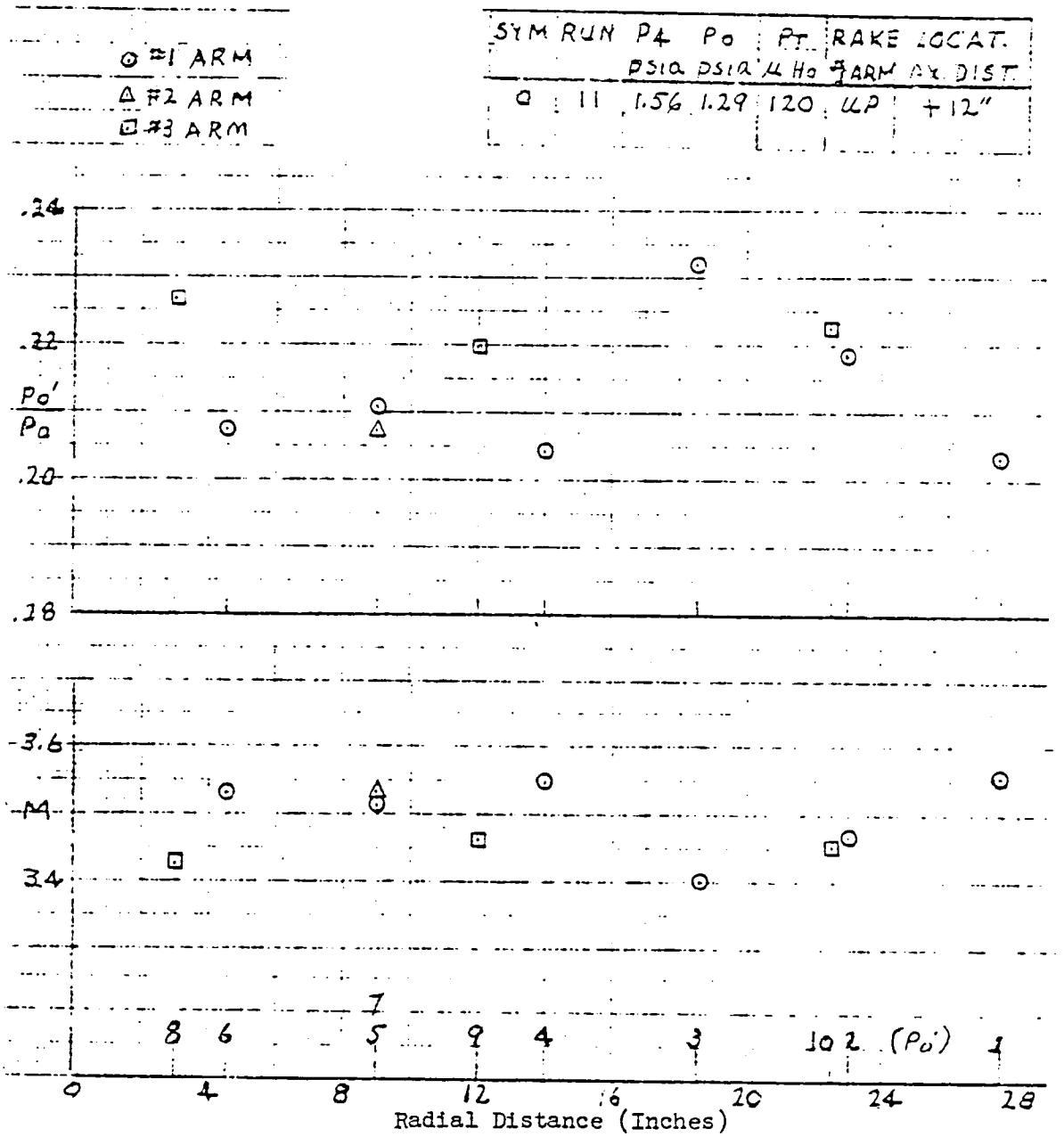

Figure D20. Run 11 Calibration Data.

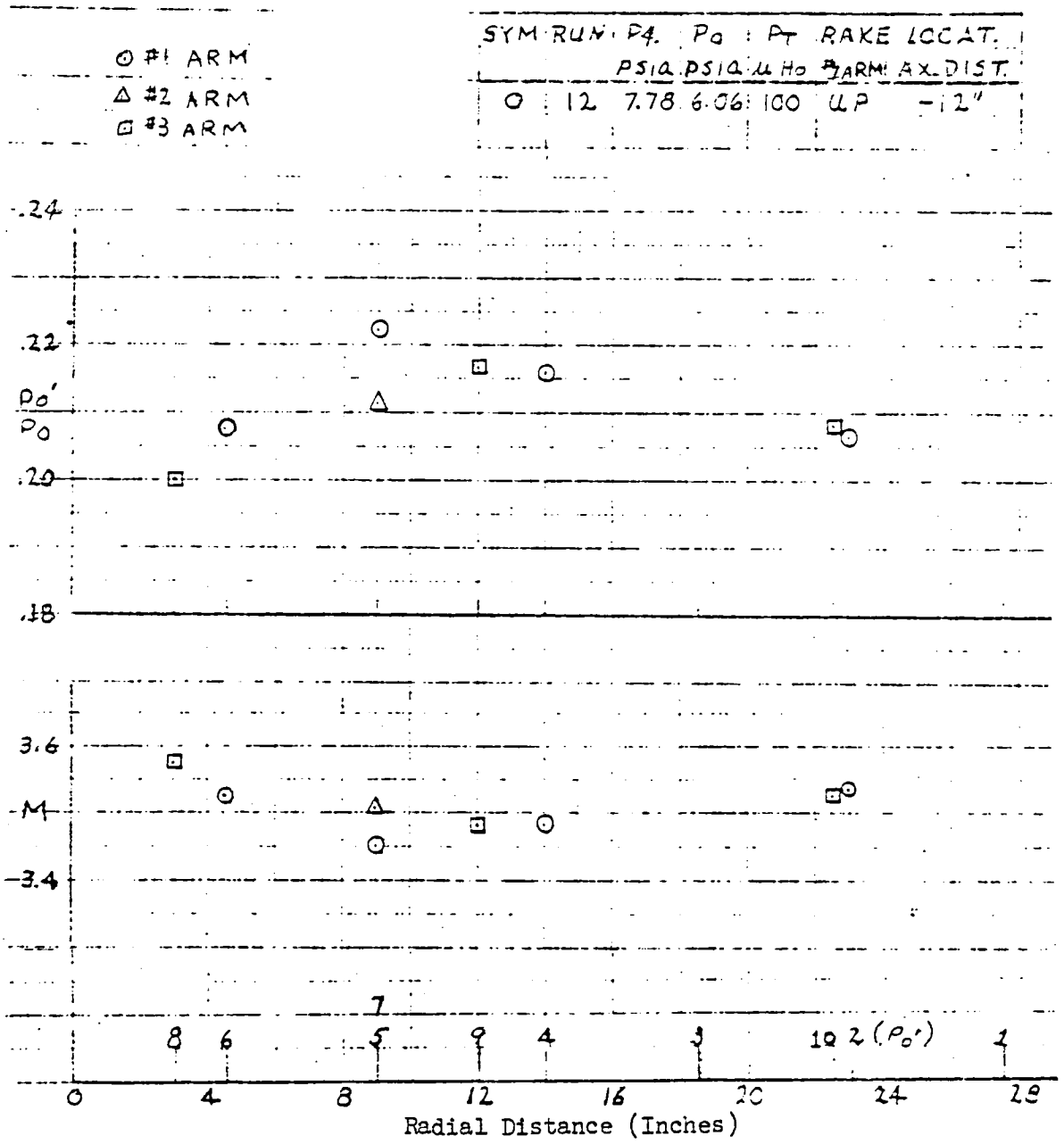

Figure D21. Run 12 Calibration Data.

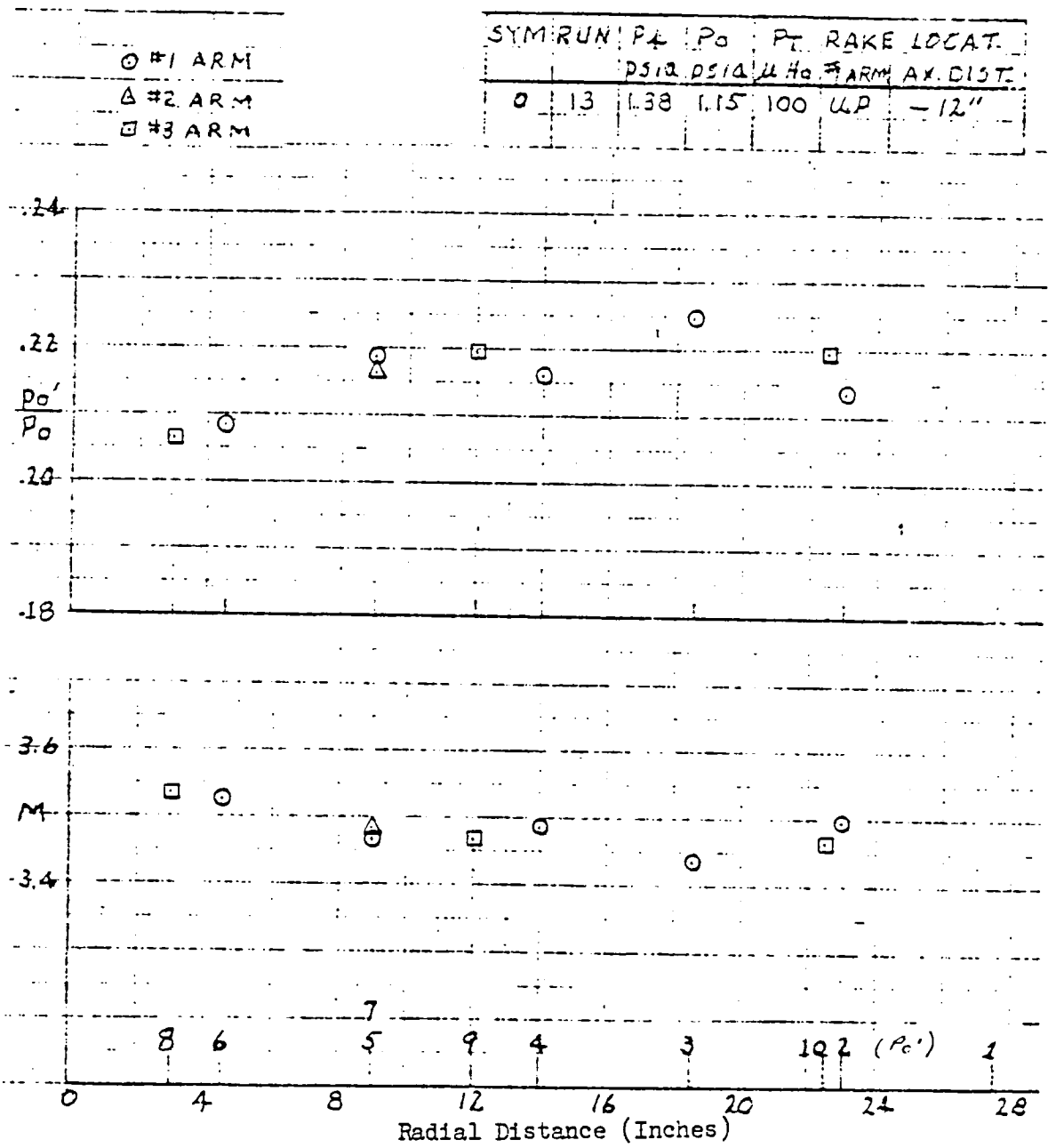

Figure D22. Run 13 Calibration Data.

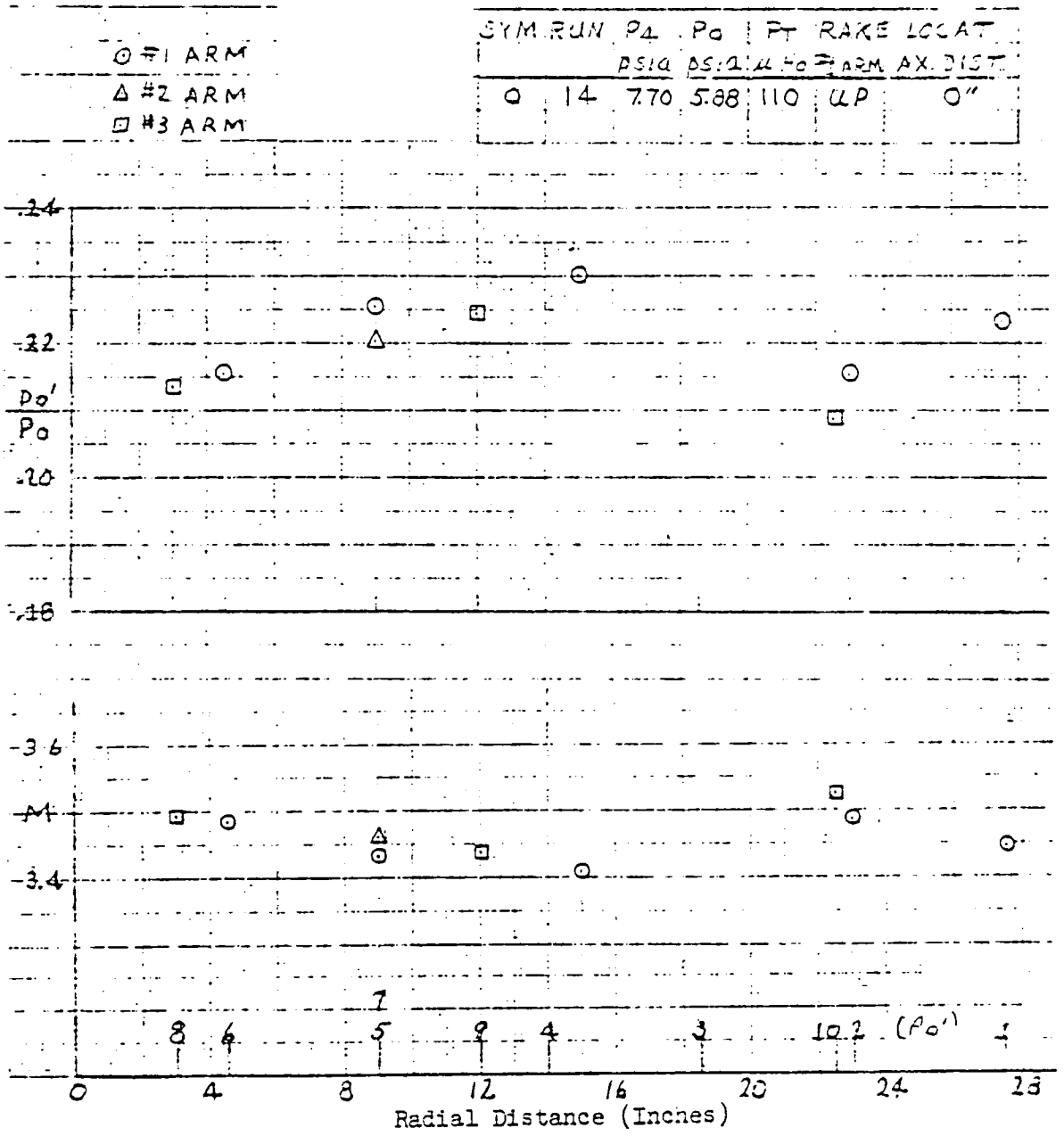

Figure D23. Run 14 Calibration Data.

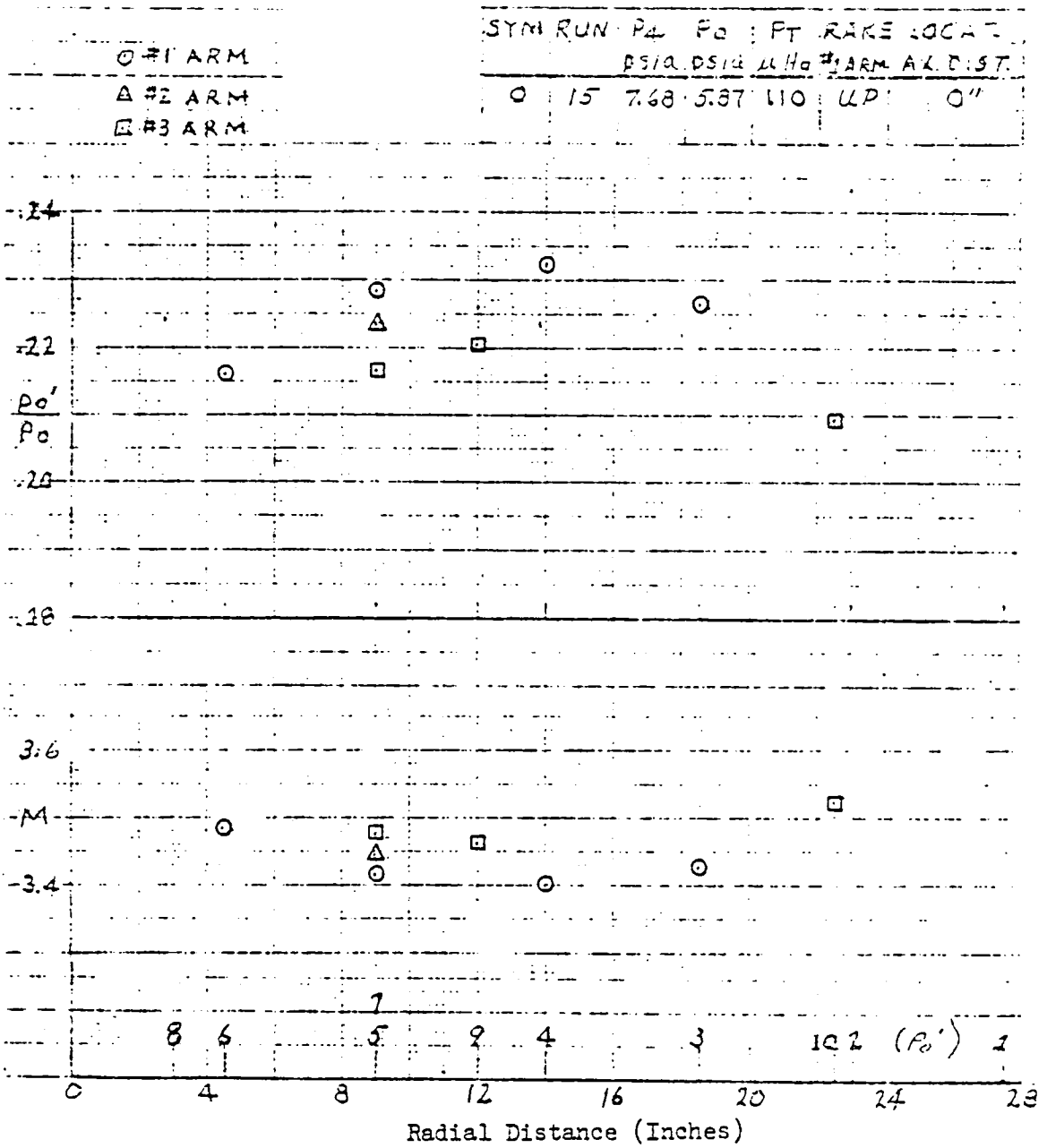

Figure D24. Run 15 Calibration Data.

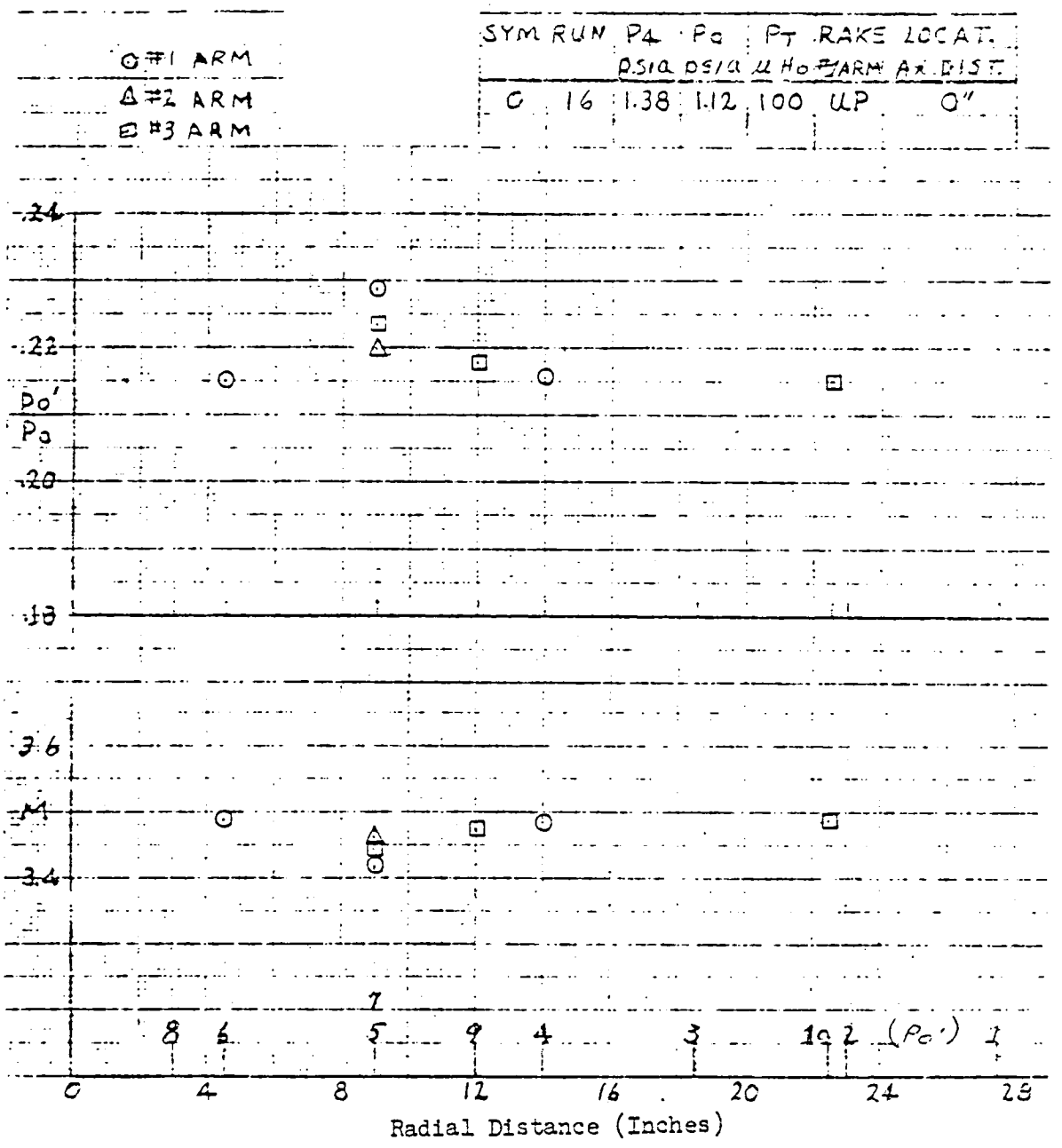

Figure D25. Run 16 Calibration Data.